CRANFIELD UNIVERSITY

G CREECH

EXPERIMENTAL AND FINITE ELEMENT DRAPING SIMULATION FOR NON-CRIMP AND TWILL FABRICS

SCHOOL OF INDUSTRIAL AND MANUFACTURING SCIENCE

MRes THESIS

ProQuest Number: 10832235

All rights reserved

INFORMATION TO ALL USERS
The quality of this reproduction is dependent upon the quality of the copy submitted.

In the unlikely event that the author did not send a complete manuscript
and there are missing pages, these will be noted. Also, if material had to be removed,
a note will indicate the deletion.

ProQuest

ProQuest 10832235

Published by ProQuest LLC (2018). Copyright of the Dissertation is held by Cranfield University.

All rights reserved.
This work is protected against unauthorized copying under Title 17, United States Code
Microform Edition © ProQuest LLC.

ProQuest LLC.
789 East Eisenhower Parkway
P.O. Box 1346
Ann Arbor, MI 48106 – 1346

CRANFIELD UNIVERSITY

SCHOOL OF INDUSTRIAL AND MANUFACTURING SCIENCE

MRes THESIS

Academic Year 2001-2

G CREECH

Experimental and Finite Element Draping Simulation for Non-Crimp and Twill Fabrics

Supervisor: A K Pickett

September 2002

This thesis is submitted in partial fulfilment of the requirements for the degree of Master of Research

ABSTRACT

For low cost and high volume composite manufacture, Liquid Composite Moulding (LCM) techniques such as Resin Transfer Moulding (RTM) are of increasing industrial interest. These techniques involve draping of fabric reinforcement layers into a mould for subsequent resin transfer. For composite materials to compete with metals in low cost, high volume manufacture, valid simulation of this fabric draping is necessary to ascertain if a fabric can be draped without forming defects. Additional permeability and mechanical analysis is reliant upon accuracy in this initial simulation stage. Therefore, this study experimentally and numerically investigates the deformation mechanisms of a woven 2/2 twill fabric and Non-Crimp Fabric (NCF) with the aim of validating a draping simulation code. PAMFORM™ is used as the basis for this work. A material model included in the code is investigated for the 2/2 twill, while a new NCF material representation is proposed to account for additional through thickness stitching constraints. Draping trials over a double hemisphere mould are conducted for final validation of material data calibrated through an extensive testing programme. Both bias extension and picture frame tests are conducted to characterise the shear behaviour of each material.

ACKNOWLEDGEMENTS

The author would like and thank Volkswagen AG and in particular Mr Lars Greve, Dr Jürgen Stieg and Dr Hillebrand at VW for their interest and support of this work. The financial support from VW is also gratefully acknowledged.

Many thanks also go to Prof. A Pickett for his training, guidance and support during the course of the project and to all in the Cranfield Motorsport Composite Research Centre for their time and assistance.

CONTENTS

1 INTRODUCTION 1

2 AIMS AND OBJECTIVES 6

3 LITERATURE SURVEY 7

3.1 MATERIALS AND MATERIAL CHARACTERISATION 7
3.1.1 DEFORMATION MECHANISMS 8
3.1.2 CHARACTERISATION TESTS 11
3.2 DRAPING TRIALS 17
3.3 DRAPING SIMULATION METHODS 19
3.3.1 MAPPING SIMULATION METHODS 19
3.3.2 FINITE ELEMENT DRAPING SIMULAION METHODS 23
3.3.3 EXPLICIT AND IMPLICIT FINITE ELEMENT ANALYSIS 27
3.3.4 FINITE ELEMENT MATERIAL MODEL 30

4 MATERIALS CHARACTERISATION 33

4.1 TESTING PROGRAMME 33
4.2 FABRIC DESCRIPTION 34
4.3 TESTING PROCEDURES 35
4.3.1 BIAS EXTENSION TESTING PROCEDURE 35
4.3.2 PICTURE FRAME TESTING PROCEDURE 37
4.3.3 FLEXURAL RIGIDITY TESTING PROCEDURE 40
4.3.4 FRICTION TESTING PROCEDURE 41
4.3.5 TOW PULL-OUT TESTING PROCEDURE 42
4.3.6 DRAPING TRIAL PROCEDURE 44
4.4 EXPERIMENTAL RESULTS 46
4.4.1 MATERIAL DIMENSIONS 46
4.4.2 BIAS EXTENSION RESULTS 47
4.4.3 PICTURE FRAME RESULTS 50
4.4.4 FLEXURAL RIGIDITY RESULTS 52
4.4.5 FRICTION TESTING RESULTS 52
4.4.6 TOW PULL-OUT RESULTS 53
4.4.7 DRAPING TRIAL RESULTS 55

5 FINITE ELEMENT SIMULATION 59

5.1 MATERIAL MODEL DESCRIPTION 59
5.2 SIMULATION PROGRAMME 61
5.3 SIMULATION PROCEDURES 62
5.3.1 TOW PULL-OUT SIMULATION 62
5.3.2 2/2 TWILL BIAS EXTENSION SIMULATION PROCEDURE 63
5.3.3 NCF BIAS EXTENSION SIMULATION: ADDITIONAL REQUIREMENTS 65
5.3.4 2/2 TWILL PICTURE FRAME SIMULATION PROCEDURE 65
5.3.5 NCF PICTURE FRAME SIMULATION: ADDITIONAL REQUIREMENTS 67
5.3.6 FLEXURAL RIGIDITY SIMULATION 67
5.3.7 DRAPING TRIAL SIMULATION 68
5.4 SIMULATION RESULTS 70
5.4.1 NCF TOW PULL-OUT SIMULATION RESULTS 70
5.4.2 2/2 TWILL BIAS EXTENSION SIMULATION RESULTS 71
5.4.3 NCF BIAS EXTENSION SIMULATION RESULTS 75
5.4.4 2/2 TWILL PICTURE FRAME SIMULATION RESULTS 77
5.4.5 NCF PICTURE FRAME SIMULATION RESULTS 77
5.4.6 FLEXURAL RIGIDITY SIMULATION 79
5.4.7 2/2 TWILL DRAPING TRIAL SIMULATION RESULTS 80
5.4.8 NCF DRAPING TRIAL SIMULATION RESULTS 85

6 DISCUSSION **89**

6.1 MATERIAL CHARACTERISATION CONSIDERATIONS 89

6.1.1 BIAS EXTENSION RESULTS DISCUSSION *89*

6.1.2 PICTURE FRAME RESULTS DISCUSSION *92*

6.1.3 FLEXURAL RIGIDITY RESULTS DISCUSSION *94*

6.1.4 FRICTION TESTING RESULTS DISCUSSION *95*

6.1.5 TOW PULL-OUT RESULTS DISCUSSION *97*

6.1.6 DRAPING TRIAL RESULTS DISCUSSION *98*

6.2 SIMULATION DISCUSSION 100

6.2.1 NCF TOW PULL-OUT SIMULATION DISCUSSION *100*

6.2.2 BIAS EXTENSION SIMULATION DISCUSSION *101*

6.2.3 PICTURE FRAME SIMULATION DISCUSSION *104*

6.2.4 FLEXURAL RIGIDITY SIMULATION DISCUSSION *106*

6.2.5 DRAPING TRIAL SIMULATION DISCUSSION *107*

6.2.6 MATERIAL MODEL DISCUSSION *110*

7 CONCLUSIONS **113**

8 FUTURE WORK **115**

9 REFERENCES **117**

1 INTRODUCTION

Many industries are today taking advantage of continuous fibre composite materials in high performance applications. Using a combination of continuous, high strength fibres held in a rigid polymeric matrix has permitted numerous performance improvements over many traditional materials for which the limits of usability are being rapidly approached. The advantage of using composite materials is different for each application but can include such factors as weight reduction due to low plastic and fibre densities, higher strength and stiffness due to the reinforcing fibres, corrosion resistance and in some applications lower manufacturing costs. The added benefit of being able to tailor the fibre orientation, fibre layer thickness and lay-up sequence for each individual component also permits much greater flexibility during design and manufacture.

The aerospace and automotive industries have exploited continuous fibre composite materials in 'high-end' applications for many years. The associated research and development has permitted almost direct replacement of metals in many high stress applications such as automobile leaf springs and drive shafts [1]. This research has, however, still to permit the full applicability of fibre reinforced plastics to be realised in lower cost and higher volume production. With this aim in mind industrial attention has become focused on the use of woven and engineered fabrics as an alternative to pre-preg[1] technology. The aim of this is to permit design and manufacturing cost reductions at higher production volumes. Further reductions in cost are possible through research into developing design simulation tools to replace prototyping, a task that is complicated by the two phase structure and generally orthotropic material properties. It is in the interest of developing such a simulation tool that Volkswagen AG have sponsored this project and provided woven and engineered carbon fibre fabrics of current importance in automobile manufacture.

[1](A 'pre-preg' is a fibre fabric or unidirectional fibre sheet which has been pre-impregnated with a thermoset resin and partially cured (β stage). The pre-preg sheets remain flexible and drapeable until curing is complete and are usually thin (i.e. 0.5–1mm) to permit stacking in predetermined orientations).

As with metals and bulk polymer materials a number of manufacturing options are available in the production of continuous fibre composite parts, each with cost and material property implications on the final component. At present the most attractive manufacturing methods available in the production of continuous fibre reinforced plastics are Liquid Composite Moulding (LCM) techniques such as Resin Transfer Moulding (RTM). This is due to the potential for being cost effective over a range of medium to high production volumes and the possibility for a large degree of automation.

Common to most LCM methods is the introduction of the resin matrix material into a closed mould containing the fibre reinforcement via a pressure gradient. This can be applied via a mould vacuum or applied resin pressure. The most common LCM technique used in industry today is RTM. A schematic diagram of the vacuum assisted variation of this is shown in figure 1.1.

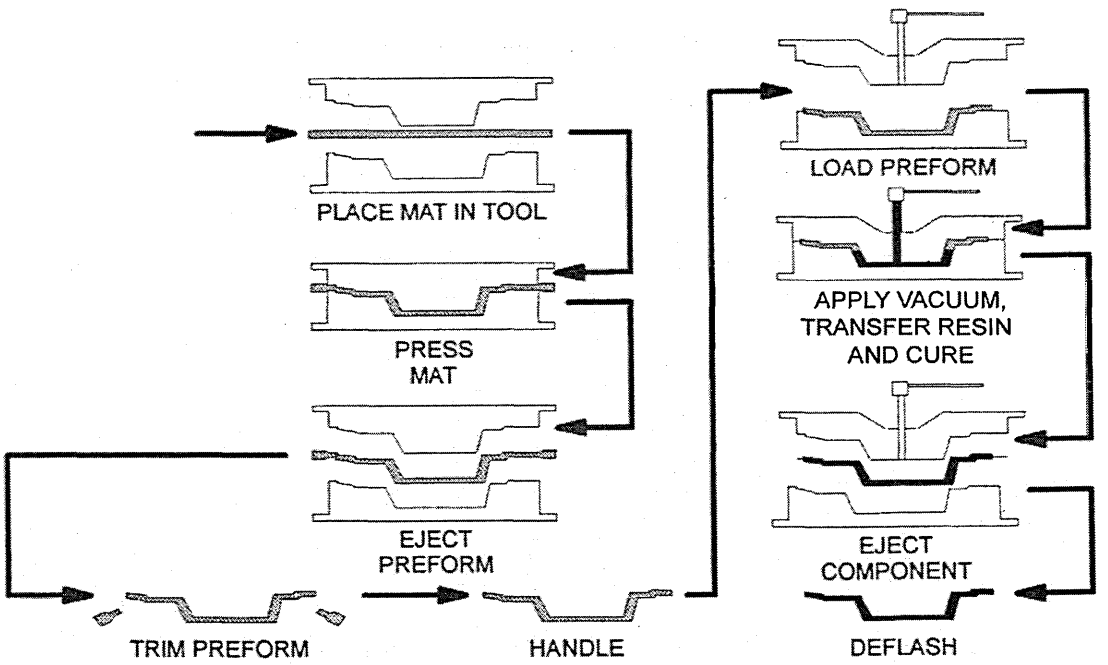

Fig. 1.1. Vacuum Assisted Resin Transfer Moulding (RTM) process schematic, adapted from [1]

Resin transfer moulding involves pre-draping the dry reinforcement fibre layers either by hand or by use of matched moulds to produce a 'pre-form'.

Pre-form draping inevitably alters the fabric architecture due to local variations in fibre orientation, volume fraction and layer thickness. This architecture affects the eventual mechanical properties of the component and also the permeability of the fibre layers during resin transfer which can lead to incomplete wet-out or resin voids within the component if not controlled. More serious is the formation of wrinkles in the fabric which results in fabric wastage and tool or component redesign. The current work is therefore aimed at validating a simulation tool for the pre-form draping process to predict the fibre architecture and occurrence of wrinkling within the fibre fabric of interest.

A summary of the design cycle usually implemented in pre-form design is shown in figure 1.2. As is shown, pre-form fibre architecture is required in any laminate or finite element analysis of the composite mechanical properties [7, 8]. It is also required in finite element flow and pressure modelling of resin transfer [1]. It is therefore of paramount importance to use valid and accurate simulation tools in the initial stages of pre-form design to obtain the fibre architecture.

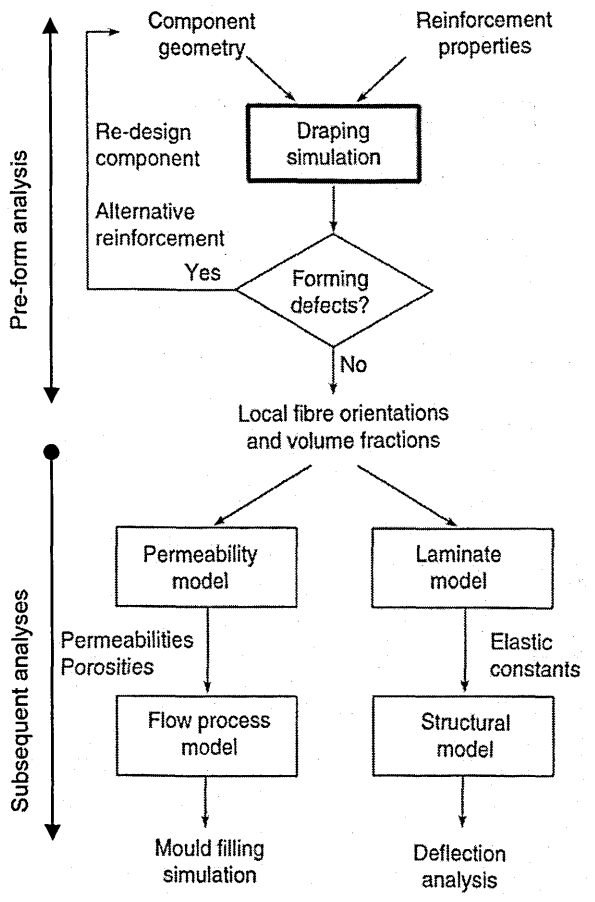

Fig. 1.2. CAE approach to pre-form design, from [1]

To date the most common methods for pre-form simulation are based upon simple geometrical models. Fibre deformation over the mould surface is represented by the closest fitting grid pattern produced after defining an initial starting node and the two initial fibre directions. This is demonstrated in figure 1.3 - the starting node and fibre directions are set at the top of the cone.

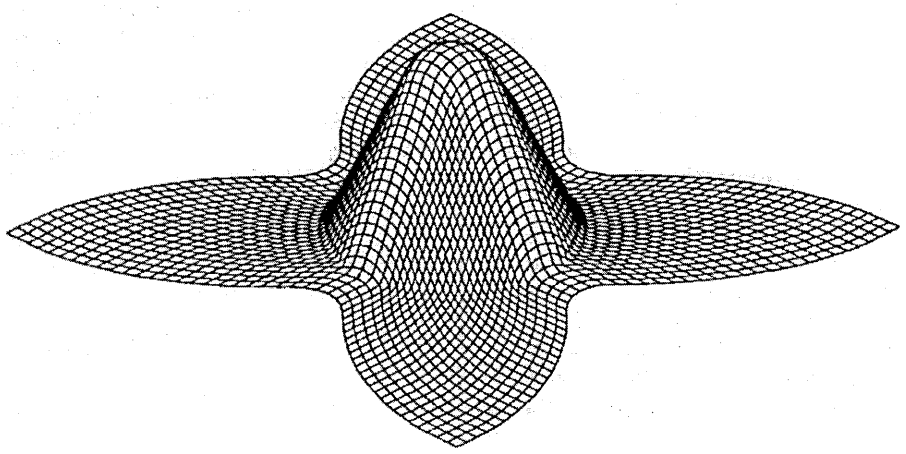

Fig. 1.3. Demonstration of mapping algorithm result on a cone shape, from [2]

Although fast solutions can be obtained, the 'mapping' methods are generally material and processing independent since no physical laws can be included. Recent research into Finite Element Analysis (FEA) has therefore sought to provide a validated tool in simulating the draping process and include sufficient material and processing data to sufficiently represent perform manufacture and improve result precision. The adaptability of FEA also permits the incorporation of any materials and processing advancements which occur through continued materials research.

Industry has become increasingly dependent on FEA as a tool in the design and manufacture of bulk polymers and metals. It has replaced the time consuming and costly process of prototyping and re-design to a degree that industry can no longer afford these methods in any volume greater than is necessary for validation of the FEA simulations. It is therefore essential for similar tools to be validated for composites if these are ever to compete as a suitable replacement for metals for which many metal stamping codes have been validated.

Accurate design and manufacturing simulation benefits industry by:

- Reducing the requirement for expensive prototyping and redesigning.
- Reducing tooling costs by design optimisation.
- Increasing part quality and consistency through manufacturing process optimisation.
- Significantly reducing design and production cycle time.
- Minimising materials waste.

Research into fabric draping simulation by FEA is a fairly recent endeavour and is currently limited, especially in comparison to the simulation of metal stamping which is in many respects a similar process using a less complicated material. This research has generally concentrated on software feasibility studies [4] and investigations of the inter-fibre angle [5, 6] of woven fabrics. Few codes advertise the ability to determine if a mould geometry is physically formable without out of plane deformation. In addition, little attention has been paid to the additional complication faced in simulating engineered fabrics.

Engineered stitch bonded fabrics are of special interest to the aerospace and automotive industries. These fabrics (termed 'Non-Crimp Fabrics' or NCF) are formed of stacked, unidirectional layers held together by through thickness stitching. Mould conformability (fabric drapeability) is good while the mechanical properties of the composite are improved, compared to the woven alternatives, by the use of straight (non-crimped) fibres.

It is therefore the aim of this study to experimentally characterise the deformation mechanisms of a woven fabric and a NCF with the purpose of validating a FEA simulation code for the drapeability and deformation that occurs during perform manufacture. A suitable method of simulating the additional complexity of NCF through thickness stitching is also to be investigated and validated. This validation will compare results obtained from experimental draping of the materials over a double-hemisphere mould to results produced through simulation of the same process.

2 AIMS AND OBJECTIVES

The aims for this project are:

- **Experimentally characterise the shear deformation of a NCF and woven fabric.**
- **Experimentally characterise the effect of stitching in NCF and its effects during deformation and draping.**
- **Calibration of the material inputs of a Finite Element (FE) code through construction of representative simulations of the experimental studies.**
- **Conduct separate draping trials of the twill and NCF fabric over a double-hemisphere mould to compare results with those produced by FE simulation.**
- **Investigate the feasibility, usability and validity of using the FE code to predict fabric drapeability.**

3 LITERATURE SURVEY

3.1 MATERIALS AND MATERIAL CHARACTERISATION

In any simulation study there will be a requirement for accurate and valid experimental data. This can be used either as inputs for constitutive material laws, to ensure precision of the results, for final validation of the model, or for both. The fact that FE draping simulation is a relatively new research area implies that both are necessary. This produces an additional industrial benefit regarding the accumulation of materials data for design consideration with or without use of the latest computer modelling techniques [1].

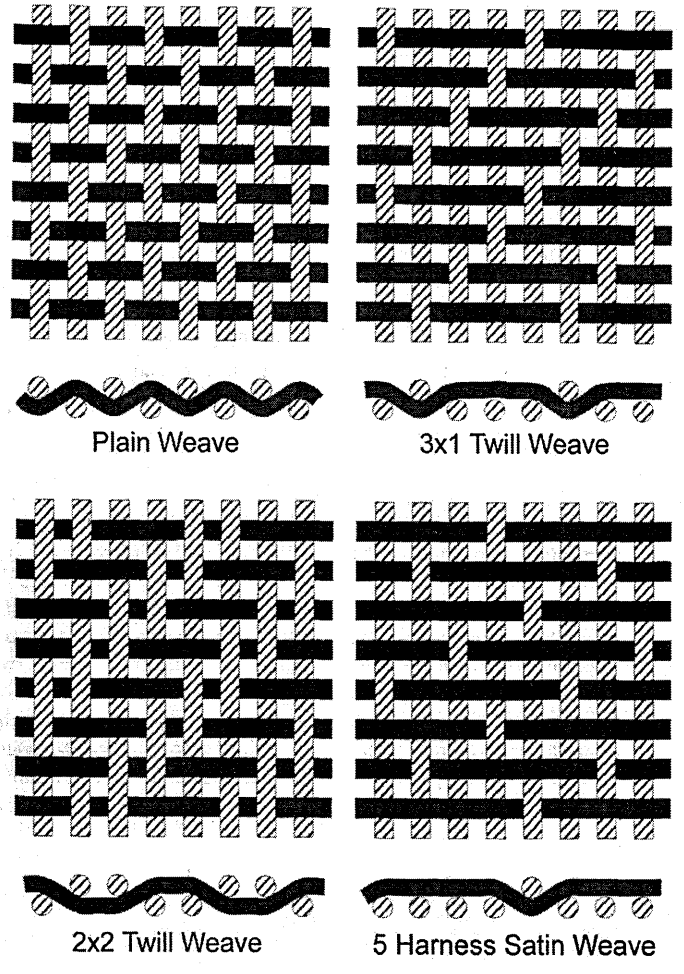

Fig. 3.1. Common weave patterns, from [1]

This study concentrates on a woven and a Non-Crimp Fabric (NCF) which are of interest to Volkswagen AG. The woven fabrics are produced by weaving individual fibre tows (bundles of fibres) in the required pattern and can be processed using conventional textile machinery. A number of different patterns are available for bi-directional (biaxial) fabrics and are summarised in figure 3.1. Fibre directions are termed either warp or weft (filling) as further described in [1].

The properties of each pattern vary – the plain weave producing the lowest in-plane mechanical performance and drapeability due to a high degree of fibre curvature (or crimp) and tight tow architecture [1]. Conversely, this results in the greatest fabric stability and the easiest handling during manufacture. Progressing through the twill to the satin weaves it is found that the in-plane mechanical properties and drapeability are enhanced as fibre crimp and the interlacing is reduced. Furthermore, fibre density is increased and the ability to manufacture composites of high compaction and fibre volume content increases [1]. These improvements are, however, at the expense of fabric stability during manufacture [1].

NCF differs in that crimp is eliminated by using unidirectional fibre layers which are stitched together using a rapid multi-axial warp knitting process [9]. This has been reported to produce up to 15% increased load bearing properties [10], compared to an equivalent woven fabric, and 100% increase in delamination critical energy release rate (G_{IC}), compared to an equivalent pre-preg laminate [11]. This is in part why industrial interest in NCF is so high. The stitching filament is usually polyester and can utilise a number of forms including chain or tricot stitch patterns [9]. This stitching provides the fabric stability necessary but does limit the fabric drapeability.

For this study two biaxial (i.e. constructed of two orthogonal layers) fabrics supplied by Volkswagen AG are to be investigated – a woven 2/2 twill fabric and a NCF using a chain stitch filament parallel to the warp direction and straight filaments looping the chain stitches parallel to weft. Both are constructed of continuous carbon fibres.

3.1.1 DEFORMATION MECHANISMS

Before conducting any material characterisation tests it is necessary to understand the deformation mechanisms that apply to fabric materials, so that suitable testing procedures can be implemented and the relevant data obtained.

In deforming a biaxial fabric sheet five possible mechanisms have been identified [1, 12]. These are shown schematically in figure 3.2 below.

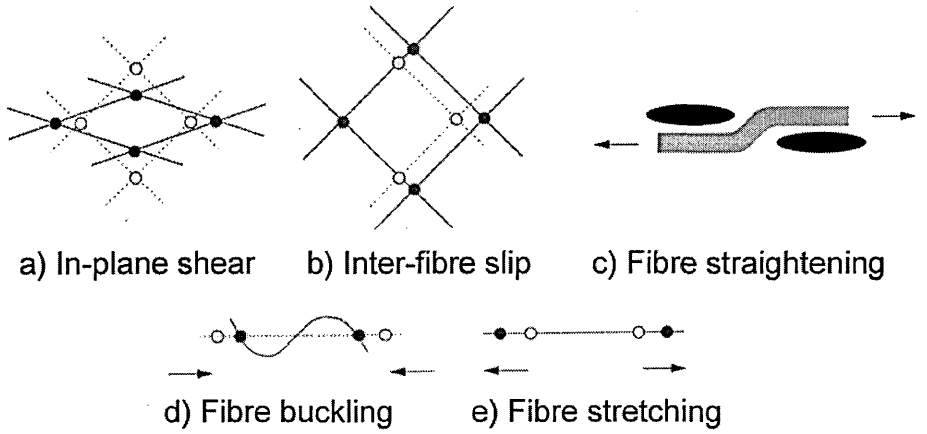

Fig. 3.2. Modes of deformation during perform manufacture, from [1, 12]

- a) In-plane shear involves fibres rotating around either the stitch or weave crossovers depending on fabric type [13]. Rotation is limited mainly by the ability of the fibre tows to become compacted and, for NCF, any stitching boundary condition which can inhibit or promote deformation [1].

- b) Inter-fibre slip occurs as fibres move relative to each other effectively resulting in crossover point sliding. This is one of the main alternatives to in-plane shear and generally occurs as the inter-fibre locking angle of the fabric is approached [1].

- c) Fibre straightening is generally limited to woven fabrics as NCF utilises layers of unidirectional fibres of negligible crimp. This mode of deformation occurs due to tension within the fibre tows resulting in layer thinning.

- d) Fibre buckling results due to local in-plane compression leading to fabric wrinkling or folding. Wrinkling can lead to a reduction of mechanical properties as well as hinder resin impregnation during resin transfer. Fitting the pre-form to the injection tool can also become problematic [1].

- e) Fibre extension is generally negligible due to high fibre moduli [1, 12].

For woven biaxial fabrics in-plane shearing is the dominant mode of deformation during draping as high strains can be achieved with low applied forces [3]. Shear of up to 60° is typically possible before the fibres 'lock' at which point alternative deformation mechanisms are required. These are usually inter-fibre slip and eventually buckling [13]. Work by Long [3] has shown this locking angle is related to the ratio between tow width and pitch, whereby a high ratio indicates a low locking angle. A material of high ratio was also shown to require a lower shear force to obtain a given shear angle. In determining the dominance of in-plane shear, Potter [16] investigated the relationship between glass fibre fabric deformation and inter-fibre slip through theoretical and experimental comparison of the fabric geometry during bias extension tests (described later). Results indicated slippage was only noticeable at high relative deformation as the fibre locking angle is approached. Further work by Wang et al. [17] also noted slip occurred in areas of high shear angle variation when testing woven carbon fibre fabrics of higher bending stiffness and fewer tow crossover points.

Fibre straightening is dependant on the fibre architecture and degree of tow crimp and is generally negligible for fabric draping.

Engineered non-crimp fabrics differ in that the stitching places additional boundary conditions on the ability of a fabric to shear. Long [18] reported that although in-plane shear is still the dominant deformation mechanism a considerable degree of inter-fibre slip was noted during the draping of some engineered fabrics into deep drawn geometries.

Further work by Long [3] has investigated the variation in shear behaviour of biaxial glass fibre NCF using pillar (similar to chain stitch) and tricot (zigzag) through thickness stitching at 45° to the 0°/90° fibre tows. Results indicate a higher shear force is required to deform the fabrics when sheared parallel to the stitching thread, to the point that the stitch filaments subsequently broke. This causes a reduction in shear force prior to tow locking. With such fabrics, deformation is non-uniform and preferential shearing will occur in orientations perpendicular to the stitch.

Similar investigations have not been conducted on NCF with stitching parallel to the fibre tows, as used in this project, although symmetry in the picture frame and bias extension shear characterisation tests would yield no theoretical variation in the obtained force against displacement data.

3.1.2 CHARACTERISATION TESTS

As previously iterated the main mode of fabric deformation is in-plane shear. Consequently most macro-scale testing of composite fabrics have concentrated on characterising the force required to produce a given shear deformation or tow shear angle. Three main methods have been utilised to characterise shear behaviour and are shown schematically in figure 3.3.

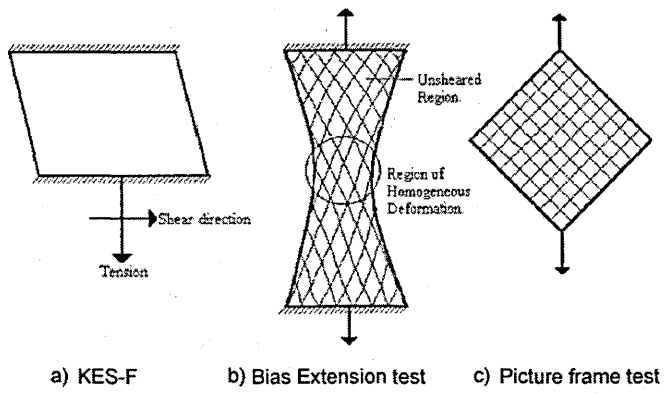

Fig. 3.3. Schematics of the three main shear test methods, from [19]

a) KES-F (Kawabata Evaluation System for Fabrics): this test involves clamping the two opposite edges of a fabric sheet with tows aligned parallel and perpendicular to the fabric edges. Specimens are usually 200x50mm and have a tensioning weight, usually 10N/m, linked to the lower edge. One edge is then moved at a constant speed to induce shearing of the fabric [19]. A FE investigation of the fibre stresses induced in the fabric by Hu and Zhang [20] concluded the shear and tensile forces produced are not uniform. Consequently the method is rarely used in current research.

b) Bias Extension: this popular test is similar to a standard tensile coupon test and involves clamping the base and top edges of a ±45° orientated fabric sheet. One clamped edge is subsequently displaced at a constant rate to determine the force per unit width as a function of axial strain (methods of data analysis are summarised in [1]). The advantage of this method is speed and simplicity in set-up and operation. The unclamped edges also permit inter-fibre slip and tow crossover rotation without placing any additional boundary conditions through requiring individual tow fibres to shear. This would artificially increase the measured force. The method is problematic in that shear distribution is not uniform. Consequently pure shear information is difficult to extract although it is a useful technique for comparing fabrics and possibly calibrate with FE models.

The clamped upper and lower edges generally cause four different shear zones to occur as shown in figure 3.4 for a plain weave fabric [21]. This emphasises the requirement for the fabric length to be at least twice the width to ensure fibre bridging and superposition of the separate zone II regions (figure 3.4) does not occur. This would lead to a substantial increase in measured shear force [1]. A higher length/width ratio also minimises the force effect of zone II and III deformations.

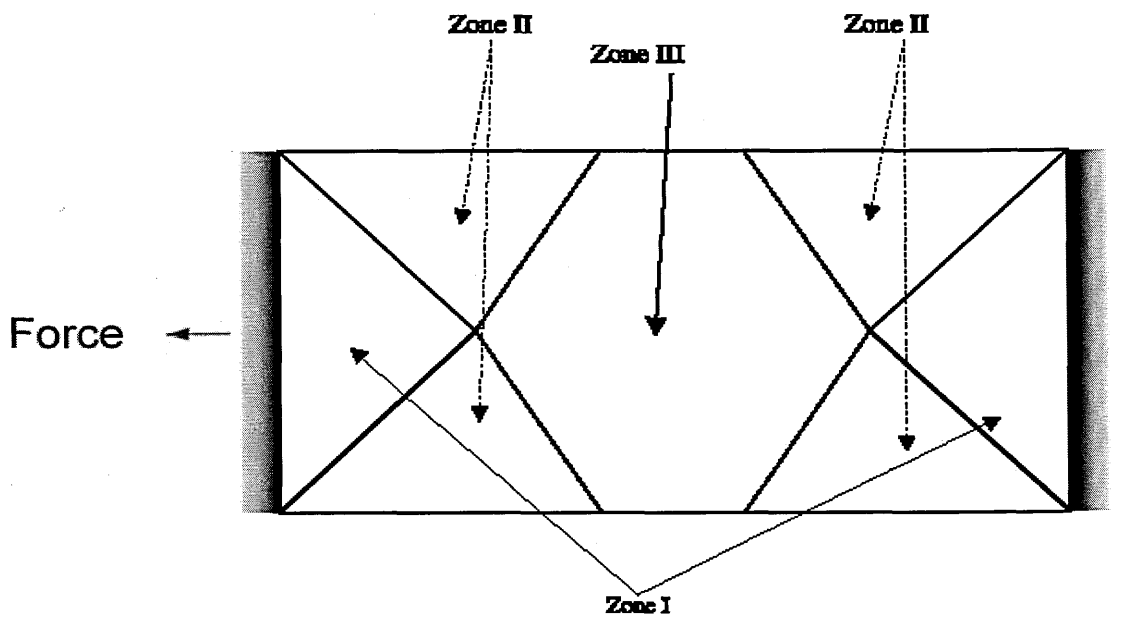

Fig. 3.4. Bias extension sample schematic showing zones of deformation, from [21]

- Zone I describes the area of negligible deformation as the constituent fibres are clamped at one end. Minor inter-fibre slip occurs at the fabric corners due to boundary conditions of the clamped tows [21].
- Zone II consists of four regions of both in-plane shear and inter-fibre slip. Slippage is highest at the free edges and some fibre reorientation occurs due to the transition between zones I and III [21].
- Zone III is the area of highest in-plane shear although this reduces towards the free edges [21]. The deformation in this area is the highest of the zones and is the region in which out of plane deformation initiates when the fibre locking angle is reached.

Results from a bias extension test are drawn schematically in figure 3.5.

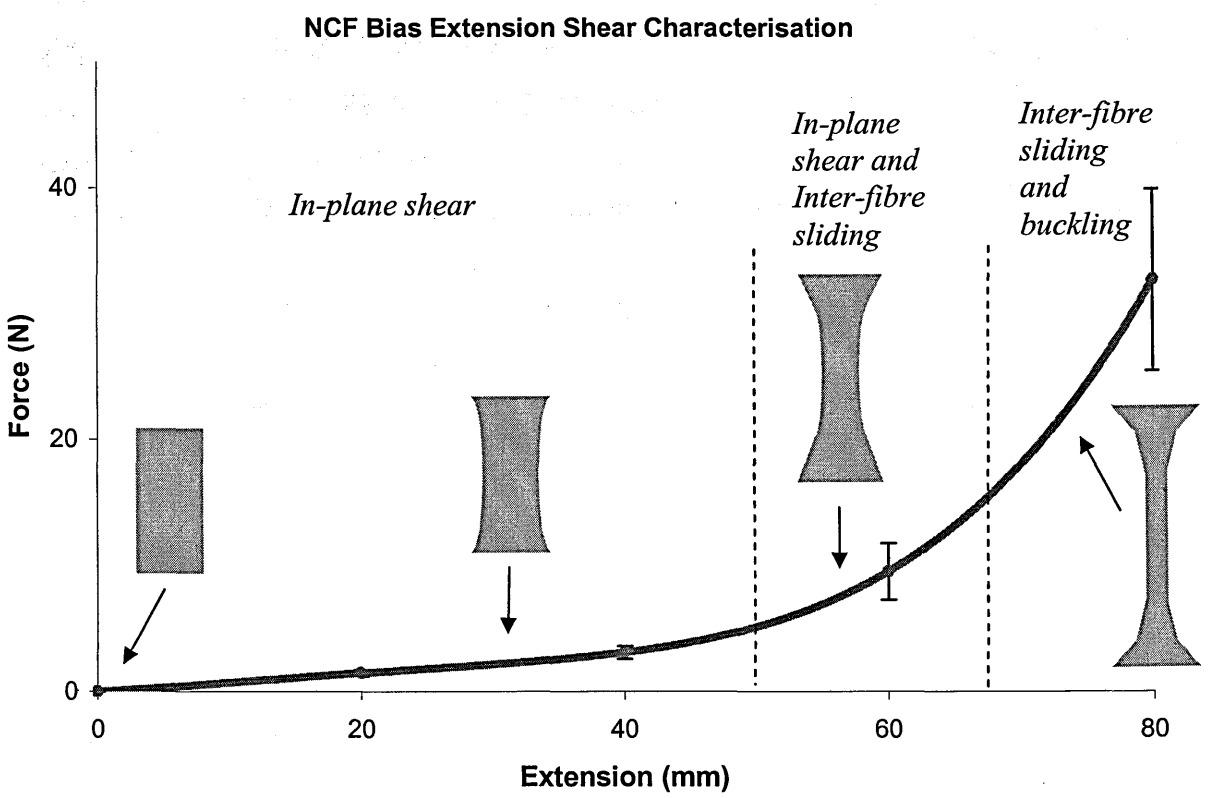

Fig. 3.5. Schematic of deformation mechanisms in bias extension tests, [21]

Picture Frame: (figure 3.6) this testing rig is preferred by many researchers as it produces uniform shear throughout the fabric [1] and permits the locking angle of the fabric to be ascertained. It uses a rhomboid frame, hinged at each corner and usually with flat plate clamps to hold the fabric on each edge [1, 22]. Some researchers prefer to let the free tow ends rotate freely [19] and prevent any boundary conditions from generating excess forces due to individual tow shear although this is difficult to implement.

The frame can be used in a standard tensile test machine whereby two diagonally opposite corners are extended. The position of the clamping edge is of paramount importance in this rig as if not in-line with the bearing centres fibre extension will occur and result in excessively high measured forces due to the high fibre modulus.

The method is also very sensitive to variations in material alignment as this also imposes fibre extension, meaning scatter in the data obtained can be high [25]. The frame dimensions are not standardised although larger frames minimise the effect of edge boundary conditions on the results. The main disadvantage of using a picture frame test to characterise fabric shear is only in-plane shear can be measured [1], which is regarded as a dominant mode of deformation for many fabrics during draping, but not the only mode.

As already discussed, inter-fibre slip can be considerable depending on the fibre architecture, moulding geometry and the state of shear imposed on the fabric. This constraint validates the use of this method when obtaining material data for use in 'mapping' pre-form simulation tools (discussed in 3.1.4) which intrinsically impose this condition [14]. Current and future draping research using FEA may require a combination of testing methods as ideally these codes should not be constrained to only simulating in-plane shear permitting more complex and accurate simulation solutions to be obtained.

Work by Harrison et al. [23] compared the boundary conditions of shearing a woven fabric with and without clamping the tows along the edges. Through micro-mechanical observations it was noted the 'waviness' (micro-buckling) of the fibre tows occurred when shearing individual clamped tows. This results in tow deformation occurring between the extremes of complete tow shear and free end rotation. Research into predicting the shear forces of woven fabrics induced in the picture frame test has been conducted by Long [3]. The model developed is based upon a Coulomb friction mechanical law. Results are good and have been applied to plain, twill and satin weave fabrics.

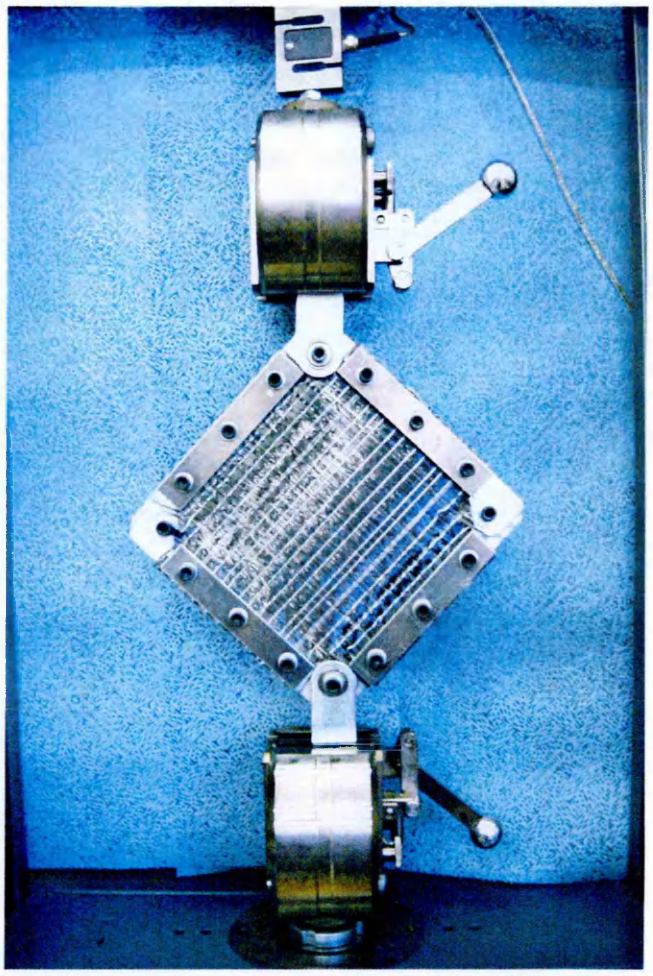

Fig. 3.6. Picture frame testing of NCF

Typical results from the picture frame test are demonstrated in figure 3.7.

Special consideration has to be taken in using this technique with pre-preg or reinforced thermoplastic materials as constant cross-head displacement of the tensile test equipment results in an increasing shear rate [22]. This can be over come through the use of a programmed rate of displacement using equations developed by Clifford and Long [22]. For dry fabrics, as used in this study, research has shown shear to be rate independent [3, 13] meaning constant cross-head displacement can be used in the current study.

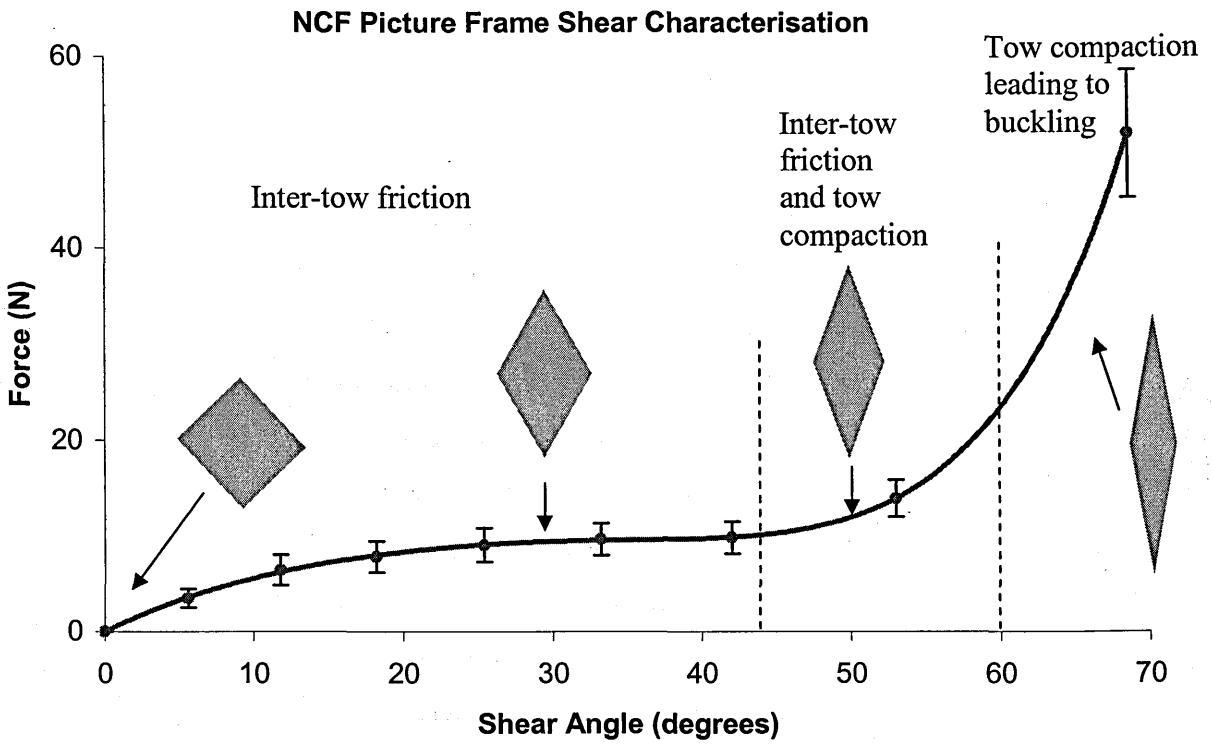

Fig. 3.7. Schematic of the dominant picture frame deformation mechanisms, [23]

As well as shear characterisation other material properties such as bending stiffness, friction behaviour and NCF stitching constraints will require characterisation to implement a valid material model. As mapping methods of simulation (described in 3.3.1) include no boundary conditions the investigation of these parameters, in the interest of pre-form manufacture, has generally been limited to research using finite element methods.

Friction testing between the fabric and mould has been conducted in work by Dong [39]. This is an important factor as additional fibre tension induced through mould contact can reduce the occurrence of wrinkles. This involved adapting ASTM [43, 44] standards and measured the static friction coefficients between two fabrics, in addition to fabric to aluminium or Perspex interfaces. Results were taken in 0°-90° and ± 45° fibre orientations.

However, the application of just the 'static' friction is questionable as this will generally only apply in areas that have yet to initiate deformation. After this occurs the forming velocity will dominantly cause consistent movement of the fabric until the draping operation is complete. These situations would require the application of the 'dynamic' or kinetic friction coefficient.

No research was found by the author pertaining to the characterisation of fabric bending stiffness, although an ASTM Standard [45] exists for the textile industry and is used in this research.

The effect of NCF stitching on shear behaviour has been researched by Long [3] using the picture frame testing equipment as described in 3.1.1 and as such can be incorporated into a FE model. However, for a more precise simulation of NCF fabrics greater test refinement of the stitching itself should be required, a topic which has had little investigation to date and for which, to the authors knowledge, no testing methods have become commonplace. For this study a test method has been utilised to characterise the force taken to 'pull-out' fibre tows from the fabric and is described in chapter 4.

3.2 DRAPING TRIALS

Current research into experimental draping has so far been unable to produce a standard test method for comparing the drapeability of different fabrics – the choice of mould geometry and methods of comparison being chosen by the individual researchers.

Commonly a simple hemisphere or cone (figure 1.3) is used as the double curvature surface can lead to a high deformation requirement. To drape, either the male mould is moved at a certain velocity into a fabric sheet held under tension by a surrounding frame [3, 24, 25] or alternatively a full male/female mould set with or without blank holders can be utilised [26].

Alternative industrial shapes have been used in research, such as a wheel hub [1] or transmission tunnel [3], to invoke higher deformation of the fabric. This condition has been attempted using a more general double hemisphere mould as proposed by Lamers [5]. The reason of using such a shape is in part to reduce the symmetry in comparison to a single hemisphere and require rapid variations of required fibre angle to accommodate the geometry. This permits investigation of the initial fibre orientations on the ability of a fabric to be draped. For this reason this double hemisphere geometry has been chosen for this project.

Draping results can also come in many forms. Early trials by Long [27] compared fibre volume fraction distributions although this gave only average distributions and no information about fibre orientations. Further research by Long [1, 18] has utilised an automatic camera and software system to obtain and record pre-marked inter-fibre angles to compare to the mapping simulations proposed. Alternatives to inter-fibre angle have been used, such as comparing the 'footprint' shape of the draped material [4, 26] or the position and style of wrinkling that is induced during draping [28].

The definition of what is an optimised drape will depend on the application of the component. Usually optimisation is defined through the production of a wrinkle free pre-form drape, confirmation of fibre orientation within limits in key structural areas or production of the lowest overall shear deformation [17]. The definition must also be considered with the optimal mechanical properties as these may not be the same [29].

Using a micromechanical approach to investigate draping Harrison et al. [23] noted that if friction between tow crossovers is high, i.e. a high normal pressure was applied to the sheet, the individual fibre tows would shear as if clamped. When this condition is not applied free rotation of the tow ends could occur resulting in micro-buckling of the tows to accommodate the required geometry.

Inspection of a woven fabric draped over a hemisphere confirmed the presence of these micro-buckles. As already stated in 3.1.1, care has to be taken with NCF fabrics as through thickness stitching can prevent deformation in certain orientations, especially when the stitching is at 45° to the fibre orientations, resulting in opposite quadrants of restricted shear [3].

3.3 DRAPING SIMULATION METHODS

3.3.1 MAPPING SIMULATION METHODS

Numerical simulation of woven fabric draping has been conducted by many researchers and has mostly utilised mapping simulation methods [3, 17, 23, 25, 30, 32]. These techniques are usually based upon on a kinematic algorithm [1], using the 'pin-jointed net' (PJN) or 'fishnet' idealisation as originally proposed by Mack and Taylor [31]. An example of a mapping simulation has already been shown in figure 1.3. The PJN idealisation requires the following assumptions to be made about the fabric:

- The fibres are inextensible.
- Fibre crossovers act as pin-joints with no relative slip.
- Fibre segments are straight between joints.
- Uniform surface contact is achieved.
- Fabric layers are infinitely thin.

In order to produce a solution an initial starting point or 'node' must be assumed on the geometry surface, along with two initial fibre directions. From this the equations of intersection between the geometry and the two connecting segment ends must then be solved. This is shown in figure 3.8.

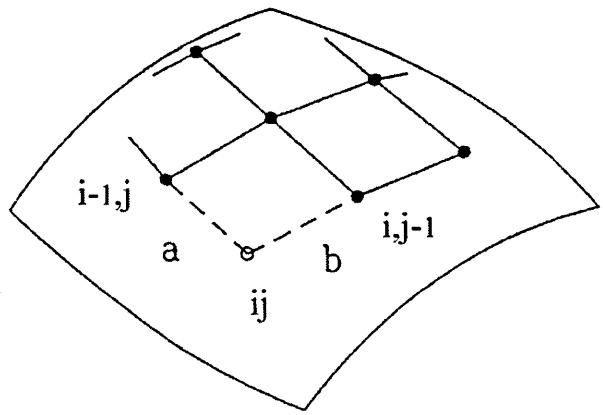

Fig. 3.8. Illustration of the pin-jointed net (PJN) model, from [17]

Crossover point *(ij)* is generated from the defined points of *(i-1,j)* and *(j-1,i)* by solving the system of non-linear simultaneous equations shown below, whereby *a* and *b* are the segment lengths in the warp and weft directions of the fabric. The solution can be found numerically, or explicitly, depending on the surface described in $F(x_{ij}, y_{ij}, z_{ij})$ [1].

$$(x_{ij} - x_{i-1,j})^2 + (y_{ij} - y_{i-1,j})^2 + (z_{ij} - z_{i-1,j})^2 = a^2$$

$$(x_{ij} - x_{i,j-1})^2 + (y_{ij} - y_{i,j-1})^2 + (z_{ij} - z_{i,j-1})^2 = b^2$$

$$F(x_{ij}, y_{ij}, z_{ij})$$

Most geometries required to be draped are unlikely to have surfaces defined by one equation therefore methods of representing a surface have been developed and commonly use a series of adjoining patches. Either curved [33] or straight [34] patches can be utilised, using a bi-directional polynomial or linear system respectively. The linear system is often preferred as the computer program is simplified and solution times reduced [17]. Result accuracy can be increased by simply utilising smaller patches.

From the initial work of Mack and Taylor [31] a number of variations to the method have been developed in the attempt to correctly take shear behaviour into account. Frequently a mould geometry is such that a unique fabric covering is defined when the initial pair of intersecting fibre directions have been specified. In defining the initial fibre directions it is possible to utilise the intersection of the geometry surface with that of two specified planes in what is termed the *planar method* [33].

When an arbitrary geometry is to be used, geodesic lines can be specified as an alternative to the plane intersections in what is called the *geodesic line method* [34].

Assuming the shear deformation is proportional to the required shear energy permits construction of a solution in which shear energy is minimised. From the initial contact point and fibre directions the algorithm calculates row by row the fibre orientation that requires the minimum amount of assumed shear energy. This is termed the *energy method* [17]. No experimental data is included in this method and should not be compared to the iterative shear minimisation method proposed by Long [3] and described later.

With mapping techniques a major limitation is that all methods can produce various solutions depending on the initial contact point and fibre orientations [29]. Usually the planes of symmetry are used to define the initial fibre orientations, although for press forming the highest point is more suitable [35].

Mapping methods are valued for their simple software requirements and fast solutions. The lack of material data requirements means solutions can be obtained without complicated material testing programs and have been developed to allow CAE mould geometry data to be imported for the simulation [40].

This simplicity comes at the expense of simulation accuracy. Boundary conditions such as tool loads and constraints are discounted from the simulation [6] and the methods described are intrinsically material independent. As such they can not include the complexity of deformation regimes as described in 3.1.1.

The only deformation that can be simulated with mapping methods is in-plane shear, the dominance of which varies upon fabric architecture, imposed geometry and state of fabric shear.

Long [18] investigated fabric draping over a block mould and found that as mould height is increased the degree of fibre slip also increased. This is due to greater variation in the state of shear which progressively invalidates the simulation results.

In addition, fabric specific phenomena such as fibre locking and out of plane buckling can not be predicted [18]. Mapping algorithms will generally continue to reduce the inter-fibre angle as necessary to represent the surface required. A consequence of this is the inability to optimise the draping process for a specific material. This problem was investigated by Wang [17] through experimental draping trials. The results indicated the initial mould contact point is important to drapeability as wrinkles can be eliminated; a feature mapping simulation would not be able to predict.

Generally the mapping methods described have been accepted for balanced fabrics and symmetric mould shapes [12] which do not involve large shear variations. This unfortunately excludes many NCF materials and complex mould shapes for which valid simulation in the design stage would be most useful to predict if wrinkling would occur.

A more recent advancement has been proposed by Long [3] with the aim of incorporating some actual material data. The proposed model uses an iterative scheme to minimise the shear energy obtained empirically from picture frame tests. In this method the total shear energy is obtained by the summation of the individual shear energies required to obtain the calculated deformation at each crossover node. An iterative Hooke and Jeeves [36] minimisation method can then be employed to vary the generator path angles, one at a time, from the initial user defined node and produce a solution of minimum shear energy. Simulation results of draping a warp-knit NCF on to a hemispherical mould show good correlation of inter-fibre angle with preferential shear in orientations perpendicular to the stitching thread being clearly illustrated [3].

The iterative method proposed by Long [3], although a vast improvement, is still based upon the PJN idealisation assumptions. As such it is still limited to simulating in-plane shear and can not include processing boundary conditions or simulate the occurrence of wrinkles. For these reasons more complex FEA simulation methods are being researched.

3.3.2 FINITE ELEMENT DRAPING SIMULAION METHODS

Finite element analysis (FEA) was first conceived in the 1950s and has since developed into a highly sophisticated simulation tool in almost all areas of engineering. With great potential for adaptation FEA has caused many numerical analysis techniques and experimental methods to become redundant and has resulted in large cost savings to industry.

The development of FEA techniques applied to metal stamping operations occurred in the 1980s. Initial research and validation of the method has permitted rapid advancements in solution precision and applicability to the point it is now an essential tool for the metal forming industry [37]. Effectively the draping of a pre-form is an extension of metal sheet forming; the main differences between the two being the anisotropic and layered properties required for pre-forms. It is therefore possible for draping codes to be extensions of the metal forming process, although in comparison these composite codes are still in the initial development and validation stages.

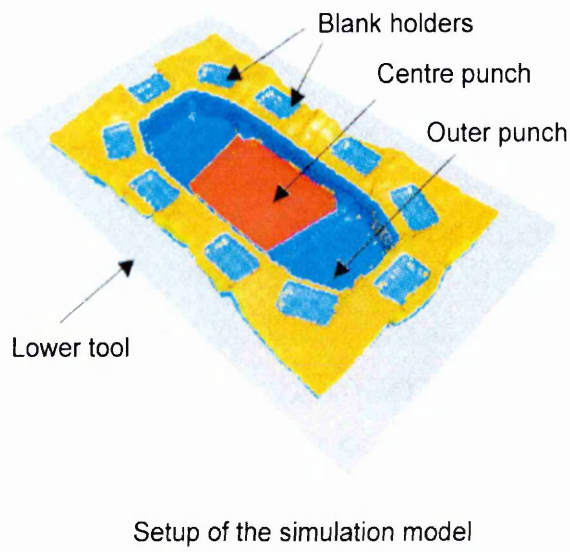

Fig. 3.9 Fabric press forming simulation, from [15]

Unlike mapping methods, FEA techniques include 3D representations of the mould and fabric (figure 3.9). The method can easily include a greater quantity of material data and can account for boundary conditions imposed by the forming tools. This last point is important for LCM processing as tooling loads can influence draping [17]. The use of blank holders to restrict fabric movement and induce fibre tension is also common to prevent wrinkling and can be included in FE simulation.

Most FEA draping simulation to date has been limited to feasibility studies of various software codes currently available. Ideally these codes should simulate in-plane shear, inter-fibre friction and sliding and fibre locking to fully characterise the fabric. Unfortunately, not all codes posses these capabilities as full characterisation of inter-fibre sliding theoretically requires a highly refined tow model. The requirement by industry for fast, more general solutions has commonly limited the ability to model deformation at this micro-scale to academic research. Simplification is therefore necessary for industrial use whereby key material factors can be included as part of a greater material law or implemented explicitly in a simplified material model.

Daniel [6] and Boisse [38] used an explicit dynamic approach to investigate the forming of a woven biaxial fabric using a hemispherical punch. Using biaxial tensile test data obtained in the study, the simulations permitted comparison of the fibre tension and shear angles to the experimental limit values of the fabric. The simulations showed good shape correlation to the experimental results but included no direct consideration of inter-fibre sliding or fibre locking in the actual model. The validity of this simulation tool could therefore be in question for more complex geometries. 2D triangular and quadrilateral membrane elements were used to simulate the fabric sheet. The use of these elements simplifies the fabric model since membrane elements have zero flexural stiffness and constant through thickness stress distribution [41]. This could therefore reduce precision when simulating complex geometries for which fabric bending stiffness could prove significant to the results.

De Luca et al [37] also used an explicit approach with the commercial software, PAMFORM™ [47], to investigate the draping of two woven fibre reinforced thermoplastics. PAMFORM™ [47] is a development of the commercial metal stamping simulation software PAMSTAMP™. Shell elements were used to represent the fabric sheets. Unlike membrane elements, shell elements include flexural stiffness and non-uniform through thickness stress distributions, usually using three integration points to integrate bending and membrane effects [41].

Parametric studies of the simulation forming velocity, fabric stacking sequence and blank holder system were conducted with the aim of investigating their effect on the internal composite layer stresses and the occurrence of wrinkles in the final part. Fibre locking could be simulated. The results proved very satisfactory in predicting the wrinkling and fibre reorientation noted during draping trials. The use of a lower forming velocity during simulation was also noted to reduce wrinkling, shear stress variation and thickness variation of the final part as also noted during experimentation. However, the applicability of these results to the current study is limited, even though the same software is being used. The materials investigated were pre-impregnated with a binding resin and therefore subject to visco-elastic deformation constraints not present in dry fabrics.

Work by Dong [39] involved conducting a sensitivity analysis of the explicit dynamic FE code ABAQUS/EXPLICIT v5.6 in forming woven fabrics using a hemispherical punch. Solution precision was investigated through varying material parameters such as punch speed, interface friction, blank holder pressure, fibre elastic and shear moduli in addition to inherent FEA variables including mesh size and time-step. Of interest from the conclusions is the mesh size should be sufficiently small to define wrinkles but not the fabric microstructure as this involved extensive computation time. Optimised friction between the fabric and mould surfaces resulted in improved stability as spatial oscillations of shear angle were noted when ratios of $\mu_{mould} : \mu_{fabric}$ were used.

The shear and elastic fibre modulus variation results obtained by Dong [39] depend on the coupling included in the FE material law so are not so useful for alternative software programs such as that used in this study i.e. PAMFORM™ [47].

Recent work by Sidhu [21] has investigated the production of a unit-cell based element model to ensure both inter-fibre sliding and fibre locking is simulated. Based upon a plain weave pattern the model uses two sets of elements to represent the fabric sheet. In-plane, two node truss elements are used to model the individual fibre tows while four node shell elements are used to account for friction and contact (figure 3.10).

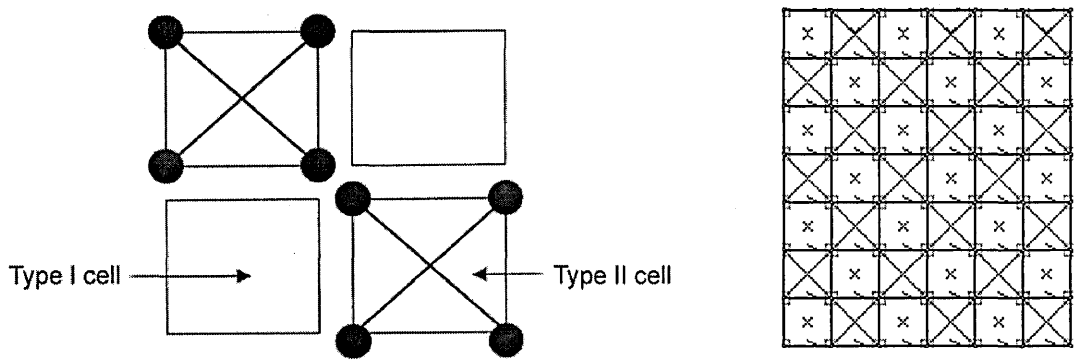

Fig. 3.10. The unit cell of the 'checkerboard' model and part of the assembled pre-form mesh, from [21]

This is implemented in LSDYNA. Bias extension experiments are conducted for comparison to the FE simulation model. The results of force against elongation are relatively good considering the level of deformation and variation in dominant mechanism. The inter-fibre angle at the centre of the specimen (zone 3 in figure 3.4) also shows good correlation with the experimental results. Subsequent draping comparison utilises a shallow pyramid punch. Simulation results are again good, although the comparison is aided by the pyramid symmetry and comparatively low level of shear variation which induces only minor inter-fibre sliding. Inter fibre sliding is controlled through shell element deformation since no two tows share a common node.

To date, Pickett [15] has published the only work found by the author to address the FEA simulation of through thickness stitching in NCF. In this review of composite FEA applications the use of 'spot-weld' elements is proposed to tie shell element sheets together.

The shell elements represent the unidirectional fibre layers that constitute the fabric and can theoretically be used to simulate any number of stacked layers. The aim of this is to simulate the additional deformation mechanism of tow 'pull-out' and stretching of the through thickness stitching. The study involved the use of the PAMFORM™ [47] simulation code. PAMFORM™ [47] is also the software to be used in this current study.

3.3.3 EXPLICIT AND IMPLICIT FINITE ELEMENT ANALYSIS

Two types of FEA have proved popular since the conception of the simulation method; namely the implicit and explicit methods. Implicit codes have proved popular for equilibrium problems such as stress analysis and thermal analysis. In explicit analysis time appears in the governing equations permitting analysis of transient problems including transient thermal analysis, impact problems and most notably crashworthiness of automotive structures. PAMFORM™ [47] is an explicit finite element software package. As such this is inherently suitable for the problem of fabric draping simulation due to the dynamic process and ability to easily treat contact and buckling, as will be discussed.

The basis of explicit FEA can be explained through consideration of a mass-spring system consisting of a mass *m*, a spring with constant *k*, and an external load as a function of time *f(t)*. This system has one degree of freedom, whereby, *x*, is the displacement, $\dot{x}$ is the velocity and, $\ddot{x}$ is the acceleration of the mass.

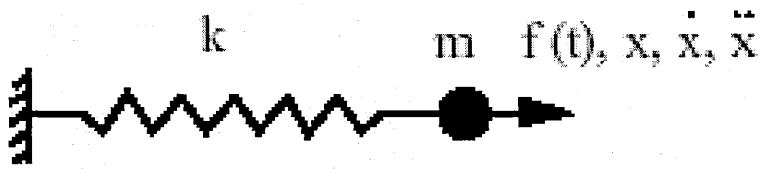

Fig. 3.11. A simple mass-spring system, from [41]

A representation of the time axes is shown in figure 3.12.

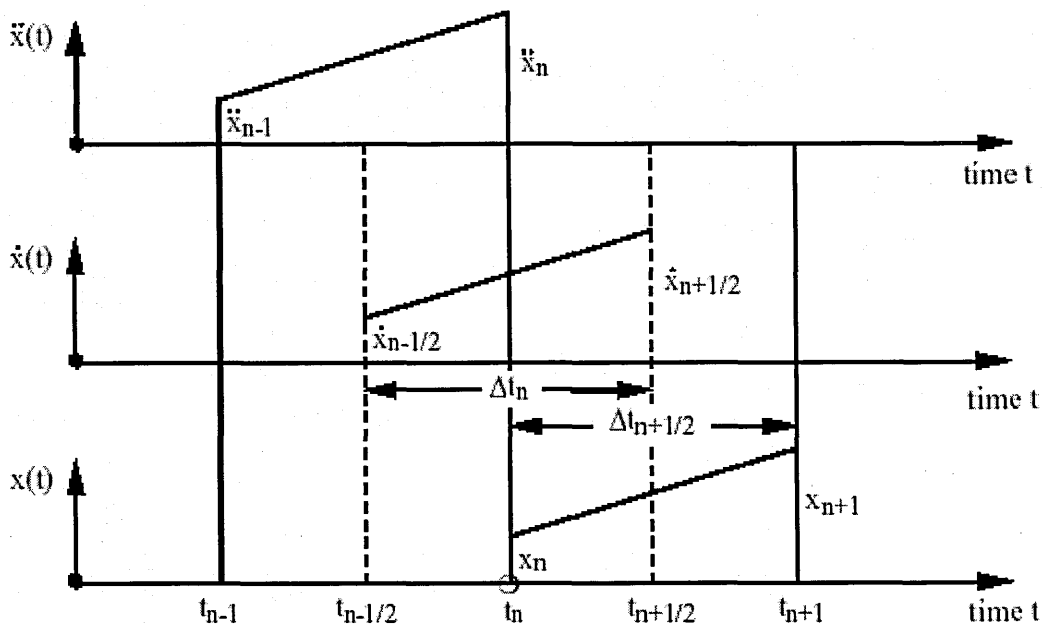

Fig. 3.12. Representation of time axes around a discrete point in time, t_n, from [41]

The known quantities are the displacement at time t_n, x_n, and the velocity at time $t_{n-1/2}$, $\dot{x}_{n-1/2}$. The required parameters are the displacement at time t_{n+1}, which is x_{n+1}, and the velocity at time $t_{n+1/2}$, which is $\dot{x}_{n+1/2}$.

Dynamic equilibrium at time t_n is expressed as:

$$m\,\ddot{x}_n = f_n - k\,x_n.$$

i.e. Resultant Force = Force $_{\text{external}}$ - Force $_{\text{internal}}$

Calculation of the mass acceleration, $\ddot{x}$, is possible as all other quantities are known. It is then possible to apply the central time integration and solve for the unknown quantities, $\ddot{x}_{n+1/2}$ and x_{n+1}, by solving, in order, the following equations:

$$\ddot{x}_n = m^{-1}\,(f_n - kx_n)$$

$$\dot{x}_{n+1/2} = \dot{x}_{n-1/2} + \Delta t_n\,\ddot{x}_n$$

$$x_{n+1} = x_n + \Delta t_{n+1/2}\,\dot{x}_{n+1/2}$$

The method results in a high number of computationally cheap iterations to produce the required solution. The criteria for solution stability depends on the *time-step,* Δt, and is satisfied when;

$$\Delta t \leq \sqrt{m/k}$$

Alternatively, substitution is possible of the equations for, *m*, and, *k*, where L = length; E = elastic modulus; ρ = density; A = bar cross section.

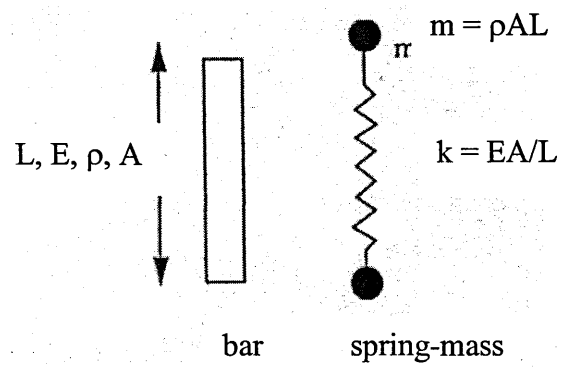

Fig. 3.13. Spring-mass parameters, from [41]

This leads to the result:

$$\Delta t \leq \frac{L}{\sqrt{E/\rho}}$$

Where, $\sqrt{E/\rho}$, is the speed of sound in the material;

$$c = \sqrt{E/\rho}$$

Implicit FEA differs in that time does not occur explicitly. Implicit FEA relies upon the assembly of each individual element equations to obtain the system equation. These take the form of;

$$[k]\{U\} = \{F\}$$

In the previous equation, [k], is a square matrix representing the stiffness of the system, {U}, is the vector of unknown nodal displacements and, {F}, is the vector of applied nodal forces [42]. To define the nodal displacements produced by the applied force it is necessary to invert the system stiffness matrix [k] and solve the sets of equations produced – it is not unreasonable to have over 50,000 equations [42]. The time-step in this process is usually 100 to 1000 times that of explicit. [41] which therefore leads to few, but computationally expensive steps to produce the solution. The solution of non-linear sets of equations also requires iterations and convergence criteria in implicit methods, which is not the case in explicit. By using smaller time increments explicit codes are justified in making small displacement approximations which negates the need for convergence studies.

Explicit codes, however, are not suitable to solve static problems. Since draping is not a static problem, explicit codes are far more suitable in this application. Explicit codes also deal with contact more effectively. Contact in implicit codes requires calculation and subsequent inversion of a new stiffness matrix, [k], for each iteration the contact changes. This is computationally expensive and leads to long simulation times. In explicit methods the use of an additional external penalty force in the equation for dynamic equilibrium is easily implemented and has negligible computational effect.

3.3.4 FINITE ELEMENT MATERIAL MODEL

PAMFORM™ [47] contains a library of many different composite material models. Of interest to the current study is material 140 used to define a bi-phase shell element material with thermo-visco-elastic matrix and elastic fibres. The basis of this model is summarised in figure 3.14.

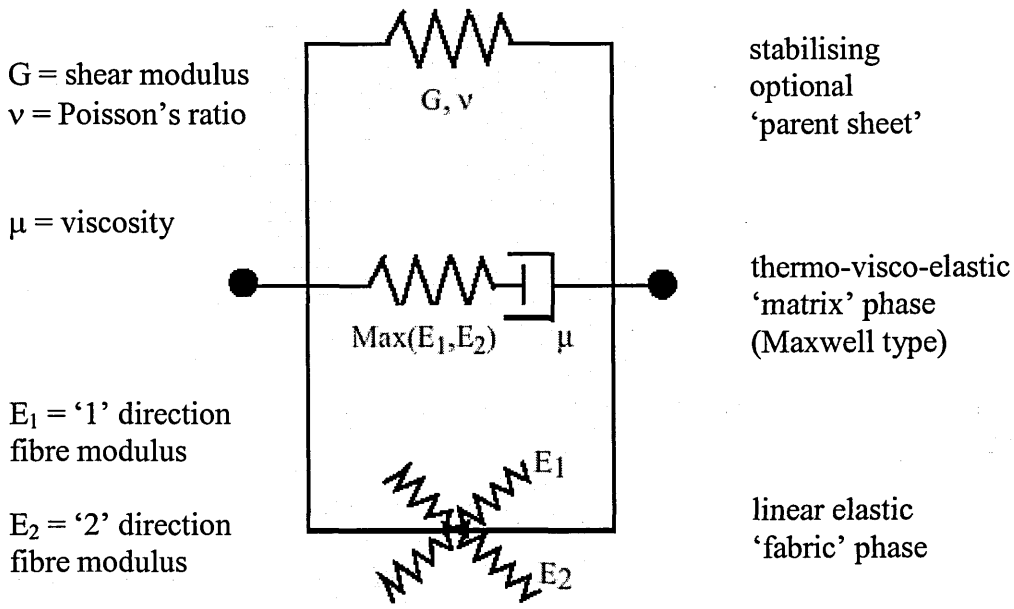

Fig. 3.14. Components of material type 140, from [41]

Material model 140 consists of three components:

- *Parent sheet:* this behaves like a standard linear elastic shell element for which the elastic properties are defined by the shear modulus and Poisson's ratio.

- *Thermo-visco-elastic matrix:* this component is used to simulate any polymeric binder that is included in the fabric, as with pre-impregnated reinforcement sheets or 'pre-pregs'. As the materials used in this project are 'dry' fabrics, with no binder present, this component will be effectively disabled through the use of a very low viscosity.

- *The Fabric Component:* this component represents the bi- (or uni-) directional fibre stiffness of the material reinforcement. Initial fibre orientations are specified by the user. The fibres are considered elastic and as such, each has an assigned Young's Modulus. Each fibre contributes not only to the fibre (or longitudinal) stresses but also to transverse shear and bending moments as calculated by classical beam theory. Therefore to account for the fibre content in composite materials a scaling factor has been included in the model to reduce the transverse shear and bending moments as required.

As of yet the validity and extent to which this material model can be applied to draping trials has received little academic attention. Through empirically characterising the material properties and behaviour it is the aim of this project to calibrate the required inputs of this material model through direct simulation of the testing procedures. These inputs can then be utilised in draping simulation trials which replicate experimental trials conducted during the project for final comparison.

4 MATERIALS CHARACTERISATION

4.1 TESTING PROGRAMME

The aim of experimental testing is to obtain material data for validation of the finite element model. It will be necessary to conduct suitable experiments to characterise the material behaviour and mechanisms of deformation that apply to pre-form manufacture. However, since the dominance of the various mechanisms mentioned in 3.1.1 depend on the fabric and state of required deformation there is currently no one testing procedure that can reliably suit both the woven and NCF materials of interest in this project. A suitable testing programme is therefore summarised as follows:

- *Bias shear extension tests:* bias extension tests are conducted for the NCF and 2/2 twill fabrics to characterise shear behaviour when inter-fibre slip and tow end rotation is permitted.

- *Picture frame tests:* picture frame testing permits pure shear characterisation of both the NCF and twill fabrics, assuming any 'edge effects' from clamping are negligible. The test also permits direct measurement of the fibre angle at which fibre locking occurs to initiate fabric buckling.

- *Flexural rigidity tests:* PAMFORM™ [47] permits the inclusion of a simple bending factor, therefore flexural rigidity tests will be conducted to ascertain the relative bending stiffness of each fabric type.

- *Friction tests:* since friction can produce fibre tension and alter the state of shear in a pre-form it is important to include this factor in the simulation.

- *Tow pull-out tests:* this test is used to obtain the force required to pull fibre tows from the fabric sheet. This is primarily being used to determine the effect of NCF through thickness stitching on the ability for tow slippage to occur.

- *Draping trials:* final validation of the simulation material model produced as a result of the previous tests will be conducted using the observations of experimental draping trials.

4.2 FABRIC DESCRIPTION

As previously described, two fabrics will be considered in this project and are summarised below;

1. *A biaxial 2/2 twill woven fabric.* Weight: 430gm^{-2}

   Manufacturer: C. C. Cramer.

   Grade: Atlas 2/2 constructed of 12K TENAX, carbon fibre tows.

   (12 thousand fibres per tow)

The 2/2 twill is a balanced woven fabric utilising identical fibre tows in both the warp and weft directions. The material is generally considered orthotropic

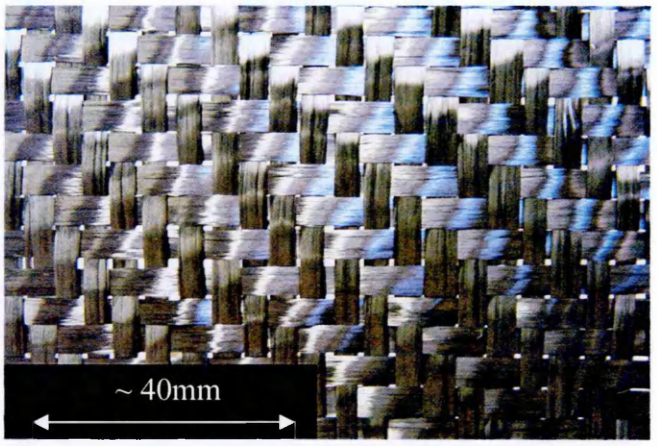

Fig. 4.1. The 2/2 twill fabric used in the current study

2. *A biaxial NCF fabric.* Weight: 430gm^{-2}

   Manufacturer: SAERTEX.

   Tow grade*:* 24K TORAY, carbon fibre.

   (24 thousand fibres per tow)

The NCF is constructed of two orthogonal, unidirectional fibre layers. The stitching consists of polyester filament chain stitches parallel to the warp direction and straight filaments passing through the chain stitches parallel to weft. As can be seen in figure 4.2 the effective tow size differs in the separate unidirectional layers of the fabric. The tows in the weft direction are constrained by the size of the chain stitch loops while the wider warp tows are constrained by the chain stitch spacing.

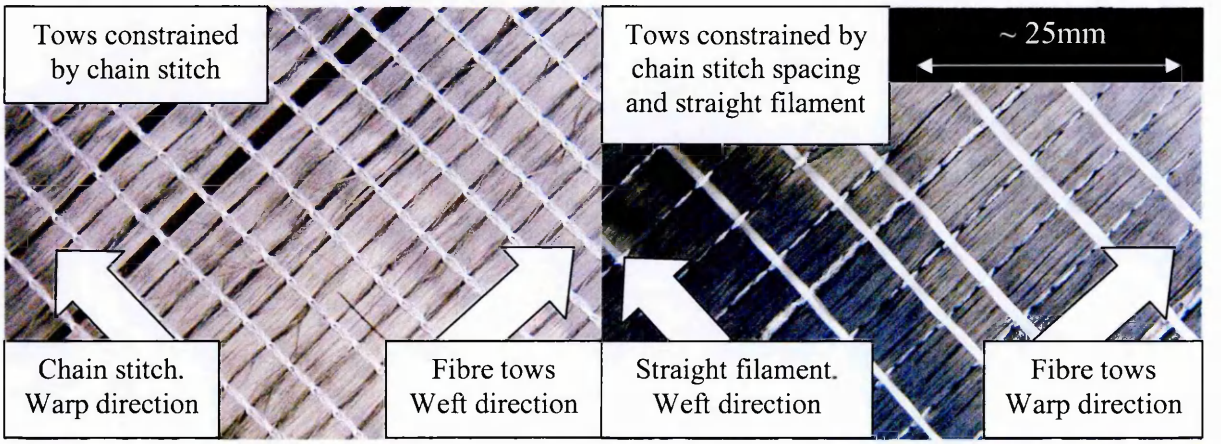

Fig. 4.2. Fibre architecture of the two NCF layers

Before testing commences it is necessary to define the fabric thickness for use in the FE analysis. This is conducted by simply using a Vernier calliper to measure the thickness of ten fabric sheets ten times to permit an average individual sheet thickness to be calculated. Measuring ten sheets prevents excessive errors through the measurement of a single sheet only.

4.3 TESTING PROCEDURES

4.3.1 BIAS EXTENSION TESTING PROCEDURE

Utilising standard tensile coupon testing equipment, the bias extension test is relatively simple to setup. Fabric coupons are cut with a ±45° fibre angle to the coupon edges. It is necessary to ensure the fabric fibres are at this angle before cutting as the low fabric shear modulus permits easy deformation when laying the fabric out on the cutting table or during coupon measurement.

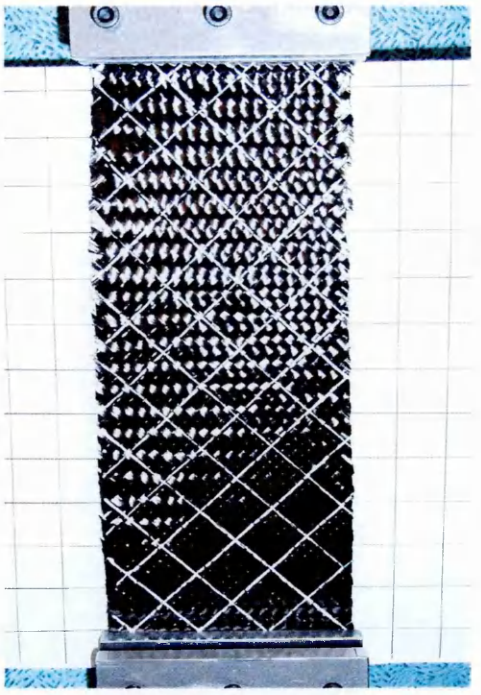

The size of the coupon depends on the testing equipment and clamp width available. Wide coupons are generally preferred to maximise the shear area and the coupon length should be at least twice this width to ensure fibre bridging does not occur. This can artificially increase the required shear force [1]. Usually 200mm x 100mm or 250mm x 100mm coupons are tested and in this study both are used with an additional 40mm length for clamping purposes.

Fig. 4.3. A 250x100mm bias extension coupon of 2/2 twill fabric.
(Upper and lower plate clamps are shown along with a 2cm grid sheet, placed behind the fabric for imaging of the deformation during testing).

For imaging of inter-fibre angle during testing it is necessary to mark the fabric with lines representing the fibre directions. A 20mm grid is therefore applied to the coupons using a water based correction fluid through a thin plastic template. In this study it was only necessary to mark one NCF direction as fibre stitching could be used for the perpendicular direction. Care has to be taken to ensure the fibre tows do not become 'glued' together through excess application of the fluid as this would restrict fibre deformation. Paints and white paint markers were found to be too thin and bleed into the dry fabric.

The clamping arrangement utilises a standard set of plate steel clamps which have a suitable attachment for the tensile testing equipment being used. Once the material has been placed in the clamps the setup can be transferred to the tensile test rig and checked for dimensional and fibre angle precision.

In the current study a Zwick Z010 tensile testing unit is utilised with a 2.5kN load cell. This has been calibrated to 0.1% error. Once the material has been loaded and the equipment readied, testing can proceed under displacement control.

For the 200mm length coupons a displacement rate of 200mm/minute has been specified while for the 250mm coupons 400mm/minute is used as much greater extension is possible before locking. As dry fabrics are being tested the shear force can be assumed independent of deformation rate [3, 13] permitting direct comparison of results from different lengths.

Automatic image processing systems are available to record inter-fibre angle variations during testing. However, the use of this is not required for this project therefore manual measurements are taken when the fibres have effectively locked.

An output of force against axial extension is produced and can be subject to data analysis for comparison to other fabrics as described in [1]. Usually a plot of force per unit width (Nm^{-1}) against axial strain (%) is produced although in the current study the test will be directly simulated therefore a direct force displacement graph is of greater use.

As previously iterated, for NCF materials utilising a stitch pattern at 45° to the fibre tows it is crucial that tests are conducted with extension both parallel and perpendicular to the stitching as differing shear behaviour will be recorded. Stitch breakage will also be necessary to accommodate even moderate strains when testing parallel to the stitching [3].

No variation in shear behaviour will be recorded with NCF stitching parallel to the fibre tows, as used in this study, due to axial symmetry within the bias extension test.

4.3.2 PICTURE FRAME TESTING PROCEDURE

The picture frame test is preferred by many researchers for characterising fabrics in uniform shear. However, the testing procedure and equipment are more complex and can be subject to high errors if set-up precision is not maintained.

The equipment consists of a rhomboid deformation cell in which the fabric can be clamped at each edge. A standard tensile testing machine is then used to apply a force to diagonally opposite corners of the frame. Currently no testing standards exist for applying the picture frame tests to composite fabrics. Therefore, researchers tend to use 'in-house' designed and built frames to fit the equipment available and suit the fabric being tested.

A picture frame (figure 4.4) was required to be built for testing to proceed. The key parameters regarding the design of the frame is the clamping edge length *c*, spacing between parallel edges *l*, and position of the bearing rotation centres.

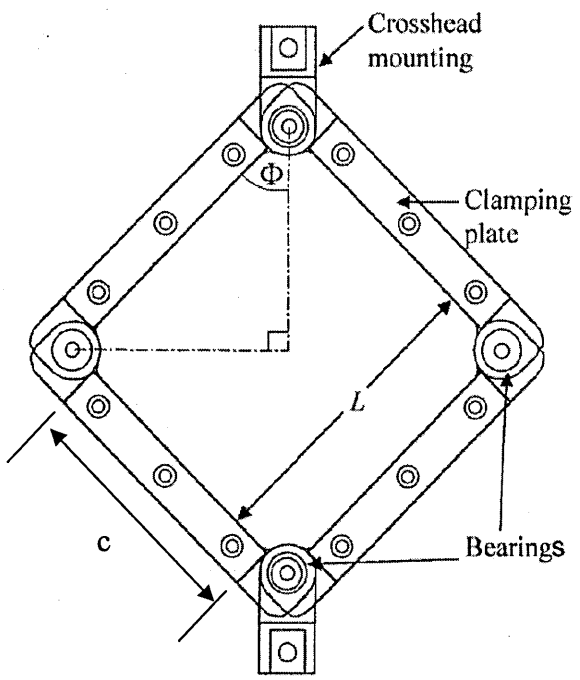

Fig. 4.4. Picture frame schematic, from [23]

To permit comparison of results and promote standardisation a similar picture frame to that used by Long [3, 23] is constructed. Therefore, *l*, is 145mm; *c*, is 115mm and the rotational centres of the bearings are positioned directly in-line with the clamping edge. This is important to ensure fibre extension and compression does not occur during deformation as the fibre modulus is high in comparison to the fabric shear modulus.

The CAD drawings of the main parts constituting the picture frame test rig are included in Appendix A.

In cutting material for the test allowance must be made for the crosshead mountings and bearing bolts. It is therefore necessary to cut the fabric into a cruciform to allow the fabric to fit the frame without interference. The fabric should be cut so fibre tows are parallel to the clamping edges with suitable overhang from the frame edge to ease tow alignment.

When laying the material coupon in the frame a base plate is used to permit the fabric to rest on a surface which lies in the clamping plane. This prevents any undue deformation or 'slack' in the fabric.

The clamping of the material into the frame is the most important stage of the setup procedure. Any misalignment of fibre tows causes fibre extension as the frame shears, again, requiring an excessively high deformational force due to the high fibre modulus. To minimise these errors careful placement and comparison of individual tow positions on opposite clamping plates is necessary. Ruler markings on the clamp plates are a useful aid in this exercise. Once the material is in place the frame can be carefully transferred to the tensile testing machine in which diagonally opposite corners of the frame are extended. The Zwick Z010 tensile testing unit is used for this purpose once again. As dry fabrics are being tested it is not compulsory to use a programmed displacement control to ensure a constant shear rate [3, 13]. A displacement rate of 10mm/minute is used during all picture frame tests of the NCF and twill fabrics.

The output of the test is once again shear force against crosshead displacement to permit. These outputs are converted to shear force against shear angle. Methods of data analysis for comparing different fabric types are provided in [1]. In characterising the in-plane deformational properties of a fabric the picture frame test also permits observation of the fibre locking angle.

This locking angle is calculated from a value of crosshead displacement recorded at the initial observation of out-of-plane fabric deformation. Using trigonometric relationships, the shear angle, θ, can be calculated from the crosshead displacement, x, and picture frame edge spacing, l, using the following equation;

$$\theta = 90 - 2.\cos^{-1}\left(\frac{\sqrt{\frac{l^2}{2}} + \frac{x}{2}}{l}\right)$$

As with the bias extension test, picture frame symmetry prevents the need for conducting test parallel and perpendicular to the NCF stitching in this study.

4.3.3 FLEXURAL RIGIDITY TESTING PROCEDURE

The textile industry already has a standard in place for the measurement of fabric rigidity; ASTM D1388-96 [45]. The *'cantilever bending'* variation of test is conducted using strips of material 200 x 20mm in size. The fabric coupon is placed upon a horizontal platform with a 20mm edge aligned to that of the platform (figure.4.5).

A moveable measuring slide is placed upon the sample using care to ensure the fabric is not moved. Automatic testers can be utilised to slide the material, parallel to the coupon length, off the platform. In this study manual slide movement is used. The coupon and measuring slide are smoothly moved at a rate of approximately 120mm/min until the edge of the coupon contacts a centrally aligned knife edge at 41.5° to the horizontal platform. Data analysis is explained in [45]. A higher bending length indicates greater flexural rigidity. Testing is conducted for both the 2/2 twill and NCF.

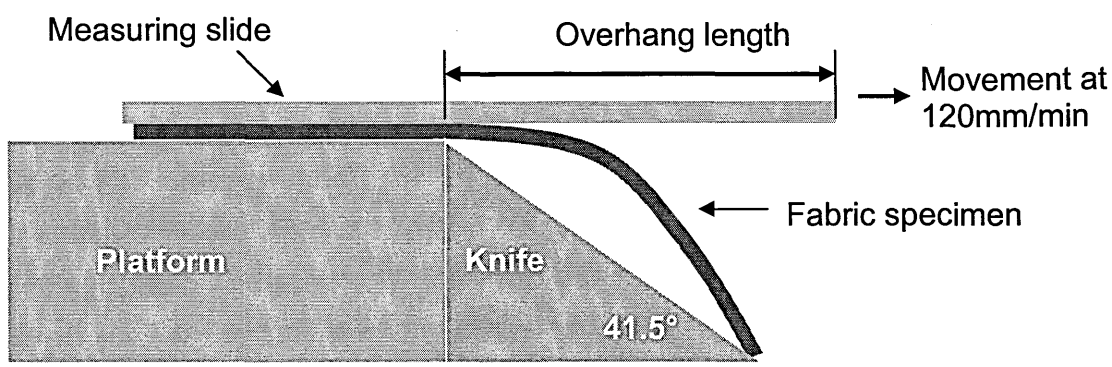

Fig 4.5. Schematic of the flexural rigidity test

Experiments using the twill fabric are conducted with a fibre angle of ±45° and 0°-90° due to a variation in the effective longitudinal fabric modulus. The NCF is more complex in that the upper and lower tows have different geometries. This theoretically requires testing to be conducted at ±45°, 0°-90° and 90°-0° with both types of tow upward facing. However, consistently placing the fabric with the wider tows upward facing during draping trials means characterisation of the bending stiffness is required in one orientation only.

4.3.4 FRICTION TESTING PROCEDURE

In defining the friction between two surfaces there are two possible coefficients that can be measured; static (or stationary) friction and dynamic (or kinetic friction).

A simple method of measuring both static and dynamic friction has been employed to permit comparison of the two values and discussion of the relevancy of each to fabric draping.

Amonton's law of friction states;

$$\mu = \frac{F}{W}$$

where, μ, is the coefficient of friction; F, the tangential force required to overcome the friction (F_S being static force and F_D the dynamic force); and W, is the total mass placed upon the contacting surfaces.

To measure the static coefficient of friction, a fabric sheet is wrapped around a metal plate, of size 100mm x 175mm, and placed on the surface of interest. This surface must be confirmed horizontal to ensure the data is precise.

A 5kg mass is then placed upon the plate and a calibrated spring balance connected horizontally. The total mass of the plate, fabric and 5kg mass must be ascertained for use in the coefficient calculation.

The spring balance is then manually extended quasi-statically at approximately 6mm/min until the frictional force is overcome and the plate begins to move. The force, F_S, at the initiation of movement is recorded for use in the above calculation. Quasi-static spring balance extension is required to ensure no extra inertial forces are induced in the system resulting in a reduced measured force.

To calculate the dynamic friction, the extension of the spring balance is stopped as soon as displacement of the fabric wrapped plate is initiated. The plate is then allowed to come to a rest at which point, F_D, is recorded for use in the above equation.

Friction measurements are taken between each respective fabric and all components that come into contact with the fabric during forming. The forming equipment and draping description is detailed in 4.1.7, for which friction testing is required between the fabric and mould; fabric and anodised base plate; fabric and forming membrane and finally between sheets of the same fabric.

Friction testing of the NCF is conducted with stitching both perpendicular and parallel to the displacement to characterise any variation due to the stitching orientation. The fabric to fabric friction is taken using sheets with fibres orientated at 0°-90° and ±45° to account for the lay-up sequence during draping experiments as described in 4.1.7.

4.3.5 TOW PULL-OUT TESTING PROCEDURE

This test is proposed with the aim of characterising the effect through thickness stitching has on the ability of NCF to deform by inter-fibre slip. Similar work is conducted on the twill fabric for completeness although data for this fabric is not required in the simulation material model.

The concept behind the test is to create a constant area of transverse fibres through which the longitudinal fibres can be pulled using a standard tensile test machine. The force against crosshead displacement curve is recorded and force is normalised for the contact area between the fibre layers.

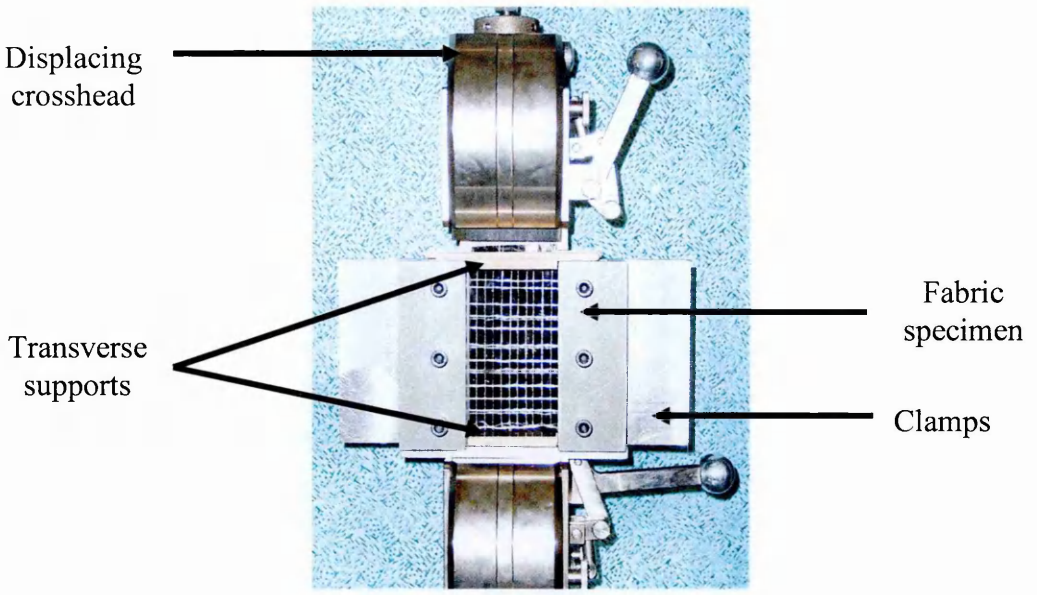

Fig. 4.6. Fibre tow pull-out testing of NCF

The equipment is shown in figure 4.6. The material is cut to a size of approximately 80mm width and 170mm length, with the fibre tows to be pulled orientated to the length of the specimen.

20mm of transverse tows are carefully removed from the top of the sample to permit the longitudinal tows to be clamped during testing. 50mm of transverse tows are then removed from the base. This ensures a contact length of 100mm between the fibre layers is maintained as the protruding longitudinal tows are pulled through.

The width of tows that can be pulled is defined by the displacing crosshead at 52mm. The width is maintained as high as possible with the aim of minimising errors due to stitching irregularities and fibre crossover between tows.

Once the material is cut to size and the redundant transverse tows removed, the transverse fibres are constrained at the edges using steel plate clamps. Transverse supports are fitted before clamping to ensure the unclamped specimen width is consistent at 52mm. These supports act to prevent the edge clamps from being drawn-in during testing as this would allow the transverse fibres to bend and cause compaction of the longitudinal tows. Higher forces would be required to pull the tows in such instances.

The clamped and supported specimen is placed in the Zwick Z010 tensile testing unit as before and the upper, protruding tows clamped. The 50mm of free longitudinal tows protruding below the edge clamps should be permitted to hang freely and in this instance are hung in the jaws of the lower crosshead. The tows are pulled under displacement control at 20mm/minute and the force against crosshead displacement plot recorded. Once the protruding tows at the base of the specimen are exhausted the test is stopped. This ensures the contact area between fabric layers is not reduced which would theoretically reduce the total contact friction and thus the force required to pull the tows. The measured force can then be normalised for the area of contact between layers.

The NCF is tested in both 0°-90° and 90°-0° orientations due to the differences in stitching constraints and tow size for each layer of the NCF.

4.3.6 DRAPING TRIAL PROCEDURE

Draping Trials are conducted for both the NCF and 2/2 twill fabrics. The double hemisphere mould used for these trials is drawn schematically in figure 4.7 and is constructed from resin. This mould has been chosen to produce greater shear variation in the fabrics and avoid the complete symmetry of hemispherical moulds commonly used to investigate fabric drapeability.

The reduction to one plane of symmetry, between hemisphere centres, can be used to make obvious any preferential shear within the NCF fabric due to stitching constraints.

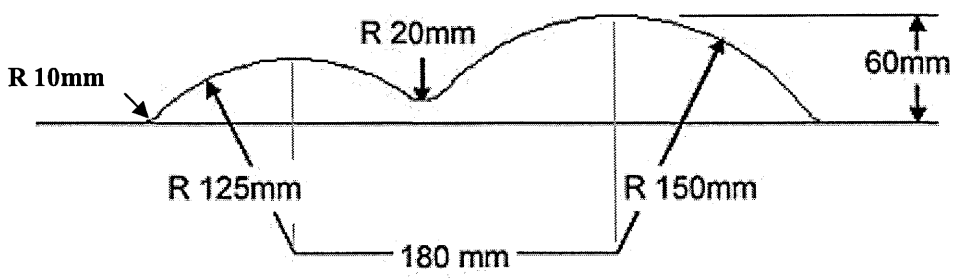

Fig. 4.7. Double hemisphere mould geometry as used in draping trials

A rubber membrane vacuum forming press is used to form the material around the mould. This equipment is constructed of a horizontal metal plate on which the desired mould can be placed as shown in figure 4.8. This metal plate is constructed of hard anodised aluminium. Once the single or double fabric sheets are placed upon the mould, a rubber membrane, held in a metal frame, is lowered over the entire plate and clamped at the edges to create an air tight seal.

A vacuum can then be applied through a framework of small holes in the metal plate to conform the rubber membrane, and thus the fabric, over the mould. The use of an underlying breather fabric may be required when pre-preg material is draped to ensure air flow is uniform and the vacuum consistent. With dry fabrics, however, air flow through the material is possible and breather fabrics can be negated.

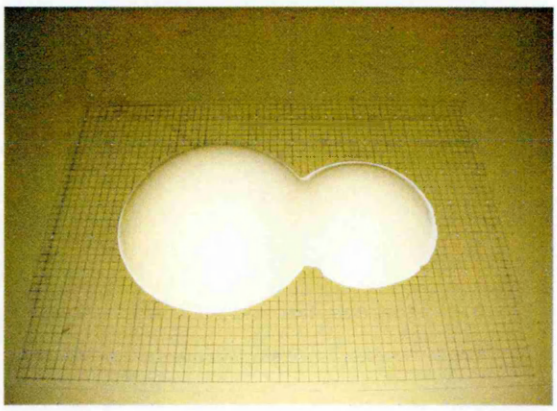

Fig. 4.8 The double hemisphere mould, placed upon the metal vacuum forming plate

The fabric specimen size for all draping trials is 550mm x 400mm (the 550mm length being aligned with the mould symmetry axis). As with the bias extension tests, care has to be taken to ensure the fibres are aligned as required before any specimen cutting occurs. The two fabric fibre directions are then marked with a 20mm grid pattern using correction fluid and a plastic template to ensure accuracy. The material specimen is then ready and can be aligned centrally along the mould symmetry plane with an 80mm overhang beyond the larger hemisphere. The metal base plate is marked with a 10mm grid to permit easy alignment of the mould and fabric specimen before testing as can be seen in figure 4.8.

Trials are conducted for both fabrics with the following fibre orientations, defined to the mould symmetry axis;

- ±45°
- 0°-90°
- a ±45° sheet on top of a 0°-90° sheet
- a 0°-90° sheet on top of a ±45°sheet

The aim of using two layers during draping is to induce greater wrinkling for validation of the simulation and produce a more representative experiment of industrial pre-form construction. In all tests the NCF material is draped with the larger, warp tows upward facing and perpendicular to the mould symmetry plane when a 0°-90° fibre angle is required.

The rubber membrane is semi-transparent and allows imaging of the deformed material shape while the vacuum is still applied. The grid on the metal base also permits perimeter deformation measurements of the material specimen to be taken. Measurements of material contraction are taken every 10mm and recorded along with the occurrence of any wrinkling for comparison to simulation results.

4.4 EXPERIMENTAL RESULTS

4.4.1 MATERIAL DIMENSIONS

Average values of the material thicknesses are as follows;

2/2 twill sheet thickness = 0.54mm
NCF sheet thickness = 0.51mm

The average *sheet* densities can subsequently be calculated using these thicknesses and known sheet densities of $430gm^{-2}$;

2/2 twill sheet density = $8.43x10^{-7}$ kg/mm^3
NCF sheet density = $7.96x10^{-7}$ kg/mm^3

The average density of carbon fibre is $2.2 \times 10^{-7} kg/mm^3$ [48], therefore the fabric sheet densities are comparatively low and result in long simulation times.

4.4.2 BIAS EXTENSION RESULTS

Initial procedural trials of the bias extension test were conducted with 100mm x 200mm NCF material. Results from these trials showed good consistency and are therefore used in the data analysis, resulting in a total of ten tests for this coupon type. Four tests are conducted for the 250mm x 100mm NCF coupons and three for both sizes of twill fabric to permit a mean average shear force to be plotted against displacement.

Error bars are calculated using a Student t-distribution method to a 95% confidence interval (i.e. 19 out of 20 tests will yield results in the range plotted). This statistical method permits calculation of specified lower and upper confidence intervals for a dataset of unknown variance assuming a normal distribution. This method is described in [46]. All data analyses are included in appendix B. From the force against extension data obtained, mean values are plotted and the confidence intervals calculated for every 10mm displacement. The corresponding data and test curves of all bias extension tests are presented in appendix B.

4.4.2.1 NCF BIAS EXTENSION RESULTS

The bias extension results for the NCF coupons are shown in figures 4.9. and 4.10.

A consistent 18° minimum inter-fibre angle is observed for both coupon sizes. A central fabric width of 40mm has been recorded at 55mm extension for the 200mm coupon and 65mm extension for the 250mm length coupon.

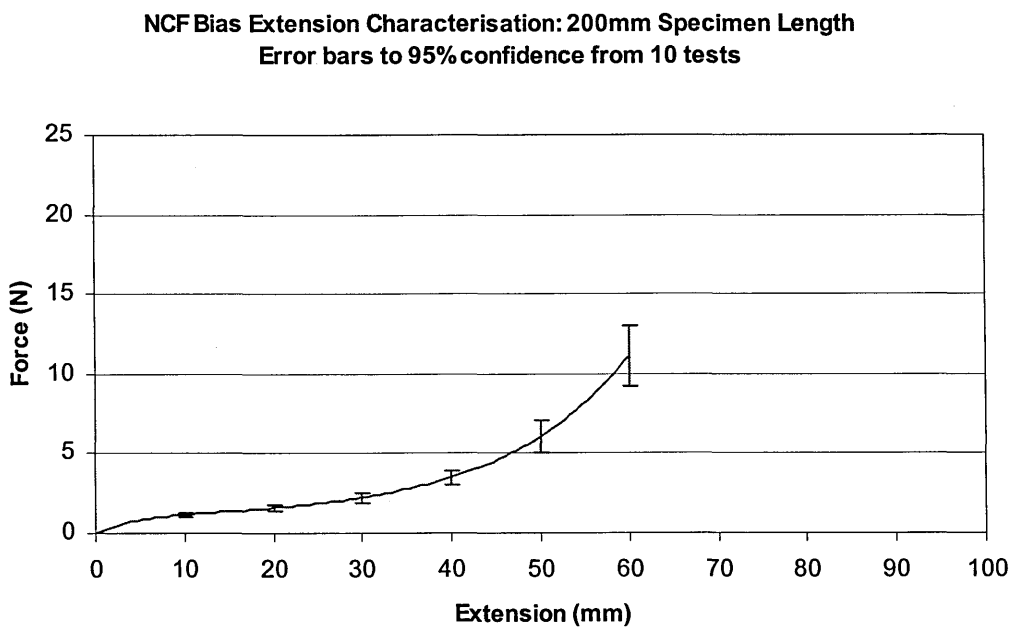

Fig. 4.9. NCF bias extension results for 200mm x 100mm samples

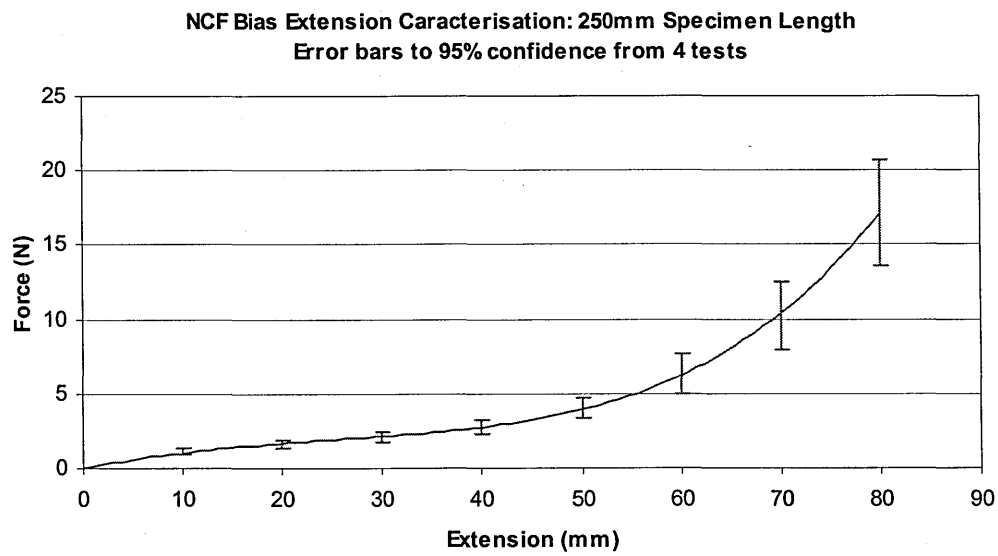

Fig. 4.10. NCF bias extension results for 250mm x 100mm samples

4.4.2.2 2/2 TWILL BIAS EXTENSION RESULTS

The bias extension method of shear characterisation has been found to be of limited applicability for the twill fabric due to coupon separation occurring at a low inter-fibre angle.

Figure 4.11 shows force data up to the completion of separation from tests of 200mm length coupons. Data for the 250mm length coupon are included in appendix B. Figures 4.12 and 4.13 show analysed data up to the onset of separation.

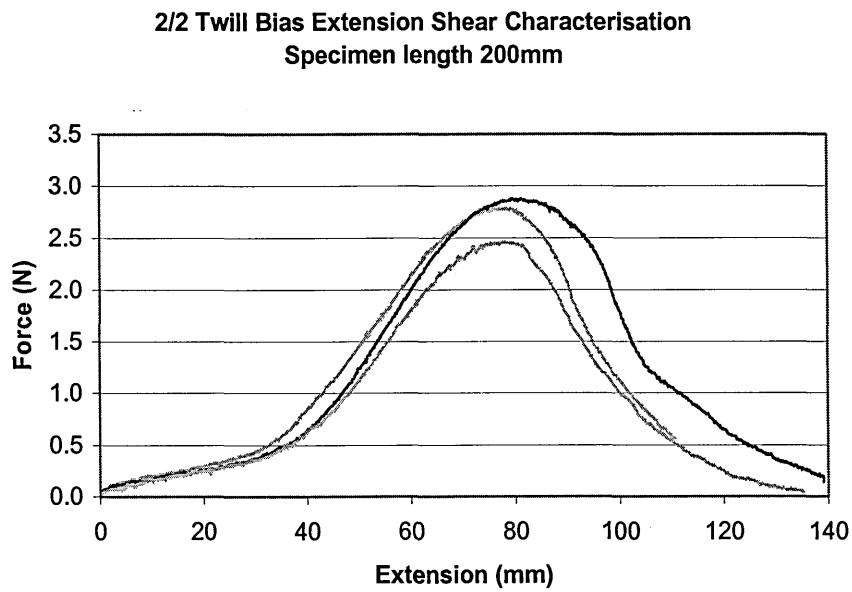

Fig. 4.11. 2/2 Twill bias extension shear data

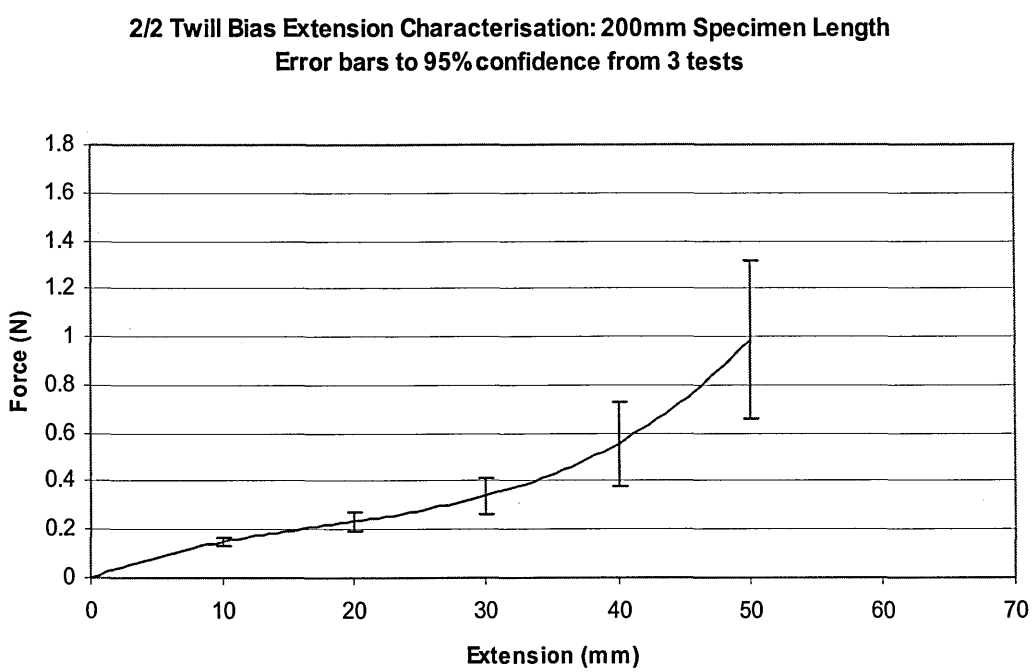

Fig. 4.12. 2/2 Twill bias extension results for 200mm x 100mm coupons

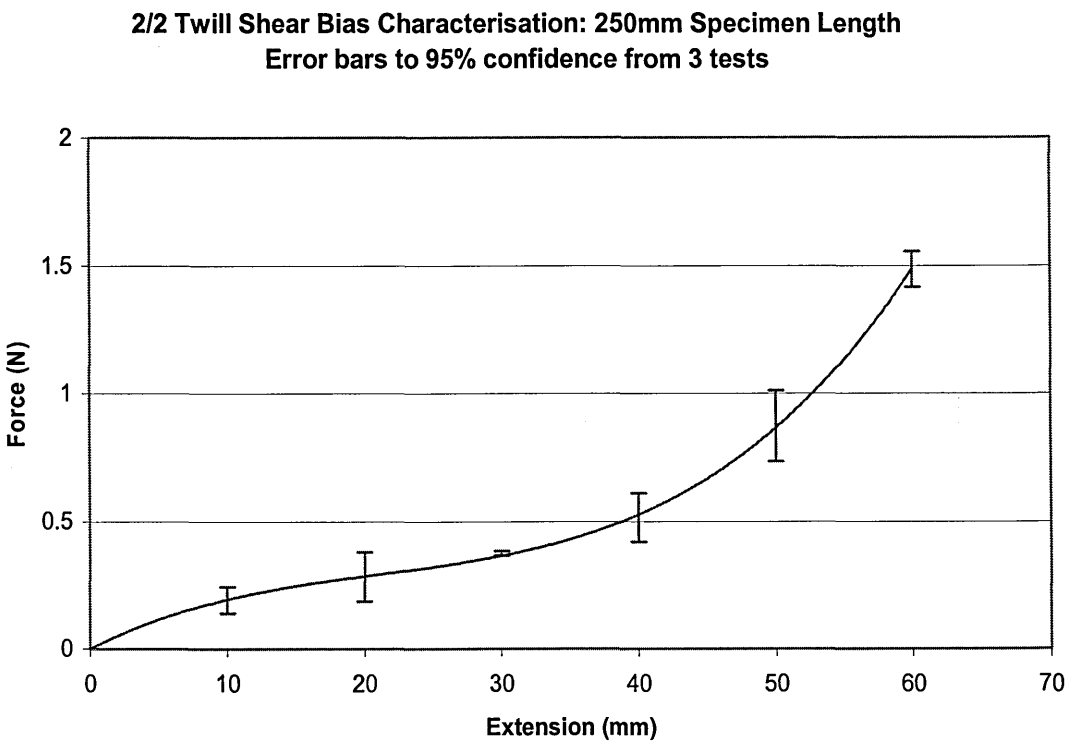

Fig. 4.13. 2/2 Twill bias extension results for 250mm x 100mm coupons

The minimum inter-fibre angle is 41° and occurs at the onset of coupon separation. The central fabric width at this point is 44mm. This width corresponds to an extension of ~48mm for the 200mm length coupon and ~58mm for the 250mm length coupon.

The data from the 2/2 twill bias extension tests are valid up to the onset of separation therefore this data has been analysed using the Student t-test method to a 95% confidence interval and included in figures 4.12 and 4.13.

4.4.3 PICTURE FRAME RESULTS

Five picture frame experiments are conducted for each fabric to permit validation of the results since errors due to tow misalignment can be high. The mean average force is plotted with error bars assessed using a Student t-test method to a 90% confidence interval [46]. The force against displacement data, Student t-test analysis data and fibre locking angle data is included in appendix B.

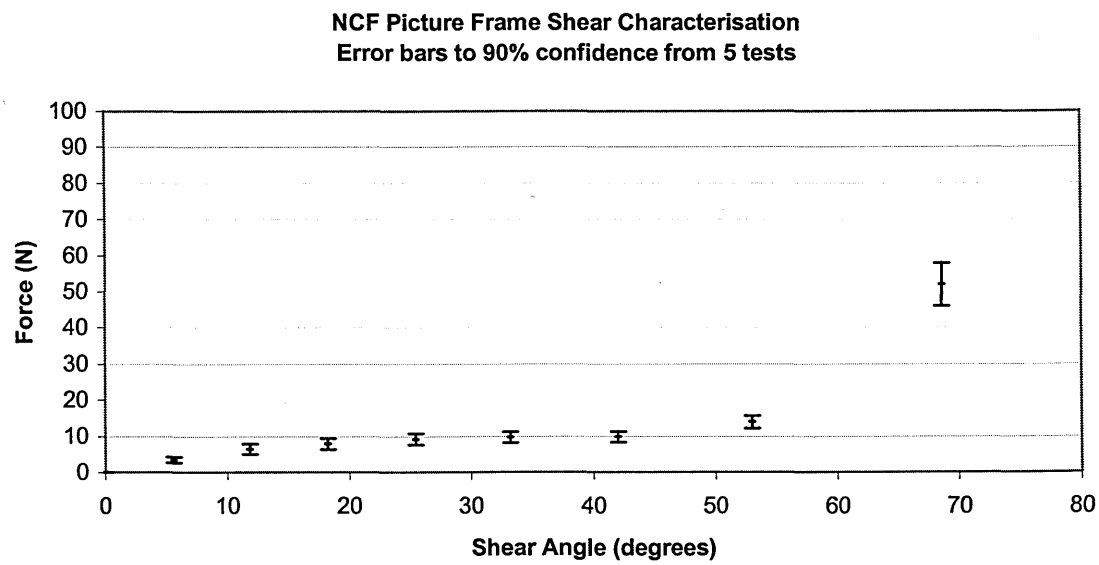

Fig. 4.14. NCF picture frame results

The NCF picture frame results are shown in figure 4.14. With the exception of edge effects, the material deforms by in-plane shear up to the locking angle of the fabric. The NCF fibres lock at an average minimum angle of 20° (calculated from extension measurement to the nearest 0.5mm).

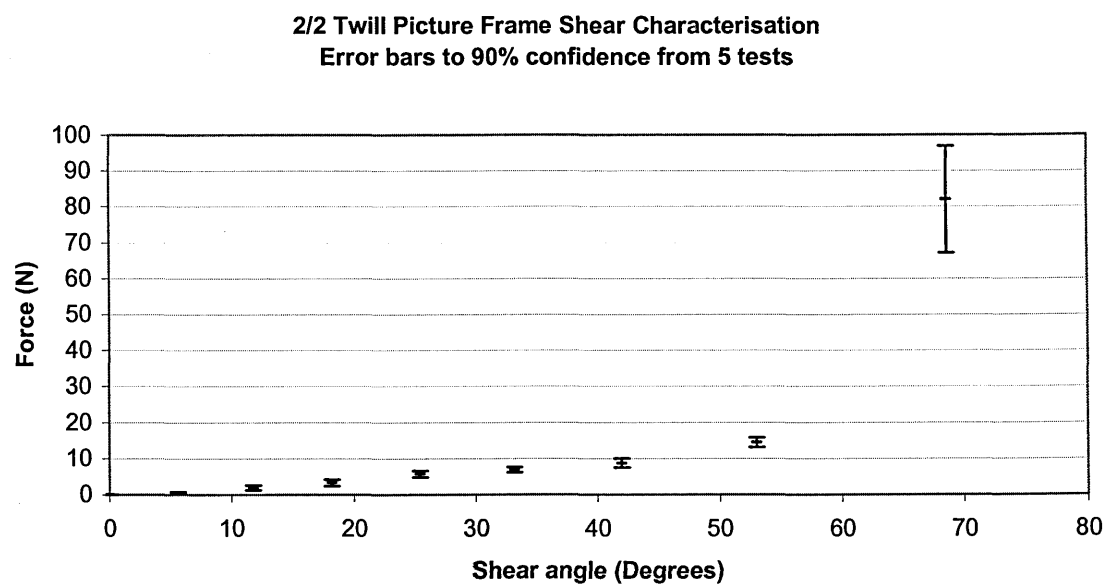

Fig. 4.15. 2/2 Twill picture frame results

The 2/2 twill picture frame results are shown in figure 4.15. The 2/2 twill fibres lock at an average minimum angle of 21°.

4.4.4 FLEXURAL RIGIDITY RESULTS

The average bending lengths from six tests for each fabric are detailed in table 4.1. Actual data values are included in appendix B.

Fibre alignment angle to coupon length	*Overhang length (mm) (to nearest 1mm)*
NCF fabric *(warp tows 'face-up')*	
±45°	81
0°-90° *(parallel to straight filament)*	188
90°-0° *(parallel to chain stitch)*	182
2/2 Twill fabric	
±45°	74
0°-90°	124

Table 4.1. Flexural rigidity results

4.4.5 FRICTION TESTING RESULTS

The calculated friction coefficients are detailed in the table below. During draping trials the NCF fabric is placed with the warp tows 'face-up', therefore the warp tows are tested against the membrane while the weft tows are tested against the mould, vacuum former base plate and warp tows of a an underlying NCF sheet. The 2/2 twill requires no such consideration as the fabric exhibits in-plane symmetry. Five tests are conducted for each coefficient to permit an average value to be calculated. The friction data is included in appendix B.

Interface 1	*Interface 2*	*Static friction coefficient*	*Dynamic friction coefficient*
2/2 Twill fabric			
Twill fabric (parallel to tows)	Vacuum former base plate	0.16	0.16
Twill fabric (parallel to tows)	Mould	0.52	0.11
Twill fabric (parallel to tows)	Twill Fabric tows at ±45°	0.23	0.21
Twill fabric (parallel to tows)	Rubber forming membrane	0.37	0.26

Table 4.2. 2/2 Twill friction coefficient results

Interface 1	*Interface 2*	*Static friction coefficient*	*Dynamic friction coefficient*
NCF fabric (contact to weft tows)			
Weft tows (parallel to chain stitch)	Vacuum former base plate	0.17	0.10
Weft tows (perpendicular to chain stitch)	Vacuum former base plate	0.19	0.10
Weft tows (parallel to chain stitch)	Mould	0.32	0.25
Weft tows (perpendicular to chain stitch)	Mould	0.32	0.23
Weft tows (parallel to chain stitch)	Warp tows at ±45°	0.34	0.29
Weft tows (perpendicular to chain stitch)	Warp tows at ±45°	0.31	0.26
Warp tows (parallel to chain stitch)	Rubber forming membrane	0.34	0.23
Warp tows (perpendicular to chain stitch)	Rubber forming membrane	0.34	0.26

Table 4.3. NCF friction coefficient results

4.4.6 TOW PULL-OUT RESULTS

The NCF tow pull-out results show poor consistency. Graphs of all tow pull-out results are shown in appendix B. Three tests are conducted and analysed using a Student t-test method to calculate 90% confidence intervals, figure 4.16.

The force output is normalised by the contact area between the individual NCF fabric layers which is equal to 5.2×10^{-3} m^2 (52mm x 100mm). Data and analyses of these tests are included in appendix B.

The force per unit area required to remove tows from the weft direction are significantly higher than that in the warp direction. This is demonstrated in figure 4.17.

For completeness, the tow pull-out results for the twill fabric are included in appendix B. These results are not required as inputs or for validation of any FE simulation.

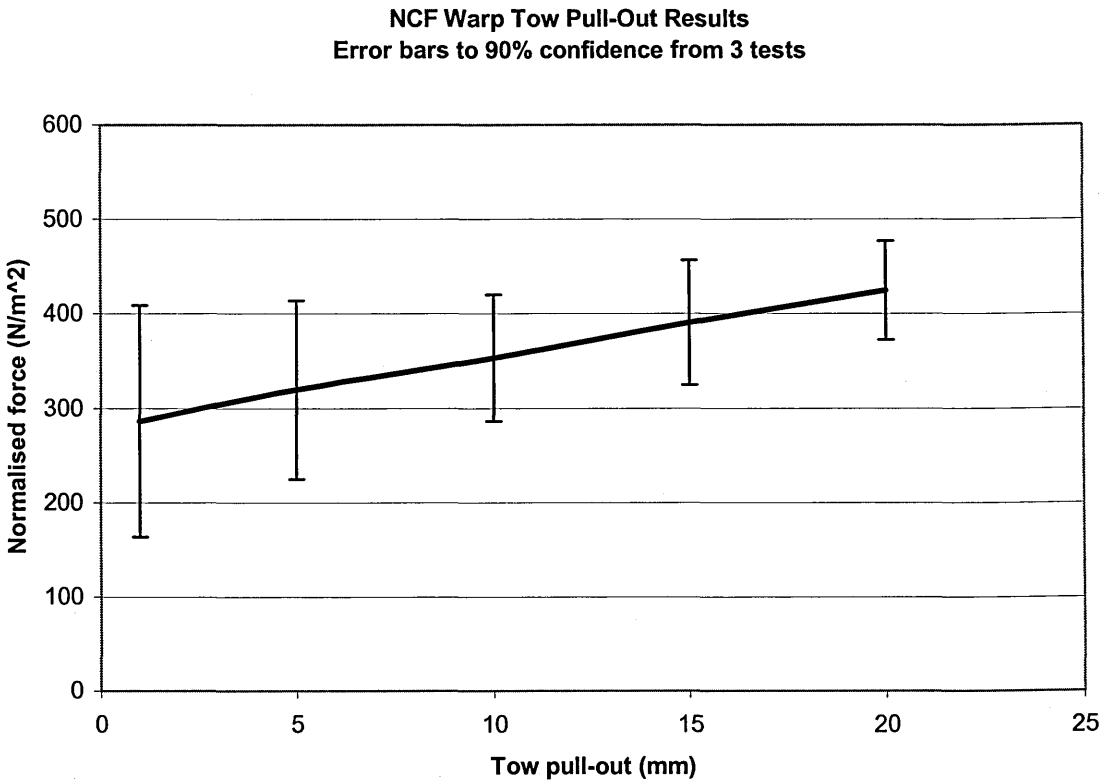

Fig. 4.16. Analysed results of selected NCF warp tow pull-out tests

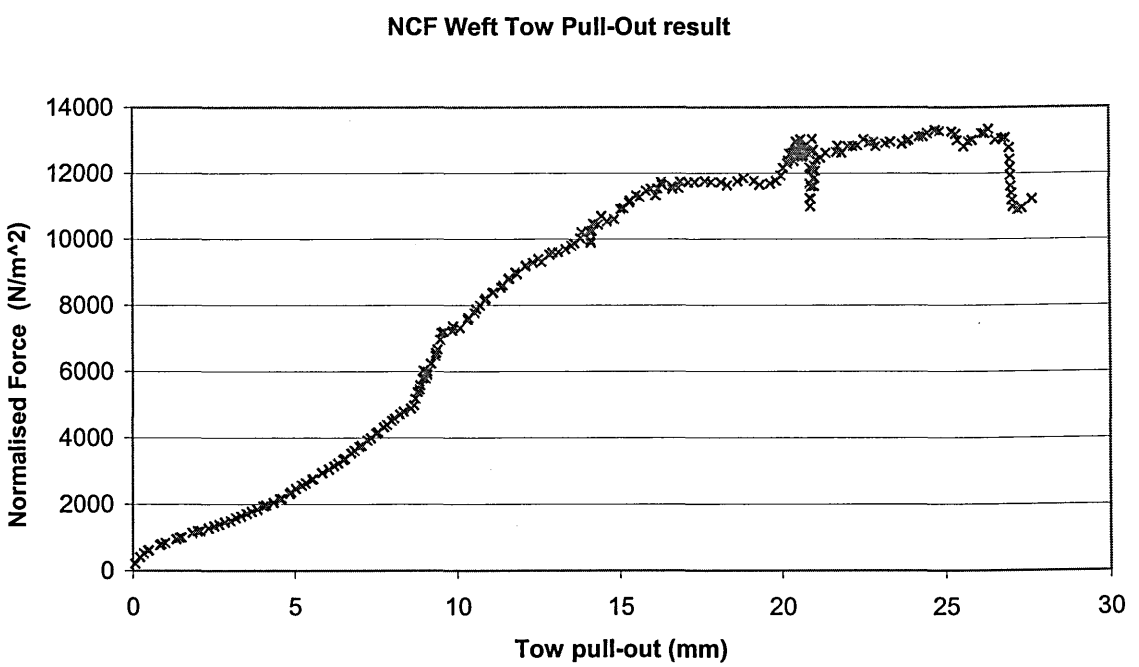

Fig. 4.17. NCF weft tow pull-out result

4.4.7 DRAPING TRIAL RESULTS

Results of the measured fabric shape obtained during experimentation are displayed in section 5.4.8 as a comparison to the draping simulation data. Images of the draped NCF fabrics are included below in figures 4.18 to 4.21 with the presence of wrinkles denoted by arrows. Images of the draped 2/2 twill fabrics are included in figures 4.22 to 4.25.

4.4.7.1 NCF FABRIC DRAPING RESULTS

With fibres aligned 0° and 90° to the mould symmetry plane (figure 4.18) the contraction of the fabric perimeter can be seen to be at a maximum in areas where the fibres are aligned at *0°-90°* with the hemisphere centres. Bridging between the hemispheres is observed and is dominant where aligned with the mould symmetry plane.

Fig. 4.18. NCF 0°-90°fabric

Figure 4.19 display the results of draping a NCF fabric sheet aligned ±45° to the mould symmetry plane. As expected the greatest perimeter contraction occurs where fibres are aligned with the hemisphere centres, but with a ±45° fibre orientation the fabric shape is very different.

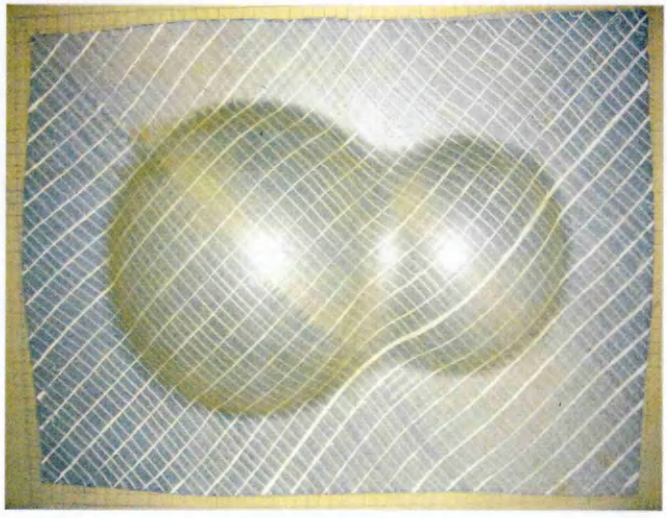

Fig. 4.19. NCF ±45° fabric

Perimeter contraction occurs dominantly at the fabric corners proximal to the large hemisphere and at edges perpendicular to the symmetry plane where between the hemispheres. Minor bridging between the hemispheres is also observed.

Figures 4.20 and 4.21 show the draping results of placing a ±45° sheet onto a 0°-90° sheet and placing a 0°-90° sheet onto a ±45° sheet respectively. In each case the individual layers maintained the characteristic shape as noted in figures 4.22 and 4.23 although the magnitude of perimeter contraction is reduced.

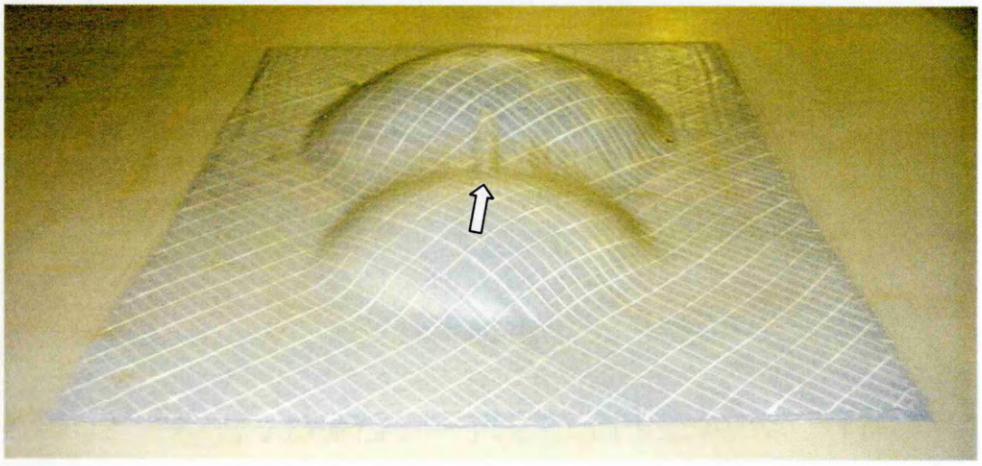

Fig. 4.20. NCF ±45° fabric sheet draped upon a 0°-90° fabric sheet

In both situations wrinkling is generated. When a ±45° upper sheet is used the wrinkling is dominantly observed between the hemispheres with minor wrinkling occurring at the base of the larger hemisphere, at a 45° angle to the hemisphere centre. When a 0°-90° upper sheet is used the wrinkling at 45° to the large hemisphere centre is minor, as more prominent wrinkling is observed close to the symmetry plane at the base of the large hemisphere. Bridging between the hemispheres is more pronounced than that of the single fabrics.

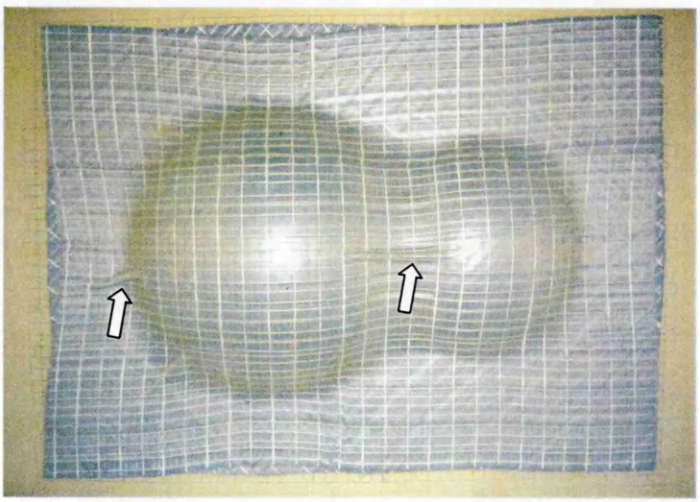

Fig. 4.21. NCF 0°-90° fabric sheet draped upon a ±45° fabric sheet

4.4.7.2 2/2 TWILL FABRIC DRAPING RESULTS

Fig. 4.22. 2/2 Twill 0°-90°fabric.

Fig. 4.23. 2/2 Twill ±45° fabric.

The shape of the draped 2/2 twill fabrics are similar to those of the NCF material. This is demonstrated in figures 4.22 and 4.23. The main fabric perimeter contractions occur in areas where fibres are aligned to the hemisphere centres. Similar hemisphere bridging is produced with the fabric in both 0°-90° and ±45° orientations. No wrinkling is produced with either of the single sheet draping trials.

Draping trials using two fabric sheets, figures 4.24 and 4.25, once again demonstrate that individual layers retains the characteristic shape as noted during draping trials of single sheets only. This results in the lower fabric sheet protruding from the upper sheet in many locations, as demonstrated at the fabric corners of figure 4.24. Bridging between the hemispheres is once again more prominent than when draping a single fabric sheet. Wrinkling is only induced between the hemispheres when the fibres are orientated to ±45° in the upper sheet.

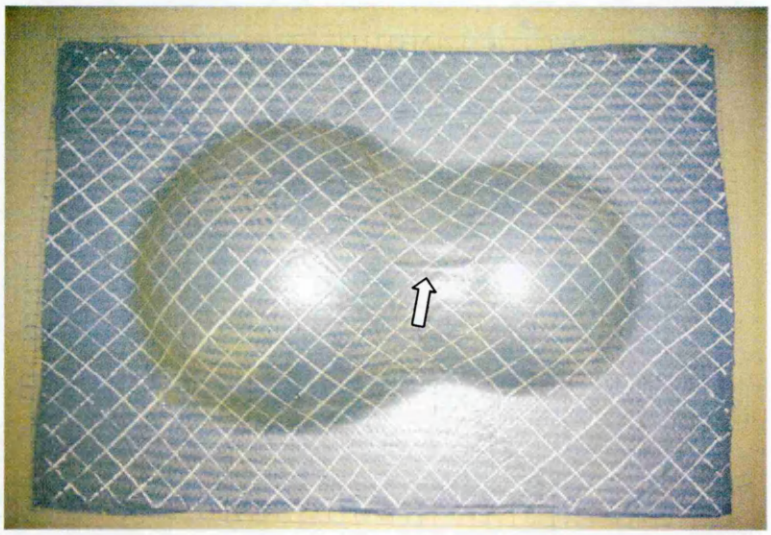

Fig. 4.24. 2/2 Twill ±45° fabric sheet draped upon a 0°-90° fabric sheet

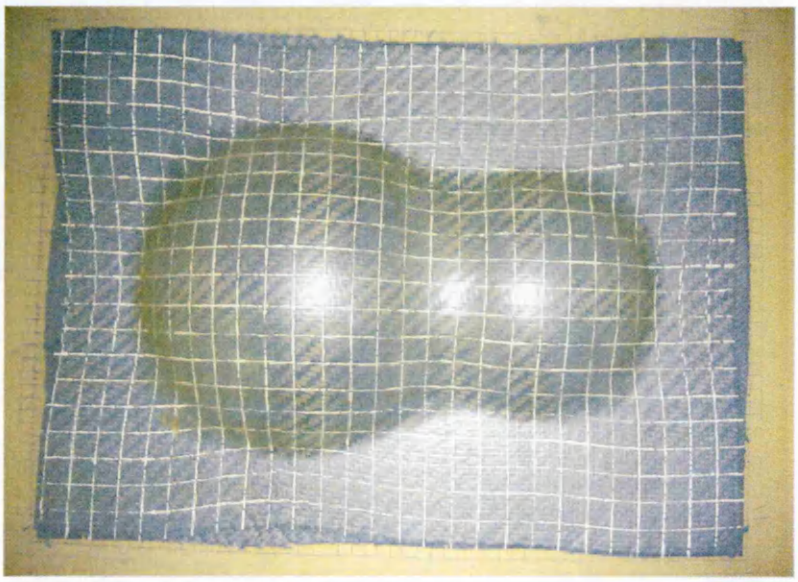

Fig. 4.25. 2/2 Twill 0°-90° fabric sheet draped upon a ±45° fabric sheet

5 FINITE ELEMENT SIMULATION

Material model 140, included in PAMFORM™ [47], is designed to permit a high quantity of material data to be included in the interest of producing precise simulations. With the aim of calibrating these material model inputs, direct simulations of the experimental characterisation tests are necessary. Once the optimum parameters are ascertained the final material model can be utilised in simulations of the draping trials for final validation.

5.1 MATERIAL MODEL DESCRIPTION

Simulation of the 2/2 twill fabric will be conducted using the material 140 model (described in 3.3.4) to represent each fabric sheet required.

Material 140 is designed to represent a bi-phase, bi-directional (direction '1' and '2') pre-preg material. This model can be used to simulate dry fabrics, as in this study, by assigning a low viscosity to the matrix material. A matrix viscosity of $1x10^{-20}$ $kg.mm^{-1}.ms^{-1}$ is used in all simulations.

The required parameters of material model 140 are listed below;

FIBRE PARAMETERS

- Fibre direction (directions 1 and 2)
- Elastic fibre modulus (directions 1 and 2)
- Out-of-plane shear modulus (directions 1 and 2)
- Bending factor (directions 1 and 2)

PARENT SHEET PARAMETERS

- Density
- Thickness
- Shear modulus*
- Post-lock shear modulus*
- Locking angle*
- Poisson ratio

* the shear data can alternatively be input as a user defined curve.

Accurate NCF representation requires a more complicated representation than material 140 model permits. This is to suitably account for through thickness stitching on the ability of the material to deform. The NCF representation proposed for PAMFORM™ [47] by Pickett [15] will therefore be utilised.

The model proposed by Pickett [15] uses shell element layers to represent the separate unidirectional layers of the fibres. These layers are simulated using the material 140 model. Using identically discretised shell element layers permits additional elements (defined as 'spot-welds' in PAMFORM™ [47]) to be created between adjacent nodes in each layer to represent the through thickness stitching (figure 5.1). These elements are more complex than simple beam elements as differing shear and normal moduli can be applied. These element moduli also require calibration, in addition to the material 140 parameters of the shell element layers.

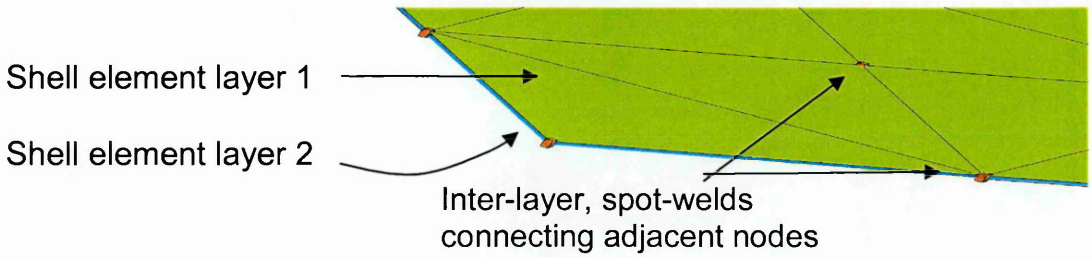

Fig. 5.1. A close-up of the proposed NCF representation

To prevent the shell element layers from penetrating one another during simulation a contact interface is defined. The most suitable contact algorithm available in PAMFORM™ [47] is 'type 33'. This is a master/slave, segment-to-segment contact algorithm for which a 'thickness' is assigned to the master layer. Continuing penetration of a slave element into this thickness results in the linear addition of a defined penalty force during calculation of nodal acceleration (equated in 3.3.3). Additionally, a mean average inter-fabric dynamic friction coefficient is applied to the contact, i.e. $\mu = 0.28$. The type 33 algorithm is described in detail in [41].

Half the total fabric thickness is applied to each shell element layer, i.e. 0.255mm. As shell elements are defined centrally to the assigned thickness, the spacing between these layers is also half the total fabric thickness. The master surface contact thickness is, therefore, also defined as 0.255mm.

In all situations of fabric simulation, isosceles triangular shell elements are used. Shell elements are chosen to include flexural stiffness and non-uniform through thickness stress distributions, using three integration points to integrate bending and membrane effects. Isosceles, triangular elements, with 10mm edge lengths adjacent to the right angle, are chosen for both the 2/2 twill and NCF representations.

Initial trials of the bias extension simulations were conducted with quadrilateral shell elements. Results produced unfeasibly high forces of up to 20kN to deform a 200mm bias extension specimen when a realistic fibre modulus of 300GPa was utilised. Triangular elements are considered to be more stable and produce no such artefacts.

5.2 SIMULATION PROGRAMME

From the experimental results obtained in section 4.4, the frictional data, material thickness and calculated density can be directly input into the material model. The effective Poisson ratio of the fabric will vary depending on the state of shear already present in the fabric. As a single value is to be applied to the material model, 0.4 will be used in all simulations. In obtaining the remaining parameters for input to the material model the following simulation programme is proposed:

- *Tow Pull-Out Test Simulation:* A representative simulation of the NCF pull-out test is required to optimise the effective normal and shear 'moduli' of the inter-layer bar elements. This is conducted first as the simulation is reliant on no other material parameters. The calibrated bar element parameters can then be utilised in subsequent NCF simulations.

- *Bias Extension Test Simulation:* Direct simulation of both the NCF and 2/2 twill fabrics will be conducted at both the 200mm and 250mm specimen lengths for comparison to the experimental results shown in 4.4.2. The aim of these simulations is to optimise the fibre out-of-plane shear modulus, elastic modulus and fabric shear modulus, post-lock shear modulus and locking angle.

- *Picture Frame Test Simulation:* Direct simulation of the picture frame tests are also used to optimise the fibre out-of-plane shear modulus, elastic modulus and fabric shear modulus, post-lock shear modulus and locking angle, for both the 2/2 twill and NCF materials.

- *Flexural Rigidity Test Simulation:* Direct simulation of the flexural rigidity tests is conducted for the 2/2 twill and NCF to optimise the material 140 bending factor. These simulations are dependant on the fibre material properties and, therefore, must be conducted after the bias and picture frame characterisation simulations.

- *Draping Trial Simulation:* Final validation of the optimised material model and NCF representation will be conducted through simulation and subsequent comparison of draping trial results.

5.3 SIMULATION PROCEDURES

5.3.1 TOW PULL-OUT SIMULATION

Tow pull-out simulation involves displacing one shell element layer of the NCF material model relative to the other. Extension of the connecting inter-layer 'bar' elements requires a force defined by the effective normal and shear moduli assigned. This force can be normalised to the area of contact between the element layers and compared to the experimental results.

The shell layer element size and distribution is identical to that used in the shear characterisation and draping trial simulations. This is to ensure the density of inter-layer spot-welds and reaction forces are also identical. The shell elements used are isosceles triangles with 10mm edge lengths adjacent to the right angle.

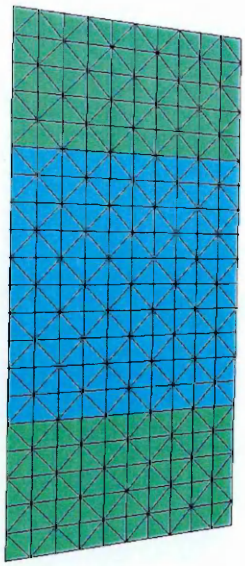

The longer shell element layer is 200mm x 100mm in size (figure 5.2) and constrained to prevent displacement and rotation in all directions. The second shell element layer of the NCF representation is smaller at 100mm x 100mm and undergoes displacement in the plane of the fabric, parallel to the length of the simulated coupon. A smaller second layer is utilised to ensure the area of frictional contact between the surfaces is constant. Null material properties are used for both element layers, as opposed to the material 140 model, to prevent element strain from distorting the results. The NCF contact 'type 33', described in 5.1, is maintained.

Fig. 5.2. NCF tow pull-out representation

The velocity profile of figure 5.4 is applied to the leading edge of the smaller element layer. The apposing force (or 'section force' as defined in PAMFORM™ [47]) of the constrained element layer is equivalent to the force measured by the tensile testing equipment and is used to compare results. Calculation of this nodal force is described in [41].

5.3.2 2/2 TWILL BIAS EXTENSION SIMULATION PROCEDURE

Simulation of the 2/2 twill bias extension tests are conducted using a single layer of triangular shell elements to the required coupon size of 200mm or 250mm x 100mm.. As demonstrated in figure 5.3, a regular element pattern is used with orthotropic symmetry to ensure the results obtained are not attributable to any mesh irregularities. Elements are once again isosceles with 10mm edge lengths adjacent to the right angle.

The nodes of the lower width edge are constrained to prevent movement in x, y, and z directions, simulating the lower clamp. The nodes of this lower edge are also selected to provide the reaction or 'support' force required to constrain the nodes during the simulation.

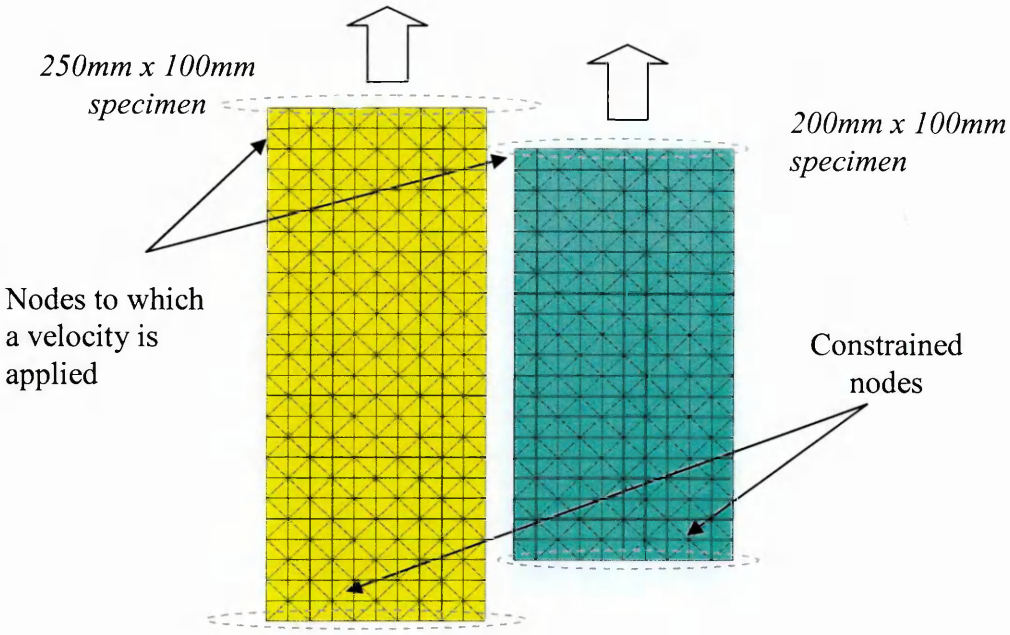

Fig. 5.3. Discretised bias extension simulation coupons

Axial strain is induced by assigning a velocity profile, as shown in figure 5.4, to the nodes of the upper width edge. Nodal movement of this edge is restricted parallel to the coupon length only. The initial acceleration of these nodes is used to reduce inertial oscillations within the coupon which are simulated using explicit dynamic techniques.

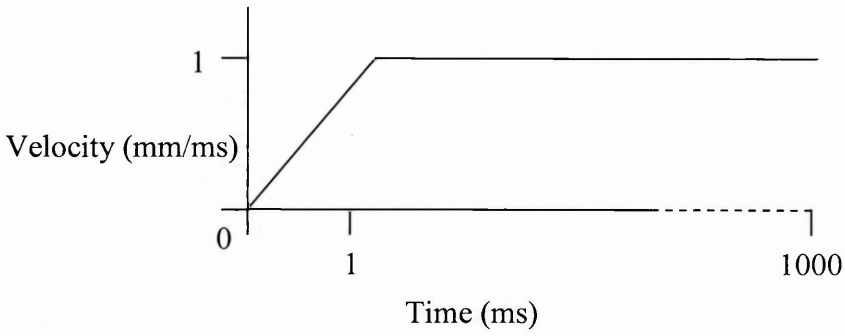

Fig. 5.4. Bias coupon velocity profile

Once the required material model data (identified in section 5.1) is defined, the simulation is ready to proceed. The fibre alignment of the material 140 model is defined at ±45° to the simulated coupon length. Once the simulation is completed, axial strain is be plotted against the section force for comparison to the appropriate experimental results.

5.3.3 NCF BIAS EXTENSION SIMULATION: ADDITIONAL REQUIREMENTS

The NCF bias extension simulation procedure is similar to that of the 2/2 twill described above with the exception of requiring the more complex material representation described in 5.1.

In addition, the boundary conditions of edge constraint and velocity must be applied to both fabric layers at the necessary edges. Results can be obtained and plotted as with the 2/2 twill simulations although the section force is defined using the upper edge nodes of both element layers.

5.3.4 2/2 TWILL PICTURE FRAME SIMULATION PROCEDURE

The picture frame simulation is more complex than that of the bias extension simulation due to the requirement for all material edges to be clamped and the pure shear movement required.

The discretised fabric mesh used for the picture frame simulation is shown in figure 5.5. A regular pattern of triangular shell elements is once again utilised to minimise errors induced through model discretisation. The specimen size is 145mm x 145mm, as defined from the experimental frame.

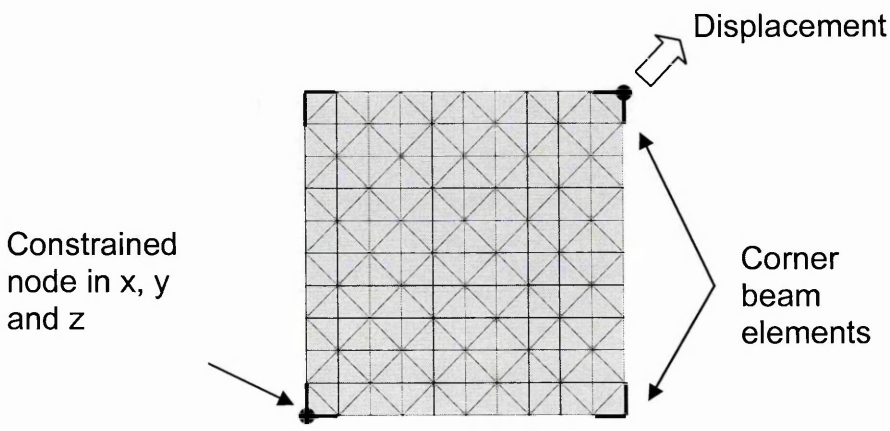

Fig. 5.5. Discretised picture frame simulation specimen

Complication occurs in simulating the actual picture frame, as rigid edges are required to constrain the fabric while permitting rotation at each of the four corner nodes.

With this aim, two 3D beam elements of one elements length are created at each of the fabric corners, as shown in figure 5.5. 3D beam elements are utilised as rotation of the element in x, y, and z is possible, unlike bar elements. Rotation is necessary to reproduce the movement permitted by the picture frame bearings.

To permit each beam element to rotate independently the corner nodes are duplicated and one linked to each separate beam element. Constraining the two co-positional corner nodes to displace together, but only in the plane of the fabric, simulates the required degree of rotational freedom of the experimental frame.

Rigid bodies are defined between the beam elements, along the edges of the fabric, to prevent any relative nodal movement, representing the clamped edge of the frame. The simulated fibre directions are defined parallel to the frame edges.

To deform the simulated frame, the 'clamps' of the tensile test equipment have to be simulated. To do this a constraint is placed on one corner to prevent displacement in x, y, and z. It is important to permit rotation of the elements at this corner to reproduce the bearing rotation of the picture frame.

A velocity is then applied to the diagonally opposing corner node. The nodal velocity profile of figure 5.4 is used once again.

The clamped, corner node is used to log the section force during the simulation for comparison to the displacement of the diagonally opposing node. These outputs are identical to those of the tensile test equipment.

Once the required material model data is defined, the simulation is ready to proceed. Force against diagonal extension of the frame is logged and is subsequently converted to force against shear angle for comparison to experimental results.

5.3.5 NCF PICTURE FRAME SIMULATION: ADDITIONAL REQUIREMENTS

The NCF picture frame simulation procedure is similar to that of the 2/2 twill described above with the exception of requiring the more complex material representation described in 5.1.

The corner beam elements and rigid bodies require definition for both layers. Additionally, the output and boundary conditions applied must utilise the relevant nodes from both layers.

5.3.6 FLEXURAL RIGIDITY SIMULATION

The flexural rigidity simulations utilise a single coupon of the representative fabric model as shown in figure 5.6 for the 2/2 twill fabric.

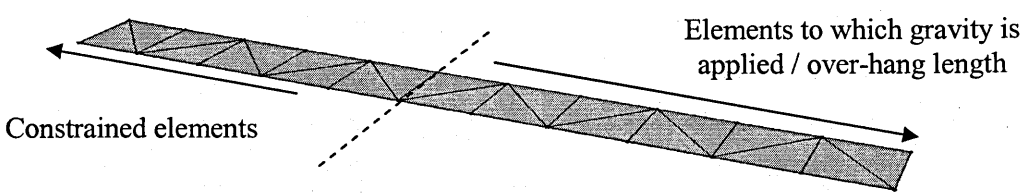

Fig. 5.6. Example of a 2/2 twill Flexural rigidity simulation coupon

The flexural test is simulated by applying nodal acceleration, equal to that of gravity, to nodes up to the overhang length found by experiment. The nodes at this length and those remaining are constrained to prevent displacement in x, y and z. PAMFORM™ [47] includes a 'gravity' option which will be used to apply the required acceleration of $9.81 ms^{-2}$ to the 'overhanging' nodes.

To compare simulated and experimental results it is necessary to log the displacement vector of the end, overhanging nodes, calculate angle θ, shown in figure 5.7, and compare this to the 41.5° angle used in the experiments.

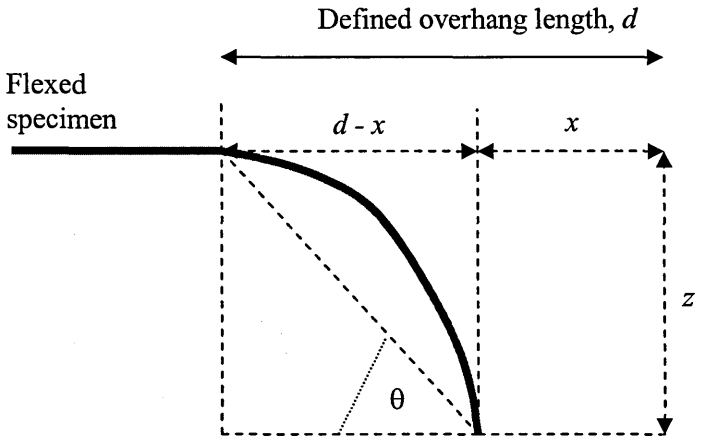

$$\theta = \tan^{-1}\left(\frac{z}{d-x}\right)$$

Fig. 5.7. Analysis of a flexural rigidity simulation

Optimised material data of the shear characterisation simulations must be used as flexural rigidity is dependent upon the fibre parameters, in particular the elastic modulus.

5.3.7 DRAPING TRIAL SIMULATION

Simulation of the draping trial tooling is conducted using separate meshes for the double-hemisphere mould and vacuum forming base plate. This is to permit the application of dissimilar friction coefficients as characterised during friction testing, i.e. 2/2 twill to mould, $\mu = 0.11$; 2/2 twill to base plate, $\mu = 0.16$; NCF to mould, $\mu = 0.24$; NCF to base plate, $\mu = 0.1$.

The geometry of the simulated mould is identical to that of figure 4.7. This geometry is meshed using quadrilateral shell elements, defined through automatic meshing in I-DEAS [49] CAE software. Local element length is defined as 4mm. The simulated base plate is constructed of a regular 5mm grid of square shell elements. The tooling meshes are shown in figure 5.8. Both base plate and mould are defined using as a null material (designation 100), as required by the software, and constrained such that all nodes can not be displaced or rotated.

The mould and base plate meshes are used to define a contact to the fabric. Shell elements are used to represent the tooling simply to permit application of a 'type 16' Lagrangian contact to the lower shell element layer of the fabric. 'Type 16' is a node-to-segment contact interface utilised, generally, for contact to constrained tooling in forming simulations. The contact algorithm is described in [41].

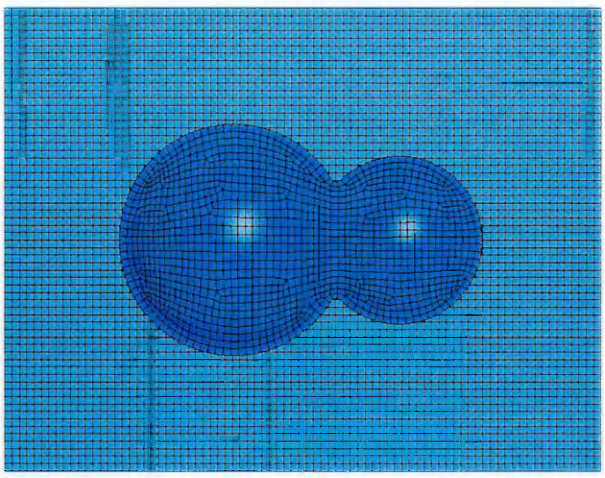

Fig. 5.8. Discretised meshes of the mould and vacuum former base plate

The size of the base plate must be greater than that of the initial fabric to permit expansion as well as contraction once the fabric is draped. An additional 50mm is therefore incorporated for each edge. Four additional bar elements are included in the plane of the simulated base plate simply to permit the original perimeter of the fabric to be recognised.

The fabric layers are initially aligned parallel to the base plate, 2mm above the larger hemisphere. The fabric layers are aligned centrally along the mould symmetry plane with an 80mm overhang beyond the larger hemisphere in accordance to the experimental trials.

A 'type 33' contact is utilised between separate sheets when more than one fabric sheet is to be simulated. This is identical to that previously described in section 5.1 with application of the appropriate NCF or 2/2 twill inter-fibre dynamic friction coefficient (μ =0.28 or 0.21 respectively).

To form the fabric to the mould a pressure is applied to all elements of the uppermost fabric element layer. The pressure initially increases linearly up to 1×10^{-4}kg.mm^2 at 1ms then remains constant. The initial pressure increase is used to prevent inertial shockwaves from being generated in the fabric.

Once the simulation is complete, key points of the draped fabric perimeter can be located relative to the four bar elements representing the initial fabric perimeter. Contraction of the simulated fabric at these key points, within the plane of the base plate, is recorded for comparison to the results obtained from the experimental draping trials.

5.4 SIMULATION RESULTS

A summary of the material data used for each simulation is given in the following text. Detailed material input data is included in appendix C with corresponding simulation designations for identification.

5.4.1 NCF TOW PULL-OUT SIMULATION RESULTS

Results of the tow pull-out simulations proved highly satisfactory and are shown in figure 5.9. The optimised shear and normal moduli data is included in appendix C.

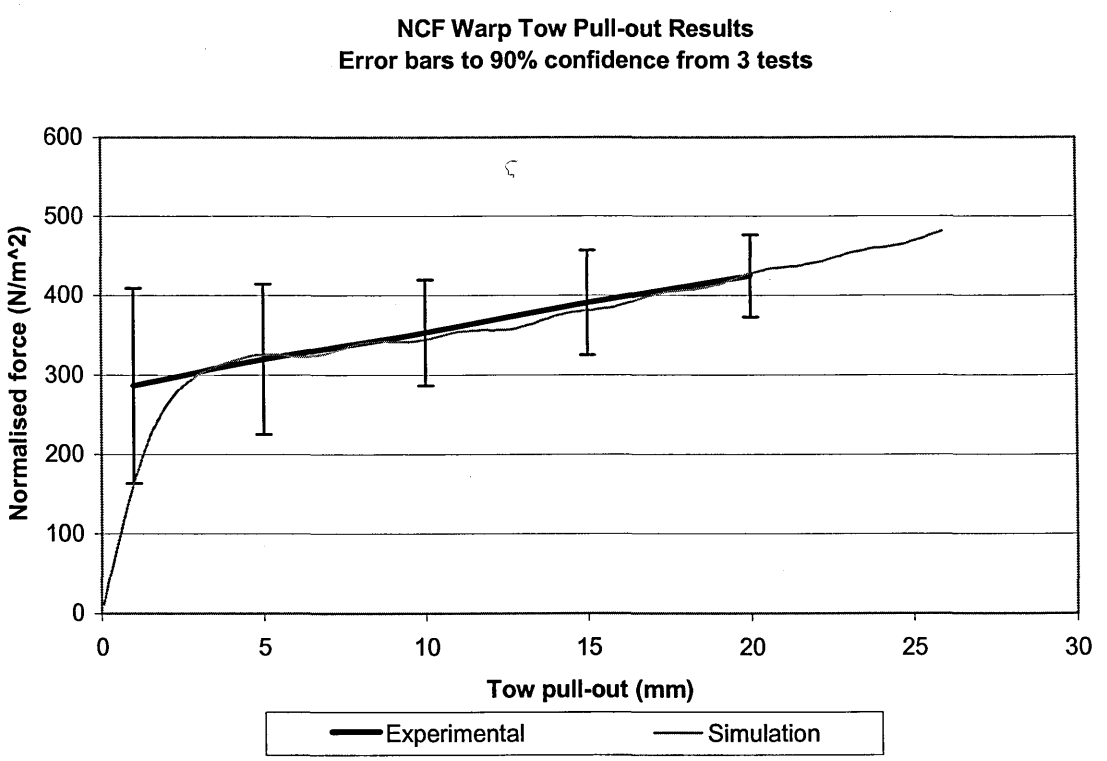

Fig. 5.9. NCF tow pull-out results comparison

The normal modulus is defined to be higher than that of the shear modulus to better characterise the actual material. A minimum factor of 19 is used in the calibrated data.

5.4.2 2/2 TWILL BIAS EXTENSION SIMULATION RESULTS

Initial simulations of the bias extension tests were conducted for the 200mm length specimens using high fibre elastic moduli of 500GPa and relatively low shear moduli of $1x10^{-6}$ GPa (simulation 1 of figure 5.10). Results indicate the level of force required to deform the fabric is high, therefore, simulation 2 has been conducted with a lower pre-lock shear modulus of $1x10^{-7}$ GPa.

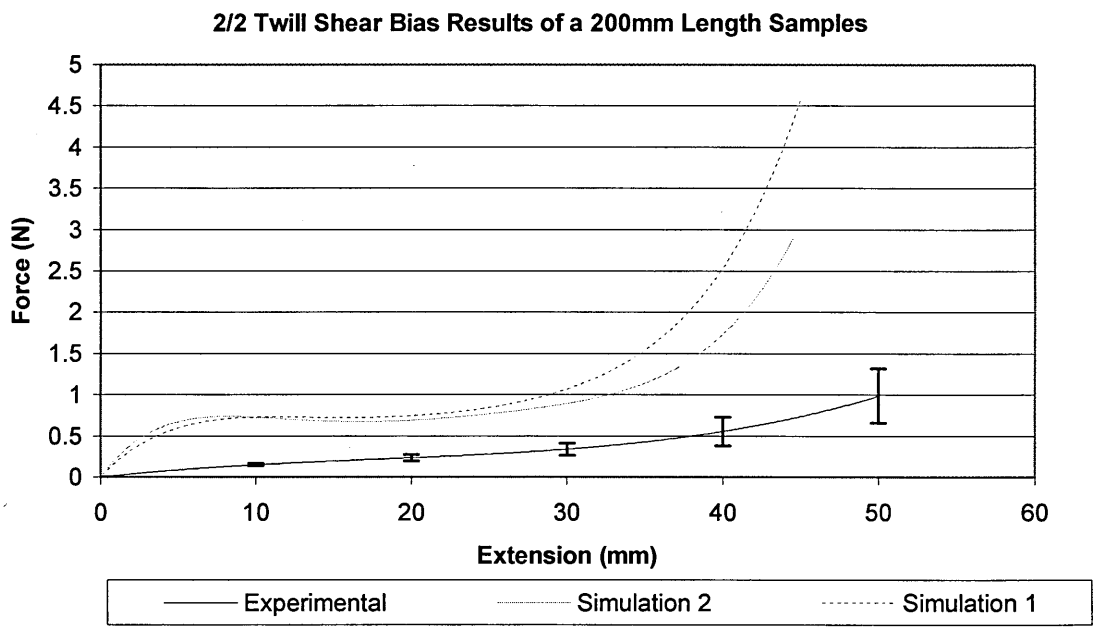

Fig. 5.10. Results comparison for 2/2 twill, 200mm length coupons

Figure 5.10 demonstrates that a lower shear modulus reduces the force required to deform the material at higher strains, but has little effect at lower strains. Similar behaviour is obtained for the 250mm length coupons when utilising the same material data. This is demonstrated in figure 5.11.

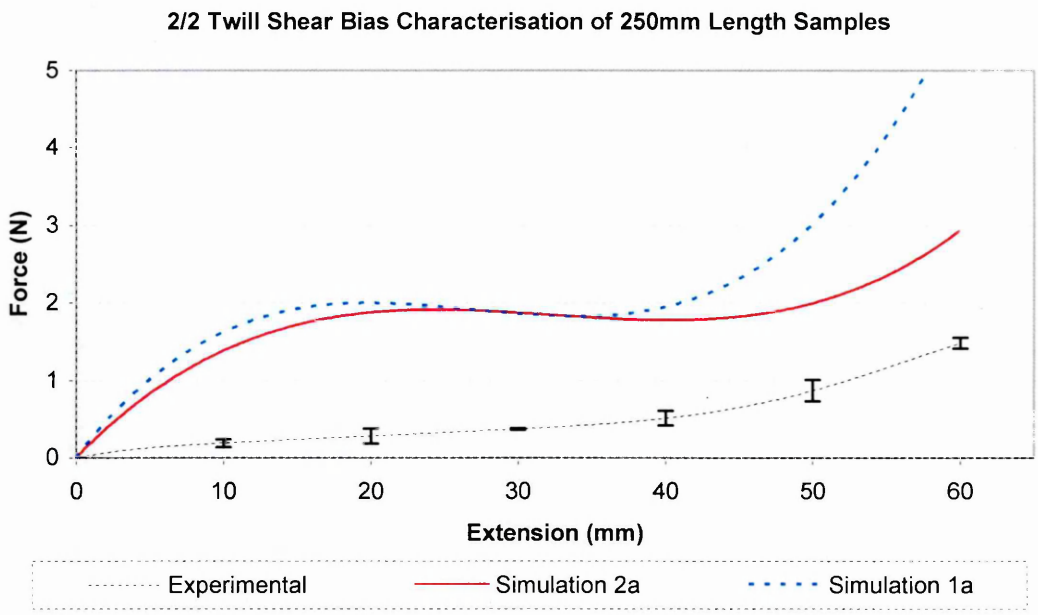

Fig. 5.11. Results comparison for 2/2 twill, 250mm length coupons

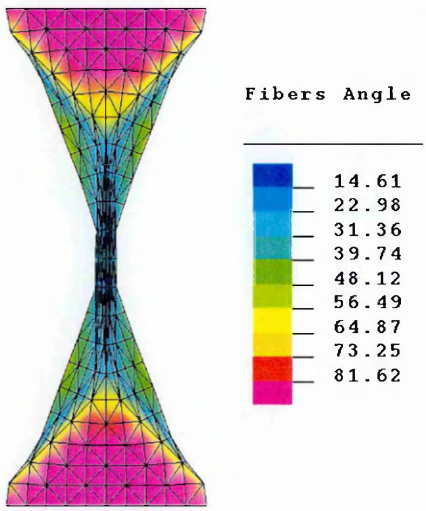

With both higher and lower shear moduli the width of the specimen centre is significantly lower than that experimentally required. The 250mm length coupon width is 23mm at 58mm extension and the 200mm length coupon width is 10mm at 48mm extension (figure 5.12), for simulation 1 and 2. These results compare poorly to the experimental width of 44mm.

Fig 5.12 Simulation 1: 200mm coupon fibre angle (°) at 48mm extension

Reducing the fibre elastic modulus was found to increase the central width of the deformed coupon. Since the deformation of the fabric is important to validate, simulations using lower moduli were conducted until the central coupon width was approximately correct. The results of figure 5.13 were then obtained.

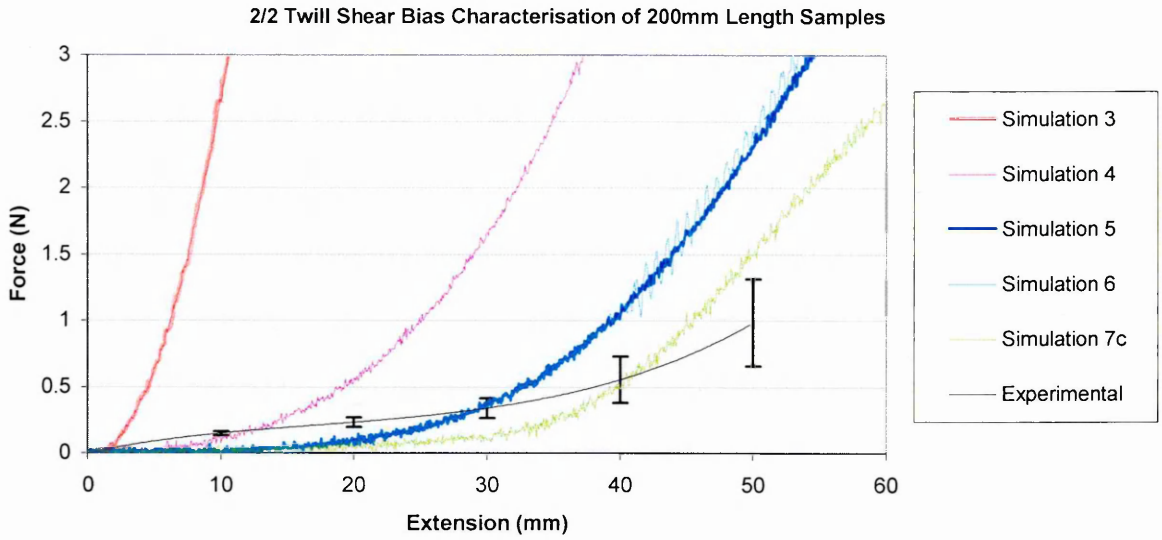

Fig. 5.13. Results comparison for 2/2 twill, 200mm length coupons

All results demonstrated in figure 5.13 have been simulated with a 9GPa fibre elastic modulus as found optimal to calibrate the specimen width. Simulations 3-5 have been conducted with the aim of optimising the deformational shear force.

Simulation 3 utilises a 0.5GPa shear modulus. Since the deformational force is overly high, the shear modulus has been progressively reduced, leading to the result of simulation 5 using a 0.015GPa shear modulus. The material model of simulation 5 produces a satisfactory 44.5mm central coupon width when extension is equal to 48mm. However, the similarity of the experimental and simulated shear force curves remain unsatisfactory. For simulation 5, longitudinal fibre strains of up to 14% occur in diagonally opposing corners of the coupon at 20% axial extension as indicated in figure 5.14.

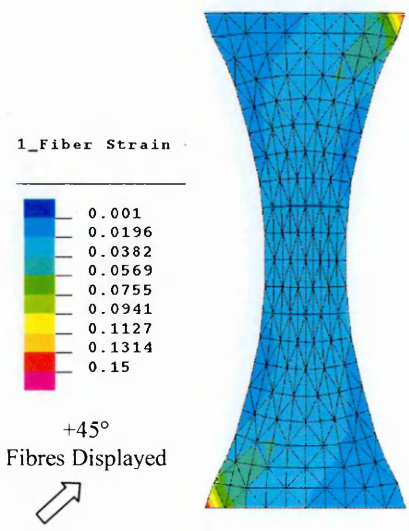

Fig.5.14. Longitudinal fibre strain of simulation 5,
a 200mm length 2/2 twill coupon at 20% axial strain

Simulation 6 is a variation of simulation 5 to verify the effect of activating the locking angle and post-lock shear modulus. A 40° locking angle has been used with a lower $5x10^{-3}$GPa post-lock modulus in an attempt to reduce the required shear force at higher extensions. Force instability subsequently occurs beyond ~40mm extension.

Simulation 7c utilises a user defined shear modulus curve. The modulus curve data is presented in appendix C and utilises a gradually decreasing shear modulus up to fibre locking. Despite this, the deformational force continues to rapidly increase at relatively low extensions.

For additional verification of the results obtained in simulation 5, identical material data has been utilised in simulation 5a for a 250mm length coupon as demonstrated in figure 5.15. A comparatively low longitudinal fibre strain of 0.14% occurs in diagonally opposing corners of the coupon at 20% axial extension.

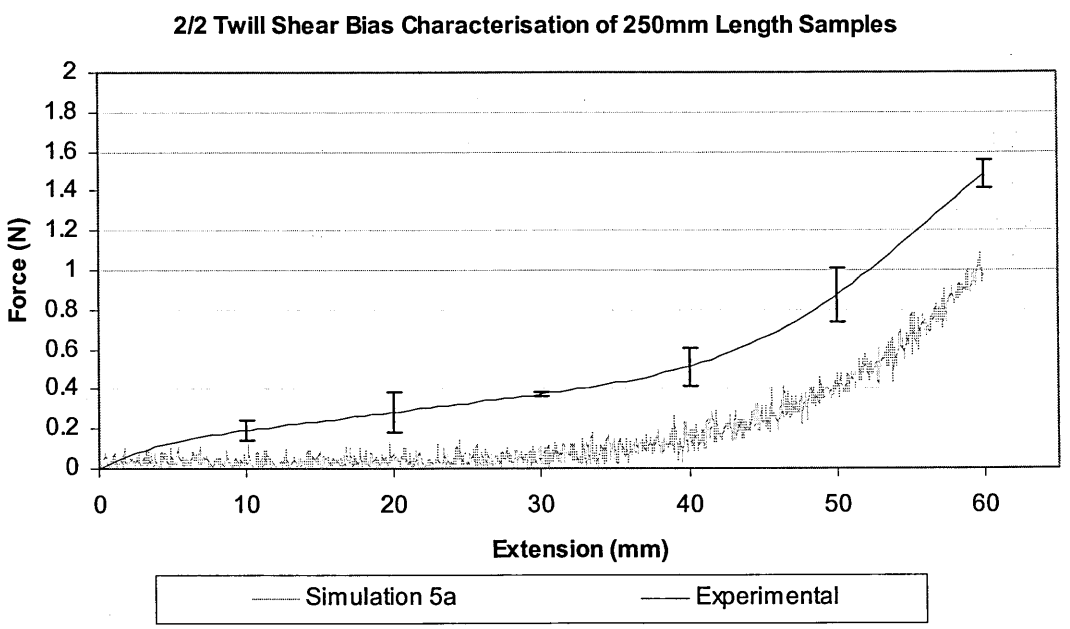

Fig. 5.15. Results comparison for a 2/2 twill, 250mm length coupons

Figure 5.15 demonstrates a simulated 250mm coupon produces improved correlation to the experimental force curve although the force magnitude is below that ideally required in all stages of the simulation. The central coupon width at 58mm extension is also low at 32mm, compared to the required 44mm.

5.4.3 NCF BIAS EXTENSION SIMULATION RESULTS

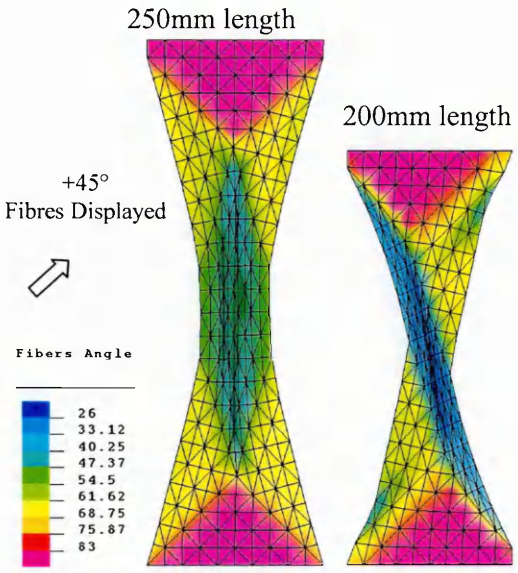

Fig 5.16. Simulation 9a and 9 fibre angles (°) at 20% axial extension

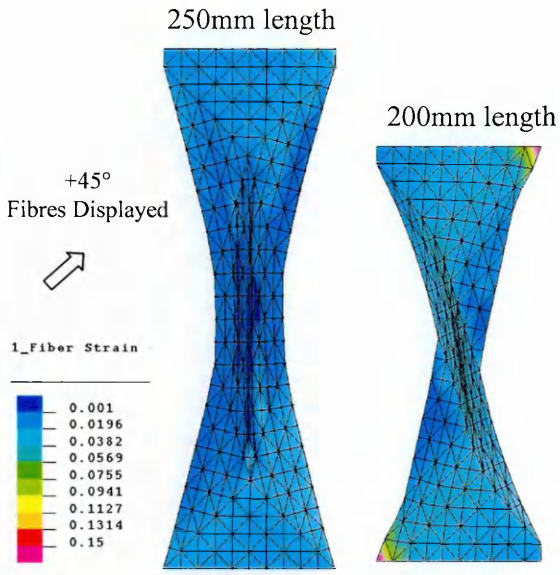

Fig5.17. Simulation 9a and 9 fibre strains at 20% axial extension

Simulations using 200mm 250mm length coupons were conducted using both high and low fibre moduli. A $1x10^{-7}$GPa pre-lock and 0.01GPa post-lock shear modulus is combined with a 20° locking angle and used in all simulations.

Simulations utilising the NCF material representation demonstrate a distinct difference in deformational style for the 200mm and 250mm length specimens. For the 200mm coupon, a region of high shear deformation is noted in the simulated transverse fibre direction of each individual element layer. This is not present in the 250mm coupon as demonstrated in figure 5.16. Additionally, higher strains of up to 15% are produced in diametrically opposing corners of the 200mm specimen, in orientations longitudinal to the simulated fibre orientation. This is demonstrated in figure 5.17.

A 40mm central width for the 250mm length coupon is attained at 50mm extension when using a low fibre modulus (simulation 8a) and 49mm extension when using high fibre moduli (simulation 9a). These results compares poorly with the 65mm extension noted during testing indicating the simulated deformation is excessively high.

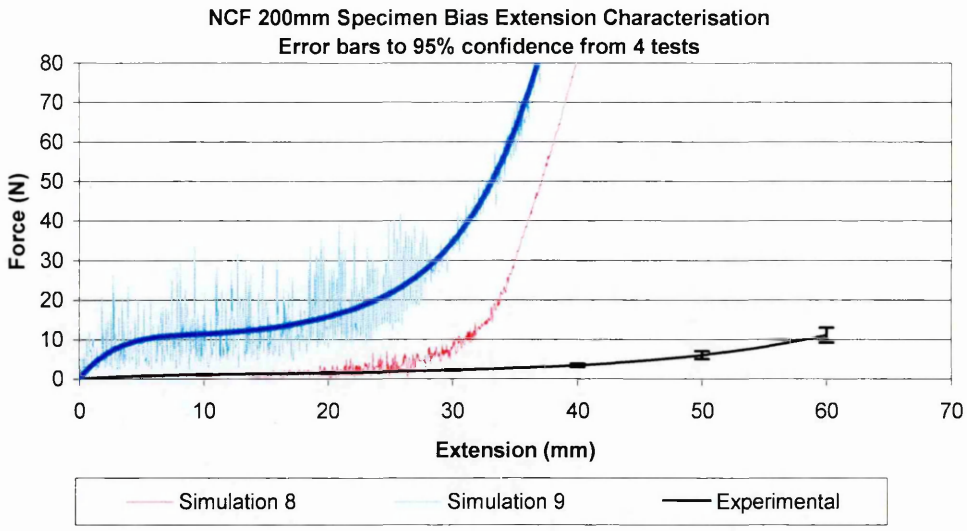

Fig. 5.18. Results comparison for NCF, 200mm length coupons

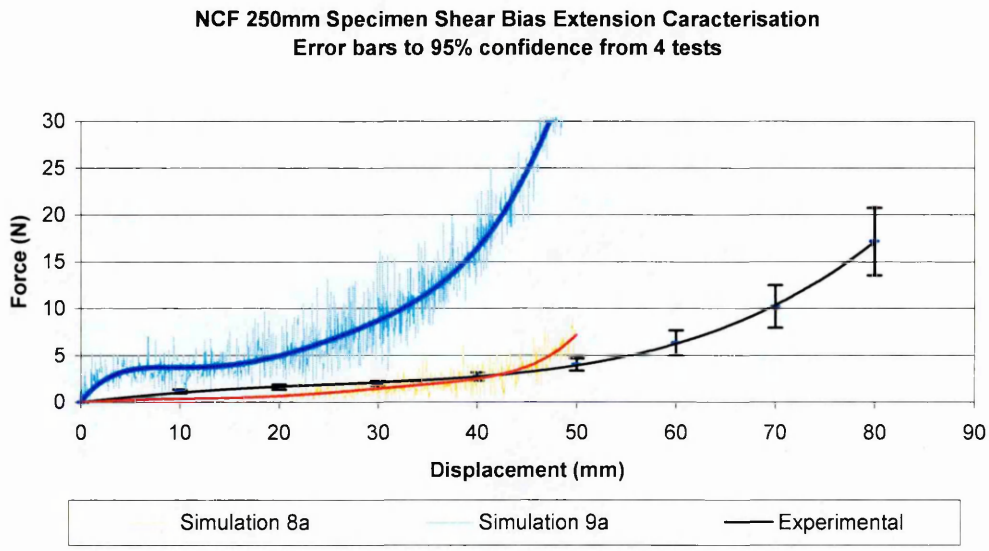

Fig. 5.19. Results comparison for NCF, 250mm length coupons

Force fluctuation is prominent with simulation 9 and 9a (figures 5.18 and 5.19) due to utilising a high fibre modulus. This is common with explicit FE methods, therefore, additional filtered lines are plotted.

Buckling occurred in the central high shear region for both sizes of simulated coupon and for both high and low simulated fibre moduli. This occurs despite a high bending factor of 100 and out-of-plane shear modulus of 10GPa. In addition, the fibre angles shown in figure 5.16 indicate locking is not initiated prior to buckling.

5.4.4 2/2 TWILL PICTURE FRAME SIMULATION RESULTS

The results of the picture frame test proved very satisfactory as is demonstrated in figure 5.20. However, the simulations required a user defined curve consisting of decreasing shear moduli up to the onset of locking at an inter-fibre angle of 20°.

The three simulation results demonstrate the effect of increasing fibre modulus. An optimum shear modulus curve of simulation A has been used for each. Simulation A utilises an elastic fibre modulus of 6GPa; simulation B, 9GPa; and simulation C, 300GPa. The deformational force increases with fibre modulus and becomes more pronounced at higher shear angles. The same force data as plotted against picture frame extension is documented in appendix C. Simulation A, with the lowest fibre elastic modulus of 6GPa, results in the optimal deformation force at shear angles up to ~55°.

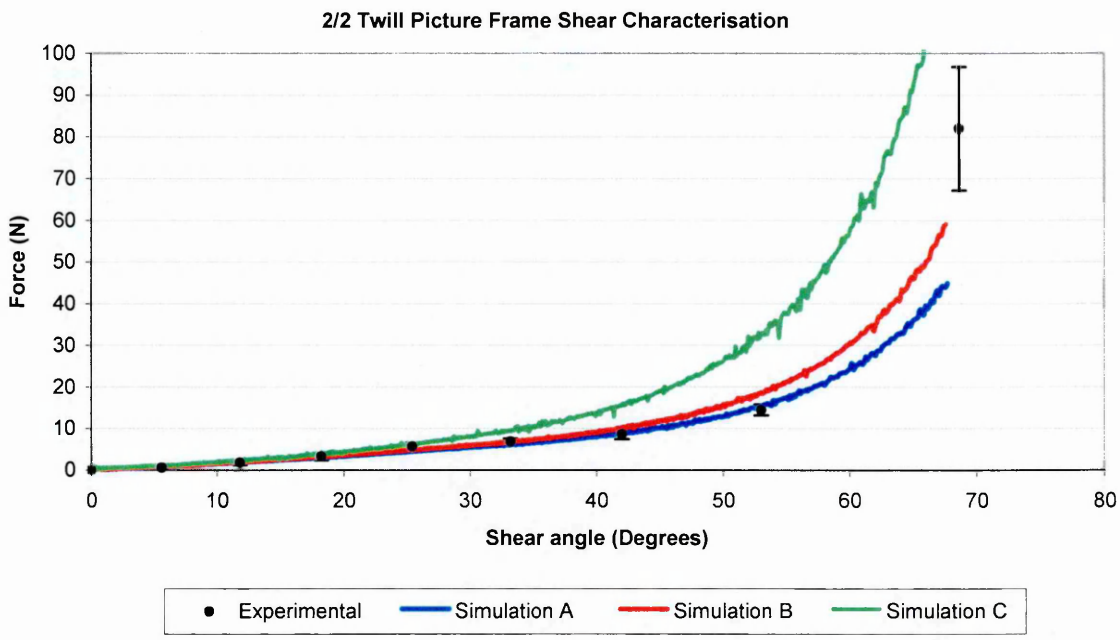

Fig. 5.20. Results comparison for 2/2 twill picture frame simulations

5.4.5 NCF PICTURE FRAME SIMULATION RESULTS

Once again, the simulations of the picture frame test produced results of greater precision than that of the bias extension simulations. These are shown in figure 5.21.

A higher fabric density, equal to that of carbon fibre, has been used during all simulations of the NCF picture frame test in an attempt to reduce the simulation time required. Simulations times are generally high for the NCF representation due to the low spot-weld element lengths.

A user defined shear modulus curve is required to prevent a rapid increase in required deformational force from occurring low shear angles. Simulation D utilised a 1GPa longitudinal and 0.01GPa transverse fibre modulus and produced the optimum force behaviour curve. However, initiation of major buckling within the fabric occurs at ~25° which compares poorly with the experimental 70° locking angle.

A higher transverse elastic fibre modulus of 0.1GPa was found optimal to initiate major buckling at a satisfactory ~65°. The force behaviour of this simulation is demonstrated as simulation E.

Simulation F is identical to simulation E but utilises a more realistic 300GPa longitudinal. Higher magnitude shear forces are produced accordingly.

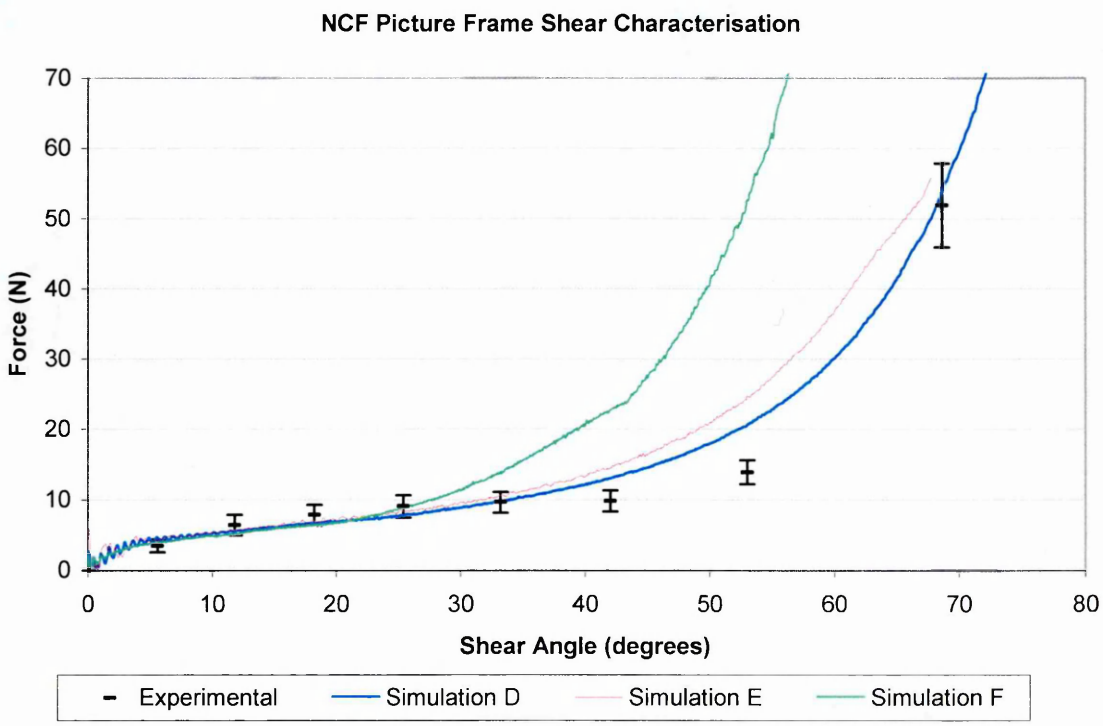

Fig. 5.21. Results comparison for NCF picture frame simulations

5.4.6 FLEXURAL RIGIDITY SIMULATION

Calibration simulations of the material 140 bending factor utilise the optimised material data of picture frame simulations A and E, for the 2/2 twill and NCF respectively. All material model inputs and bending lengths used are detailed in appendix C.

Results from the simulations conducted indicate this factor has little actual effect in the simulation code. In all simulations conducted the overhanging material drops rapidly, indicating almost negligible flexural resistance.

The bending factor was introduced to the material model to permit a reduction in bending stiffness based upon the high fibre modulus. However, in all simulations an excessive factor of 1000 is utilised in an attempt to *increase* the bending stiffness. Not all experimental test variations have been simulated due to the poor results obtained.

Poor results from initial simulations with the NCF material representation were thought due to a higher density used in the picture frame simulation to speed the simulation process.

However, subsequent simulation using the accurate material density yielded a similar result. Further simulations were conducted, first using an out-of-plane shear factor equal to 100, then utilising a higher 90GPa fibre elastic modulus in longitudinal and transverse orientations. With all variations a similar behaviour is observed, with the material displaying little flexural resistance.

A sequence of animation states from the simulation utilising 90GPa fibre moduli are shown in figure 5.22. This deformation is indicative of the results from all simulations.

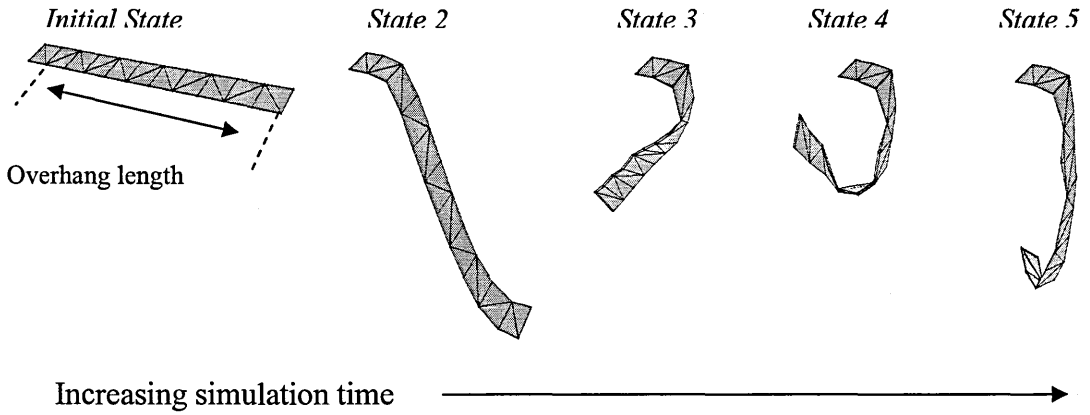

Fig. 5.22. Example of the fabric deformation during flexural simulation (simulation 'T')

5.4.7 2/2 TWILL DRAPING TRIAL SIMULATION RESULTS

2/2 twill draping trials have been conducted using the material inputs of simulation A. Additional fibre strain images and an example of the PAMFORM™ [47] simulation file is included in appendix C. A separate page of simulated results follows for each of the fibre lay-ups used during draping trials. For all images and graphs the larger hemisphere is to the left of the page.

2/2 TWILL 0°-90° SHEET RESULTS

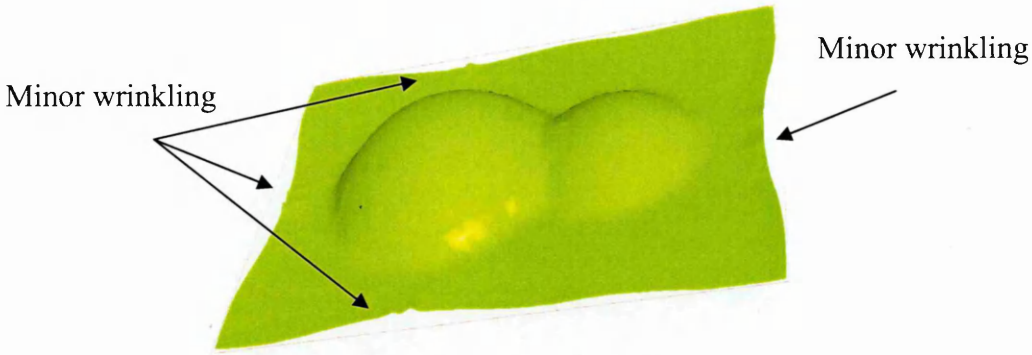

Fig. 5.23. 2/2 twill 0°-90°

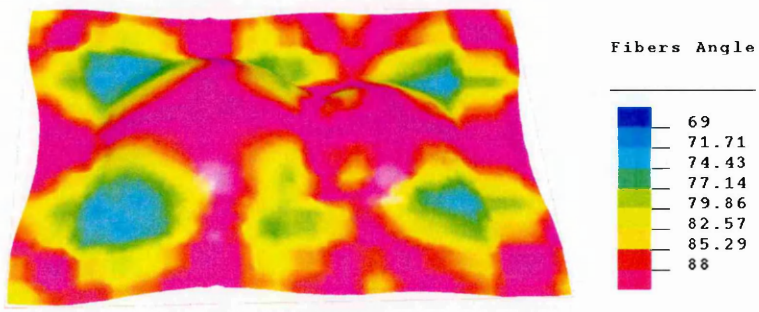

Fig. 5.24. 2/2 twill 0°-90° fibre angle variation (°)

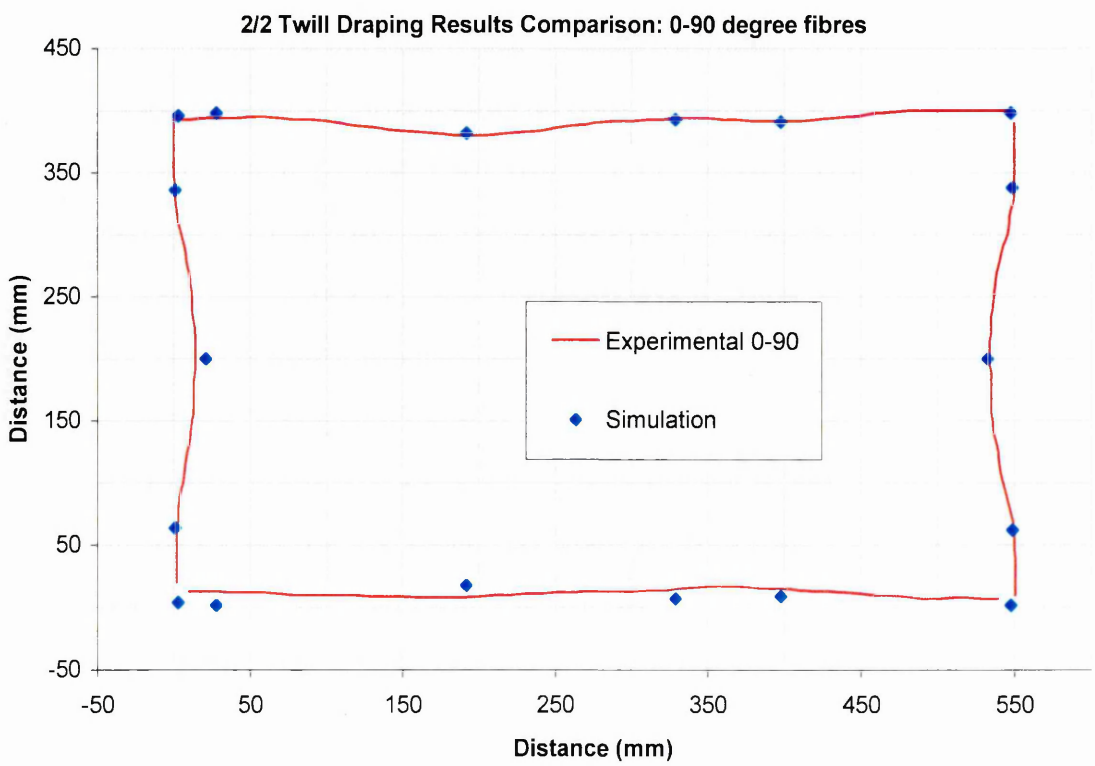

Fig. 5.25. 2/2 twill 0°-90° perimeter contraction comparison

2/2 TWILL ±45° SHEET RESULTS

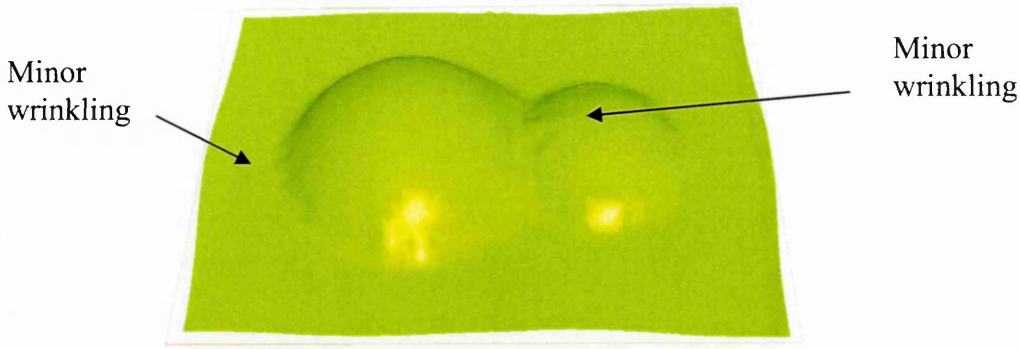

Fig. 5.26. 2/2 twill ±45°

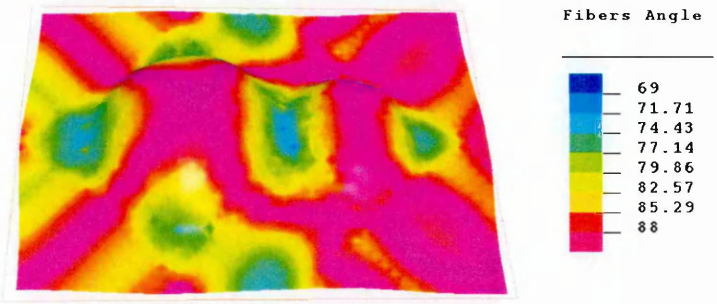

Fig 5.27. 2/2 twill ±45° fibre angle variation (°)

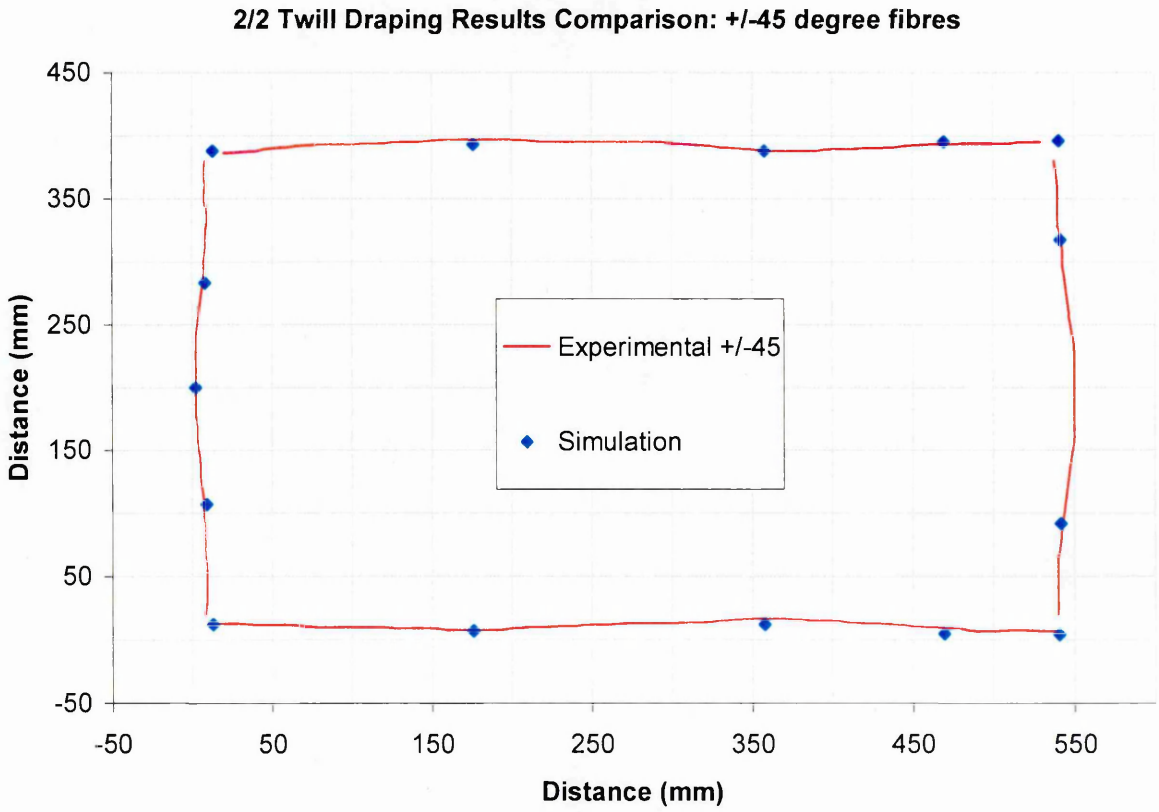

Fig. 5.28. 2/2 twill ±45° perimeter contraction comparison

2/2 TWILL 0°-90° SHEET ON ±45° SHEET RESULTS

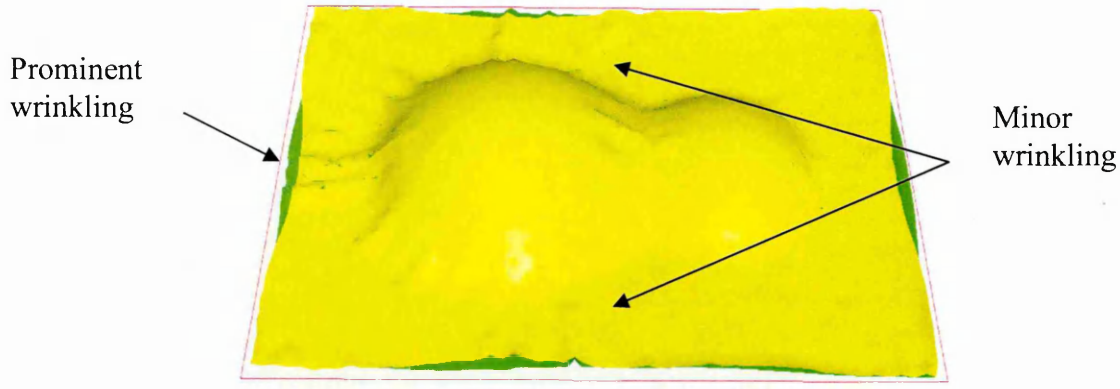

Fig. 5.29. 2/2 twill 0°-90° sheet on ±45° sheet

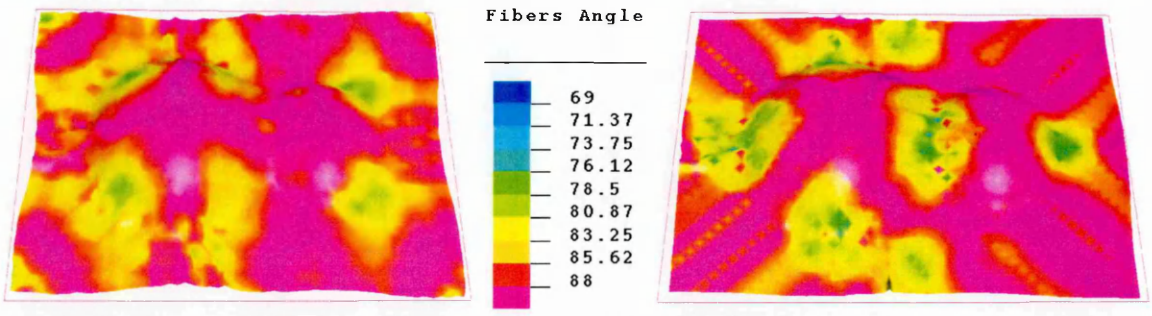

Fig. 5.30. 2/2 twill 0°-90° layer fibre angle *Fig. 5.31. 2/2 twill ±45° layer fibre angle*

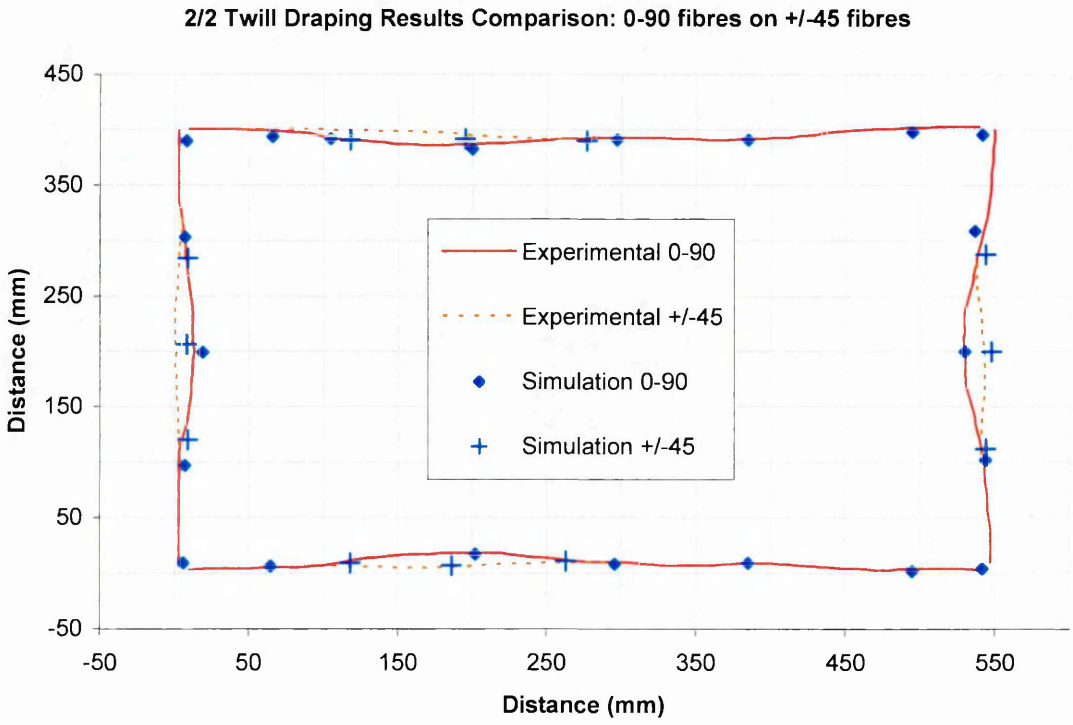

Fig. 5.32. 2/2 twill 0°-90° on ±45° perimeter contraction comparison

2/2 TWILL ±45° SHEET ON 0°-90° SHEET RESULTS

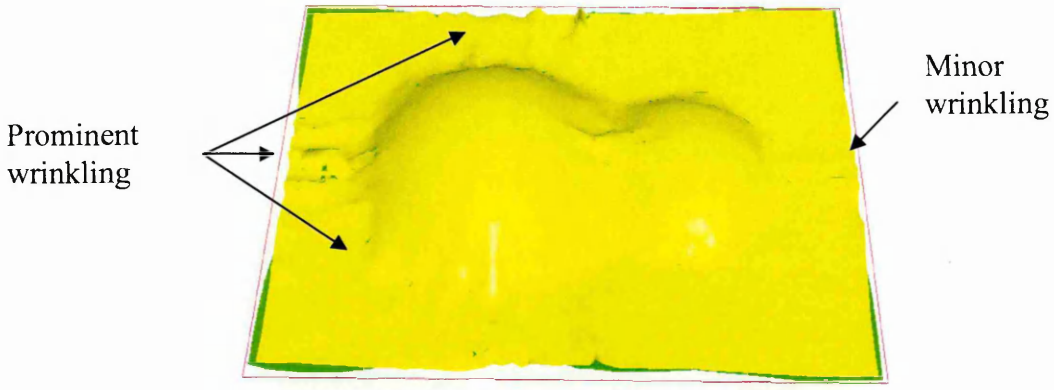

Fig. 5.33. 2/2 twill ±45° on 0°-90°

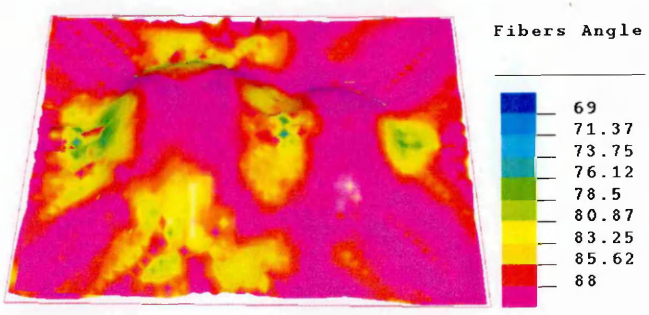

Fig. 5.34. 2/2 twill ±45° layer fibre angle

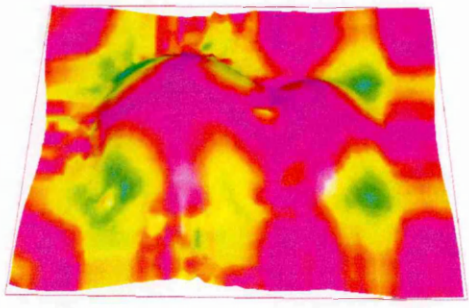

Fig. 5.35. 2/2 twill 0°-90° layer fibre angle

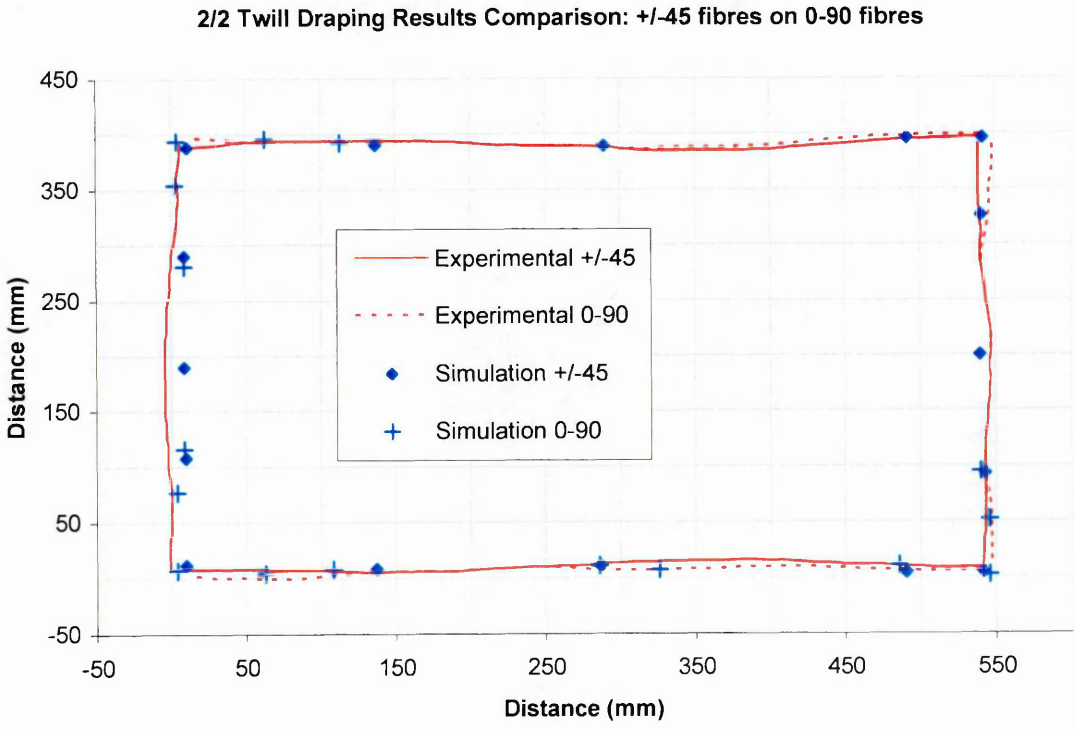

Fig. 5.36. 2/2 twill ±45° on 0°-90° perimeter contraction comparison

5.4.8 NCF DRAPING TRIAL SIMULATION RESULTS

NCF draping trials have been conducted using the material inputs of simulation E Additional fibre strain images and an example of the PAMFORM™ [47] simulation file is included in appendix C.

NCF 0°-90° RESULTS

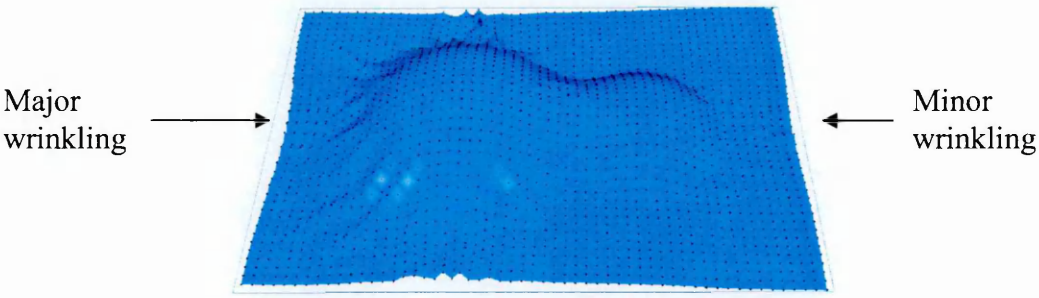

Fig. 5.37. NCF 0°-90°

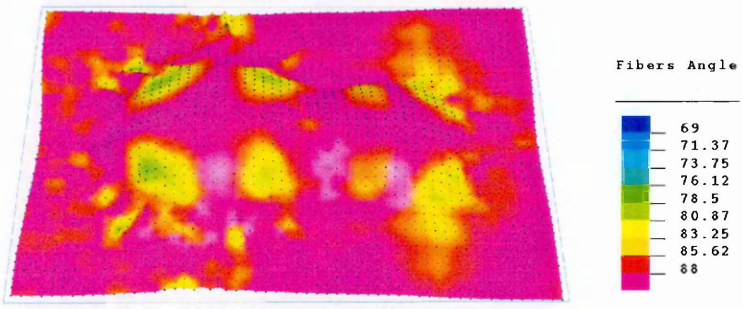

Fig. 5.38. 2/2 twill 0°-90° fibre angle variation (°)

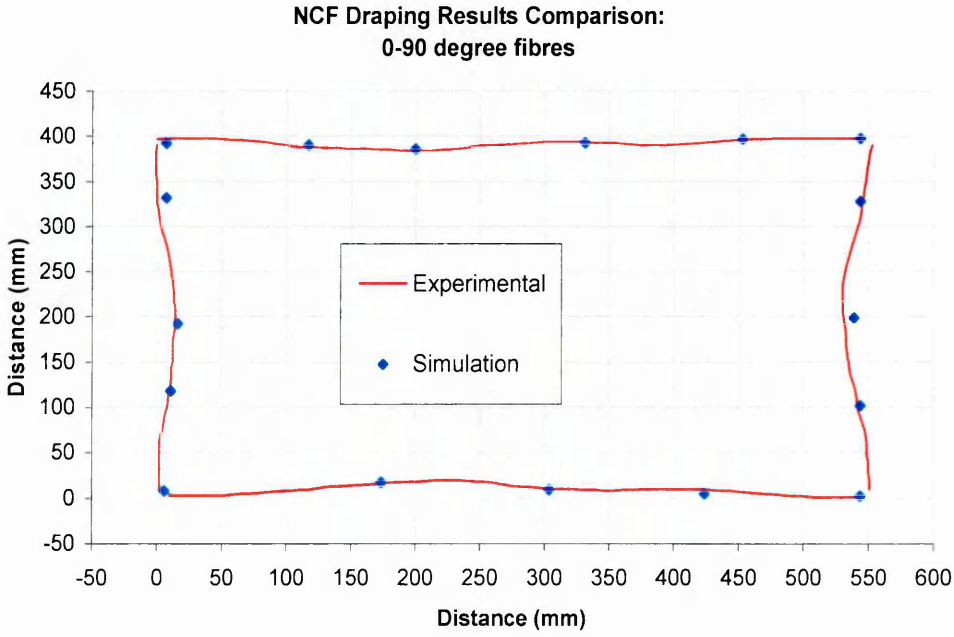

Fig. 5.39. NCF 0°-90° perimeter contraction comparison

NCF ±45° SHEET RESULTS

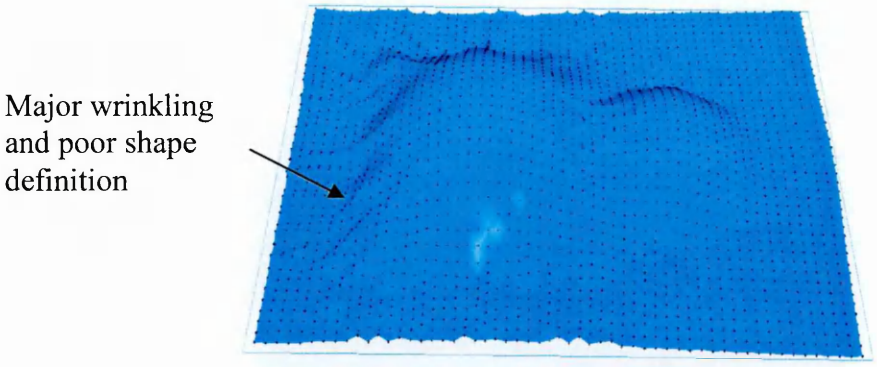

Fig. 5.40. NCF ±45°

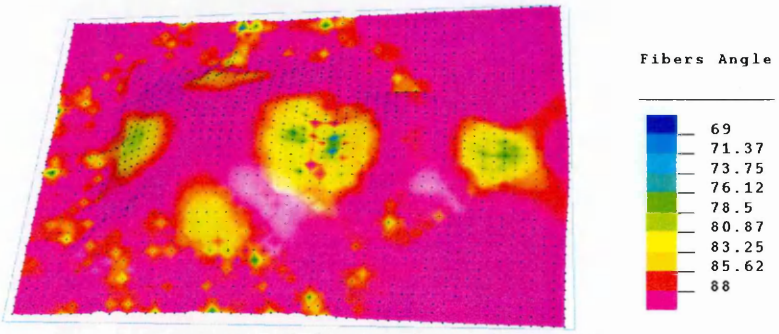

Fig. 5.41. NCF ±45° fibre angle variation (°)

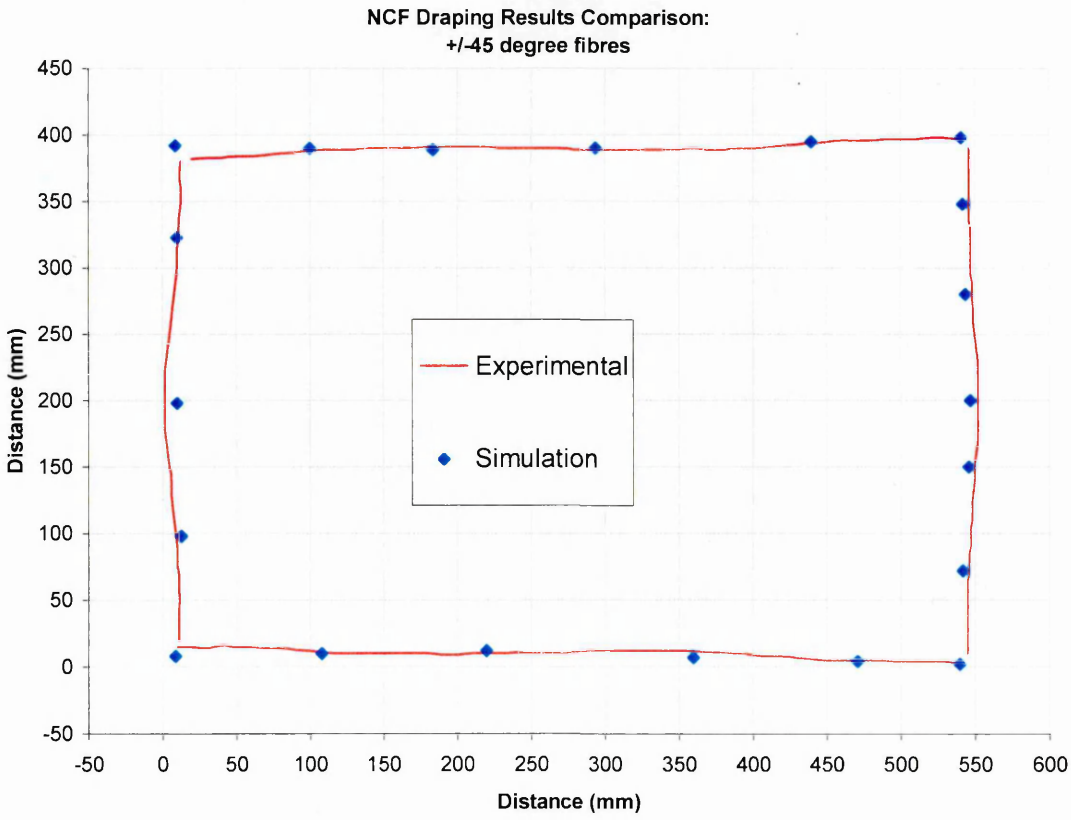

Fig. 5.42. NCF ±45° perimeter contraction comparison

NCF 0°-90° SHEET ON ±45° SHEET RESULTS

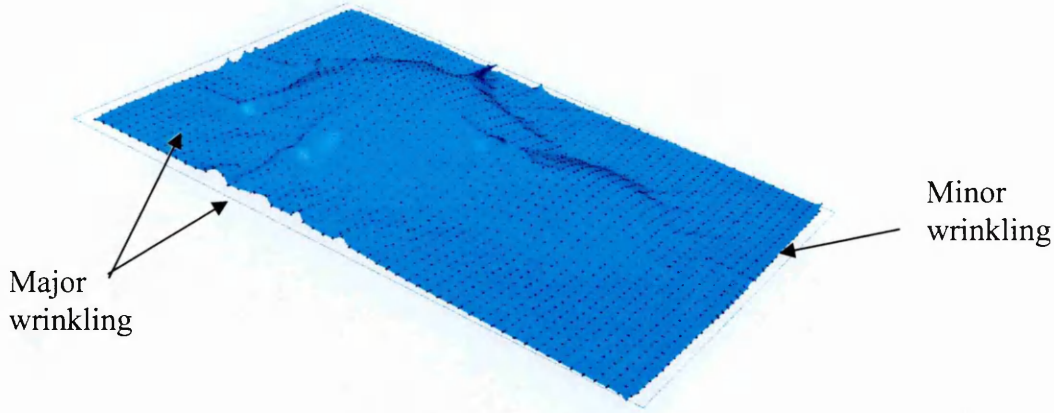

Fig. 5.43. NCF 0°-90° on ±45°

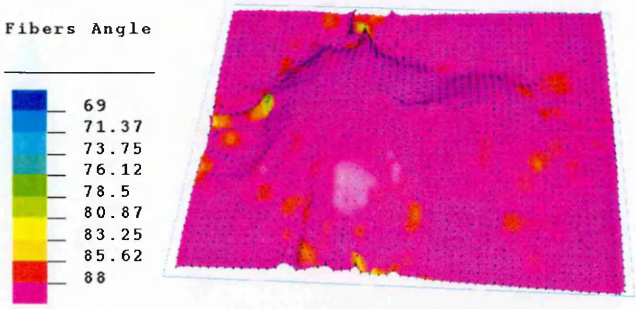

Fig. 5.44. NCF 0°-90° layer fibre angle

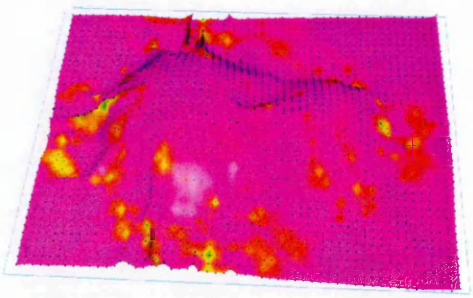

Fig. 5.45. NCF ±45° layer fibre angle

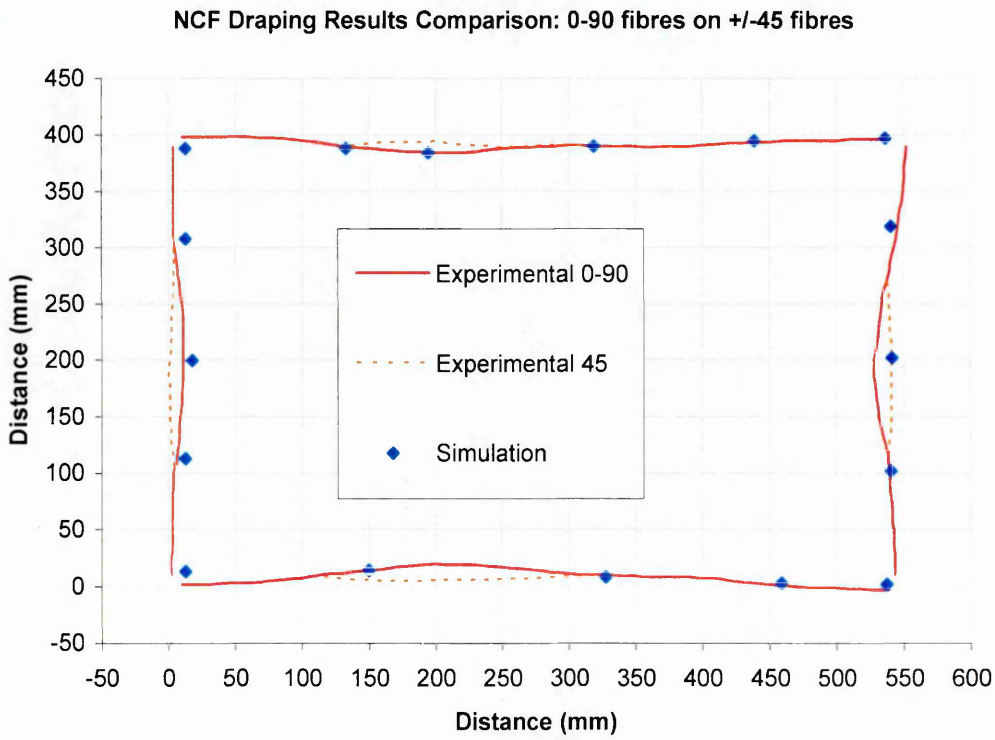

Fig. 5.46. NCF 0°-90° on ±45° perimeter contraction comparison

NCF ±45° SHEET ON 0°-90° SHEET RESULTS

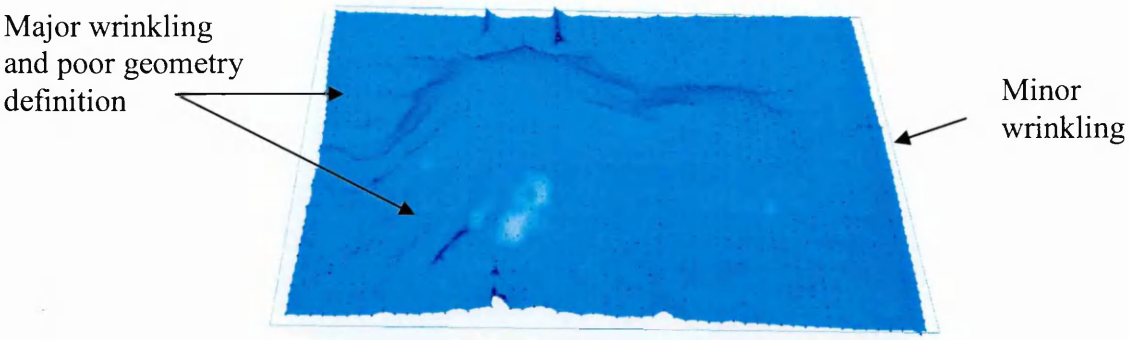

Fig. 5.47. NCF ±45° on 0°-90°

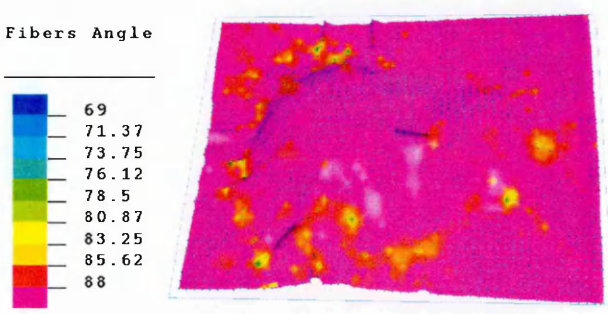

Fig. 5.48. NCF ±45° layer fibre angle

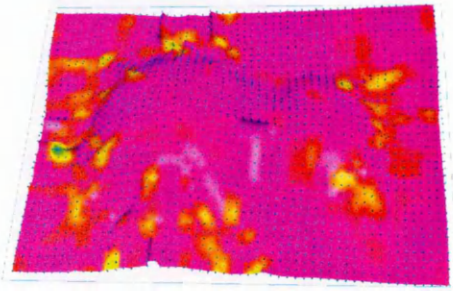

Fig. 5.49. NCF 0°-90° layer fibre angle

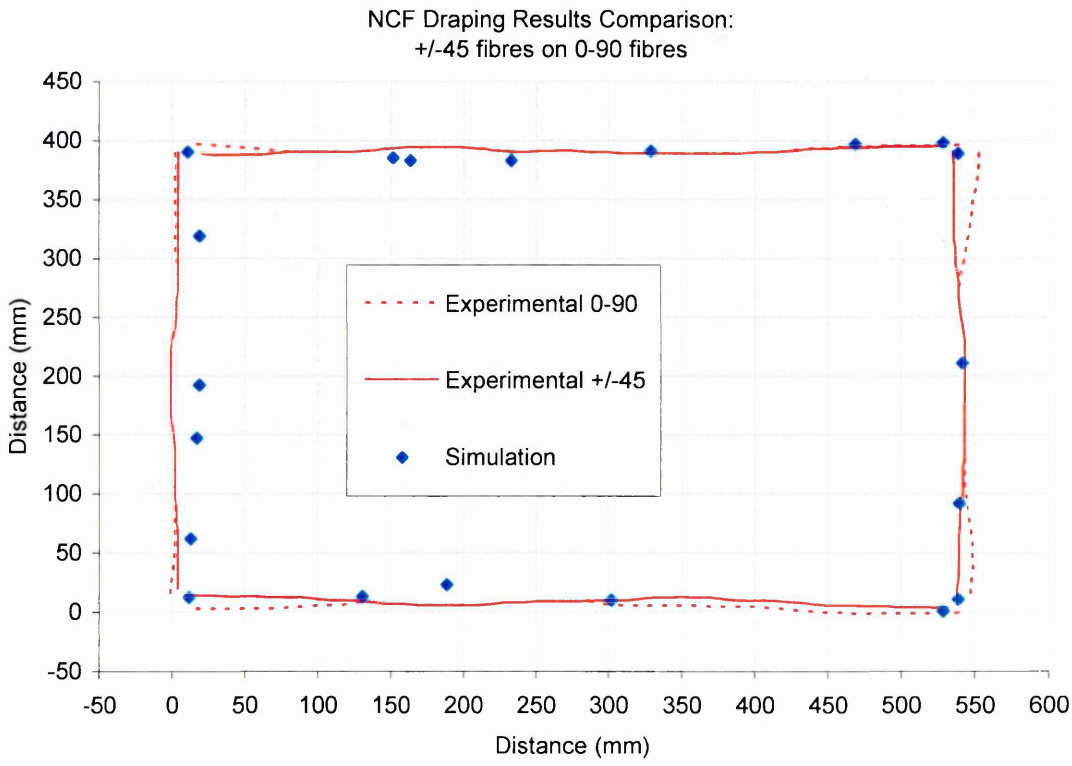

Fig. 5.50. NCF ±45°on 0°-90° perimeter contraction comparison

6 DISCUSSION

6.1 MATERIAL CHARACTERISATION CONSIDERATIONS

The extensive fabric testing programme used in this study has been developed to permit suitable characterisation of the dominant deformation mechanisms for both the NCF and 2/2 twill fabrics. The following section considers the applicability and precision of each testing procedure in addition to draping implications of the data obtained.

6.1.1 BIAS EXTENSION RESULTS DISCUSSION

The bias extension test is found necessary to better characterise the deformation of the NCF fabric. This is due to a higher degree of inter-fibre sliding and non-uniform shear when compared to the woven 2/2 twill fabric. This is induced through the use of unidirectional fibre layers.

The shear force behaviour of the NCF material is similar to that described in figure 3.5. Initial deformation of the material is dominated by in-plane shear with minor inter-fibre sliding occurring preferentially in zone II regions of the coupon. In-plane shear is dominant in the central region of the specimen (zone III of figure 6.1) where fibre tows are not constrained by tow clamping. Shear in this region is non-uniform and decreases to the perimeter of the specimen where free end rotation and inter-fibre sliding occurs. Since the required deformational force increases with shear, the majority of force required to deform the coupon is produced by material close to the central axis of the specimen.

Inter-fibre sliding is most prominent in zone II deformation regions, defined in 3.1.2. However, stitching of the NCF results in a variation in the degree of fibre slip that can occur in adjacent zone II regions, as demonstrated in figure 6.1

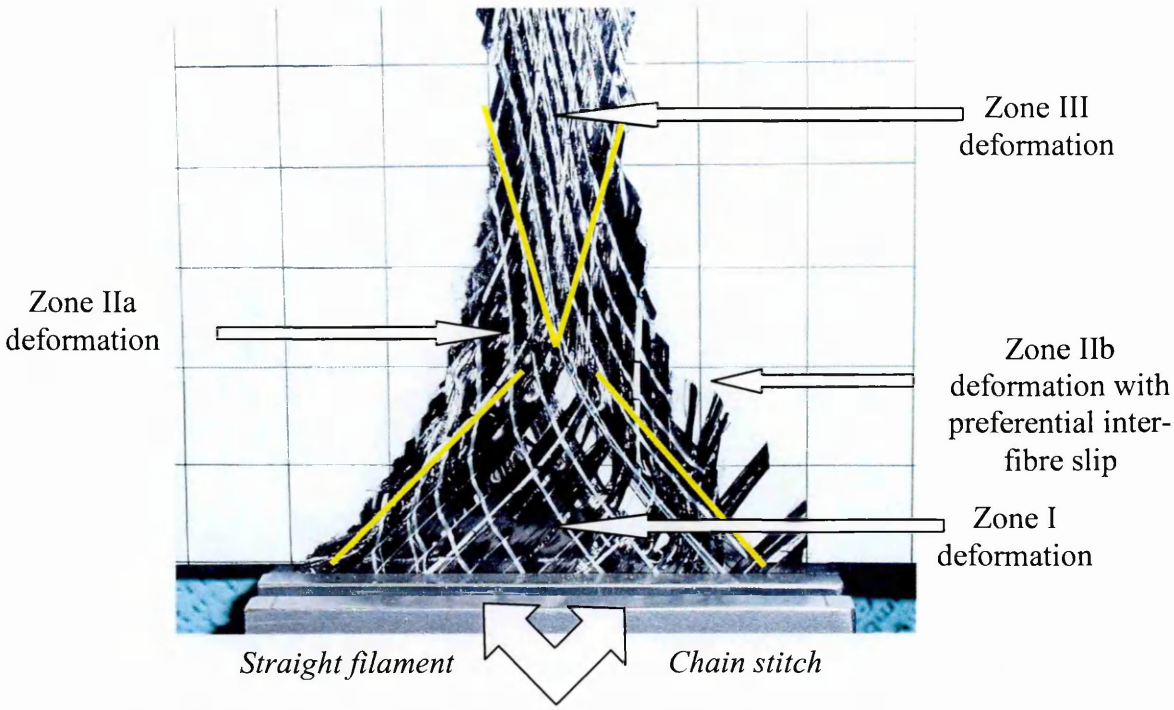

Fig. 6.1. NCF bias extension sample showing preferential inter-fibre sliding at one edge

In zone IIa, inter-fibre slip is reduced due to constraint by the chain stitch. Zone IIb displays preferential inter-fibre slip since low forces are required to permit sliding of the straight filament through the chain stitch. This filament sliding permits warp tows to 'pull-out' from the stitching constraint and results in the deformation of figure 6.1.

Zone I is defined by minimal deformation since the tows and stitches are constrained by the clamp. Deformation is, however, transitional between zone I and each adjacent zone II region.

Despite the directional variation in deformation observed, the bias extension test remains independent of initial fabric orientation. This is due to axial coupon symmetry and stitching parallel to the tows. However, the deviation in permitted inter-fibre slip can cause variation in pre-form fibre deformation unless the mould symmetry is aligned with one of the initial fabric fibre directions.

Through the observations described, the bias extension test has been proved a useful tool in ascertaining the deformational behaviour of NCF materials. These observations would not be possible when inducing pure shear through picture frame testing.

Contrary to this, the bias extension test is of limited use for woven fabrics of low stability, such as the twill fabric in this study.

During testing the twill fabric initially deforms by in-plane shear with minor inter-fibre slip in zone II regions. However, inter-tow sliding becomes dominant at a relatively low zone III inter-fibre angle of ~41°. This angle is an artefact of the test and is not related to the fibre locking angle. Sliding initiates with the unclamped tows at the zone I to zone II transition and causes the specimen to separate into two parts. This is demonstrated in figure 6.2.

Fig 6.2. 2/2 twill separation during bias extension testing
(Arrows denote the direction of observed fibre separation movement)

Prior to the initiation of separation the level of fibre-slip is noticeably less than that observed for the NCF. Tow crimp, created by the weave pattern, effectively 'locks' the tow cross-over points to prevent slip from occurring until sufficient force is applied.

The force against extension graph for the 2/2 twill bias extension tests is displayed in figure 4.12. Initiation of fibre slip at the zone III to zone II transition is indicated by the point of inflection at ~50mm (25%) axial extension. Pure shear and inter-fibre slip proceed to change dominance up to the force maxima, beyond which inter-fibre slip dominates. Continued slip dominance reduces the effective tow cross-over area of the separating sections. Therefore, the total friction and resistance to separation decreases and results in a decreasing measured force until separation is complete.

Data up to the initiation of separation is considered valid and has therefore been analysed (figures 4.13 and 4.14).

Scatter in data obtained from the picture test, for both fabrics, is of higher magnitude at higher extensions as would be expected from a curve of increasing gradient. Scatter is thought to be induced by deviation in coupon fibre orientation from the required ±45°. The NCF is also subject to variations in the degree of individual fibres 'crossing-over' between separately stitched tows. This causes local variations in deformation. Despite this the twill fabric demonstrates lower result precision due to lower fabric stability and greater variance in the dominant deformation mechanisms. Error bars indicated in figure 4.13 additionally demonstrate inconsistency for this reason.

Data from shear characterisation tests such as the bias extension and picture frame test can not be directly interpreted using relationships for shear behaviour of bulk materials. This is due to tow cross over points lying in the plane of the fabric, to which no relevant thickness can be applied as with solid materials [1]. Relative comparisons of *fabric* shear can be conducted using data analysis methods described in [1].

6.1.2 PICTURE FRAME RESULTS DISCUSSION

Fabric deformation is constrained to pure shear when using the picture frame test rig. However, after initiation of the picture frame test it has been observed that micro-buckling of individual fibre tows is induced along all clamped edges for both fabrics (figure 6.3 demonstrates this buckling for the 2/2 twill fabric). This out of plane deformation is less prominent with NCF due to stitching constraints placed upon the clamped tows.

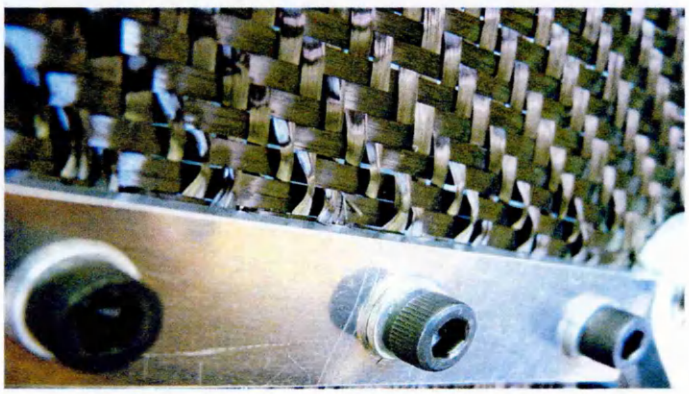

Fig. 6.3. Micro-buckling of 2/2 twill tows at the clamp edge

This fibre buckling will theoretically artificially increase the force required to shear the material, especially for the constrained NCF tows. This is due to bending stiffness of the fibre tows being higher than the fabric shear modulus. This error is difficult to quantify, is generally assumed negligible when using large fabric specimens and is minor compared to errors induced through fibre misalignment.

Operator error leading to fibre misalignment causes fibre strain and is the main cause of error due to high fibre moduli. The degree of fibre strain also increases with shear resulting in larger scatter of data at higher shear angles. However, result variation for both fabrics is relatively low as indicated by the error bars of figures 4.14 and 4.15.

Results obtained for both fabrics show similar deformational mechanisms and shear behaviour to that described in figure 3.7. Initial deformation is dominated by inter-tow friction. As shear angle increases, effects of tow compaction lead to the requirement for higher shear forces. Compaction becomes increasingly dominant until compression of the fibres, transverse to the extension direction of the test, results in fabric buckling.

Comparison of results between the fabrics indicate a higher force is required to deform the NCF at lower shear angles. It is postulated that shear of the NCF chain stitch is the dominant cause of this observation. During tow shear the chin stitch must either conform to the shear and stretch or cause compaction of the tow fibres (figure 6.4 demonstrates stitch stretching). Stitch stretching is observed to dominate. With no stitch constraint, the shear force measured for the twill fabric is attributable to inter-tow friction at low shear angles. Tow compaction is present at all shear angles for both fabrics but only dominates at higher shear angles prior to locking.

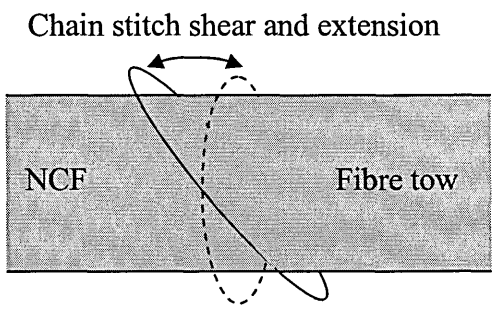

Fig. 6.4. Example of chain stitch stretching to accommodate pure shear in NCF

Conversely, a higher relative shear force is required for the twill at higher shear angles. This is attributed to constraints of the woven structure causing a higher degree of tow compaction than that imposed by the unidirectional layers of the NCF.

The fabric locking angle is denoted by a rapid rise in required shear force. Locking angles for the NCF and twill fabric are low at 20° and 21° respectively, demonstrating the high conformability of these fabrics. This is determined at the onset of out-of-plane buckling and has been calculated from crosshead extension measurements to 0.5mm accuracy. Since the shear angle is proportional to the inverse cosine of the measured crosshead displacement, the shear angle accuracy decreases with extension. At ~20° this accuracy equates to approximately ±0.5°.

As described for the bias extension test, conventional shear data analysis for bulk materials can not be applied to fabrics.

6.1.3 FLEXURAL RIGIDITY RESULTS DISCUSSION

Flexural rigidity tests were conducted to ASTM-D1388 [45]. Results indicate both fabrics to have higher bending stiffness when coupons are tested with fibres parallel to the overhanging length. This is due to a higher effective longitudinal modulus of the specimen as classical laminate theory would predict. With fibres in this orientation, the NCF also shows considerably higher bending stiffness compared to the 2/2 twill; with a bending length of 182-188mm compared to 124mm respectively. Combined with the low force shear behaviour of the 2/2 twill, this would indicate the twill fabric to be more conformable to a given mould geometry than the NCF material.

Using the ASTM standard, a defined slider displacement rate of ~120mm/min is used in moving the fabric specimen from the horizontal surface. It was noted during testing that this displacement rate may require reduction for carbon fibre fabrics since time dependant deflection behaviour is observed.

This is believed to be a visco-elastic effect, induced by polymeric 'sizing'. This coats each individual carbon fibre to prevent fibre damage and produce an adherent surface for a polymeric matrix. This is present around all types of carbon fibre. Lower displacement speeds may be more applicable to ensure equilibrium deflection is attained. This is a recommendation for future testing as the standard has been adhered to in this study.

Testing of the ±45° fabric specimens also resulted in shear extension of the specimens as the material deforms. This alignment of fibres longitudinal to the overhanging specimen would have the effect of artificially increasing bending stiffness and, thus, the measured overhang length. More importantly, the actual shear extension would also artificially increase the measured overhang. For comparison between fabrics of differing shear behaviour these effects could result in significant errors. However, for this project the increase in specimen length is also present in the FE simulations, minimising any errors.

6.1.4 FRICTION TESTING RESULTS DISCUSSION

Friction testing has been conducted using a relatively simple characterisation method. The method was used to ascertain dynamic and static friction, although only dynamic friction is used in the FE models as only one coefficient can be assigned to the simulated contact interfaces. Average dynamic friction coefficients have been utilised since the forming process is dominantly dynamic. Relative material displacement between the tooling and separate fabric layers generally occurs throughout the draping process. Exceptions to this are assumed minor and depend upon the mould geometry.

For this study fibre movement was observed to be continuous until forming was completed in all regions, with the exception of that between the two hemispheres. A subsequent deformation cycle of material bridging the hemispheres is observed as the forming membrane conforms to the mould.

The relatively high static coefficients of the mould surface therefore contribute to the occurrence of hemisphere bridging noted in experimental and simulated draping trials. The fabric conformability and rubber membrane elasticity limit are additional contributing factor to this bridging.

The results indicate friction coefficients between both fabrics and the anodised forming plate are relatively low. Higher friction contact between the fabrics and rubber membrane of the forming equipment will therefore dominate the fabric constraint and control tension within the fabric material. However, high membrane elasticity will result in low tension and additionally permit the material to slide and conform to the mould geometry.

Errors are minor for the static friction coefficients. These occur due to measurement accuracy and inertial effects transmitted to the test specimen through quasi-static extension of the measuring spring balance. A measurement accuracy of 0.5N results in minor friction coefficient errors of ±0.005.

Higher errors are induced in the dynamic coefficients obtained as inertia of the moving sample and mass cause lower forces to be measured when sliding of the sample stops. This error is thought to be demonstrated by results of the 2/2 twill and mould contact, whereby a high static measured force, and thus a high static friction, subsequently results in a low dynamic measured force, and thus a low dynamic friction.

The precision of the results obtained are suitable to the current work to induce the required degree of interaction between the simulated fabric sheets and tooling surfaces. Precision in other tests, such as NCF tow pull-out and shear characterisation, are of greater consequence to the simulation results.

6.1.5 TOW PULL-OUT RESULTS DISCUSSION

Warp tow pull out results show poor consistency as indicated by the error bars of figure 4.16. This is due to a varying degree of fibre cross-over between tows, through the NCF stitching. A high degree of fibre cross-over results in higher forces required to remove tows.

As fibre tows are removed from the fabric, fibres which cross-over stitching filaments become progressively entangled. A gradually increasing force is therefore required to continue removing tows from the fabric.

Higher forces are required to remove weft tows as shown in figure 4.17. The weft tows are constrained by individual chain stitch loops and as such have a greater tow density than the warp tows. Additionally, the observed degree of fibre cross-over is much higher than that for the warp tows. These two factors result in higher forces required to remove weft tows, i.e. 7 times the force of removing a warp tow by 5mm is required to remove a weft tow. The force gradient is also significantly higher, although this is observed to reduce as stitch breakage occurs.

The weft tows are therefore considered to be locked in the simulation model. Since the fabric will deform by the mechanism of least resistance, the spot-weld elements of the NCF representation are calibrated to the warp tow pull-out results.

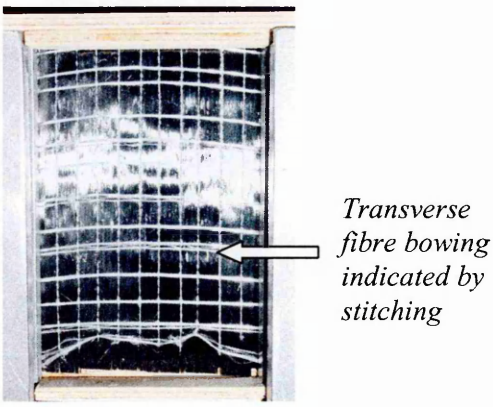

The main errors of warp tow pull-out results occur due to bowing of transverse fibre tows in the pull-out direction. This is demonstrated in figure 6.5. This deformation acts to compress the pulled fibre tows and causes higher forces to be measured.

Fig. 6.5. NCF tow-pull showing fibre bowing

This could be limited by inducing tension in the transverse tows but this is could not be implemented with the equipment available and is considered a limitation of the technique used in this study.

Included in appendix B are results for 2/2 twill pull-out tests. These have been conducted for completeness and include unusual and cyclic force behaviour. This behaviour is interpreted to be a result of initial tow crimp since the results are cyclic over two tow widths, the repeating pattern of a 2/2 twill. As tows are pulled through, the required force increases to induce an opposite crimp pattern while lower forces are then required to return the tow to an original crimp pattern.

6.1.6 DRAPING TRIAL RESULTS DISCUSSION

Less fabric deformation is produced using the double hemisphere mould than was initially believed necessary. As such, no wrinkling is produced when draping all variations of a single fabric sheet. Bridging between hemispheres, however, does occur as a combination of fabric properties, rubber membrane elasticity and frictional effects of the double hemisphere mould. This is described in 6.1.4.

The fabric shapes produced by the individual 0°-90° and ±45° fibre lay-ups are similar for both fabrics tested. This is to be expected as in-plane shear is the dominant mechanism observed in the draped fabric. As such, stitch induced differential fibre slip of a ±45° NCF sheet is not observed.

Inter-fibre slip is only observed to occur at fabric edges where tow constraints are minimal and tow end rotation is permitted.

The occurrence of wrinkling when draping more than one fabric sheet demonstrates the importance of simulating interaction between fabric plies. Although not simulated precisely in the FE simulations conducted, the ability to model these interactions is possible. This is not true for mapping simulation methods.

The wrinkling induced when draping more than one fabric sheet is mainly concentrated between hemispheres. This is produced by a number of factors. Each bi-directional fabric sheet preferentially shears at 45° to the fibres. Fabric tension between the hemispheres is high as mould friction prevents the fabrics from fully forming between the hemispheres. Therefore, tension in the separate fabric sheets induces a high degree of fabric interaction as controlled by friction. This friction is sufficient to prevent both fabric layers from deforming in their relative preferential shear directions. Fibre compression and wrinkling is therefore induced, transverse to the mould symmetry, as the fabric layers attempt to form to the smaller effective mould radius between the hemispheres.

Wrinkling is also noted to the base of the large hemisphere in figure 4.21. This is for a 0°-90° NCF sheet draped upon a ±45° fabric sheet. The wrinkle observed is thought to be an effect of local fatigue in the rubber membrane resulting in localised rubber stiffening. This is proposed since wrinkling would theoretically be observed either parallel to or at 45° to the fabric fibres; if excessive localised fibre tension or induced fibre compression causes a wrinkle, it will generally be aligned parallel to the fibre direction; if fibre locking occurs, wrinkling will generally be aligned at 45° to the fibre direction. Proximity to the 0° fibre direction indicates fibre tension to be an important factor in this example, although rubber membrane effects can be significant in inducing wrinkling.

The dominant errors in the draping trials are a result of initial misalignment of the fabric on the mould. Figure 5.25 demonstrates non-symmetry of the experimental fabric shape as an example of this problem. Ideally more than one draping experiment should be conducted for each lay-up to permit average contraction measurements to be used. Time and material constraints prevented this in this study.

Precision of the fabric perimeter measurement is affected by fibre slip and tow end rotation. With tow ends protruding from the fabric perimeter an observational average measurement is taken.

6.2 SIMULATION DISCUSSION

The aim of the simulation programme was to validate material model inputs and validate the final material models through simulation of the draping trials. The following section considers the suitability and applicability of the simulations conducted to the actual testing, in addition to discussing the results obtained.

6.2.1 NCF TOW PULL-OUT SIMULATION DISCUSSION

The tow pull-out simulation was the first to be conducted as no material data is required for the shell element layers. The test only concentrates on the deformation of the connecting inter-layer elements of the NCF representation. As such, strain in the shell element layers is not desirable. This is justified since the actual carbon fibres can be considered inextensible.

The data obtained from this simulation is valid for use in simulated draping trials since stitch element density is identical for both. This is a consequence of using an identical element distribution.

The calibration of the simulation proved very successful since the desired force curve is a close match to that obtained by experiment. However, difficulty is produced in justifying the relative dominance of the shear ('slip') and normal moduli assigned. In the calibrated inter-layer element data the shear modulus is a minimum of 19 times lower than the normal modulus. The quantitative relationship is justified since removal of a fibre tow, normal to the fabric, is considered to require higher forces since stitching strength and fibre cross-over are the controlling factors.

Slip, therefore, is controlled only by the fibre cross-over effects between stitched tows and is assumed to require a lower force. Qualitative justification of the values would require additional testing to ascertain the force required to remove a tow normal to the fabric.

6.2.2 BIAS EXTENSION SIMULATION DISCUSSION

The bias extension simulation produced a good opportunity to investigate the ability of the material models to deal with the various deformation mechanisms of the two fabrics tested.

Initial trial simulations of the bias extension test, using fibre elastic moduli of 500GPa, were conducted with a quadrilateral shell element layer of the 2/2 twill representation. These results are not included as excessively high forces were required to deform the simulated coupons. The curves produced are similar to those displayed in figure 5.10, with the exception that the force level reaches ~20kN unless the fibre modulus is reduced excessively. This is believed to be an artefact in how the material model is applied to quadrilateral elements. Subsequent trials with triangular shell elements produced more realistic results as demonstrated by figure 5.11. Triangular elements are therefore considered more stable and, as such, have been utilised in all simulations.

Results displayed in figures 5.10 and 5.11, for simulation 1 and 1a, indicate a high fibre elastic modulus of 500GPa to be detrimental to the state of deformation in the coupon. As indicated by figure 5.12 the central shear zone of the coupon is simulated to have a minimum inter-fibre angle of ~15°. This is despite using a high locking angle of 40° to increase the shear modulus from $1x10^{-6}$GPa to 0.1GPa and hinder deformation.

The results indicate a higher shear modulus should be assigned to reduce the level of deformation permitted. Conversely, consideration of the force data indicates a lower shear modulus should be used to calibrate the data as the force level is excessive. Reducing the pre-lock shear value to $1x10^{-7}$GPa has little effect on the state of deformation and only reduces the required deformational force at moderate axial strains. Only through reducing the fibre elastic modulus to 9GPa does the state of deformation better represent that obtained by experiment.

These results are believed to represent a limitation of the current material code. During experimental testing of the fabric the fibre elastic modulus is such that the fibres are assumed inextensible. The shear behaviour of the material is therefore independent of the fibre elastic modulus. Without simulating individual fibre tows, the material 140 model, included in PAMFORM™ [47], appears to utilise coupling between the fibre modulus and shear behaviour. As a result, calibration of the material code could be required, in addition to the material inputs, to ensure the coupling is precise for the fabrics being tested.

The requirement for low simulated fibre moduli is coupled by a requirement for a relatively high shear modulus value. This is to calibrate the shear force curve data, i.e. simulation 5a for a 250mm length coupon. For the 200mm specimen (simulation 5) the initial force level is lower than required but increases rapidly to be much higher than required.

Figure 5.14 indicates this increase in force may be due to simulated fibre extension. The simulated longitudinal fibre strain is twice that in a 200mm coupon than a 250mm coupon (simulations 5 and 5a respectively). The simulation code therefore appears to simulate fibre bridging for the 200mm length coupons. Bridging describes fibre tows being constrained at the central plane. This results in fibre strain and high measured forces due to the high fibre modulus. This result is emphasised when simulating the NCF material, as a low transverse fibre modulus permits excessive shear deformation in the 200mm coupon, transverse to the simulated fibre direction (figure 5.16). Figure 5.17 indicates high longitudinal fibre strain in the 200mm NCF coupon compared to the 250mm coupon, justifying the interpretation of this bridging effect. The excessive transverse shear is not comparable to the preferential slip of the experimental coupons as this deformation mechanism can not be directly simulated.

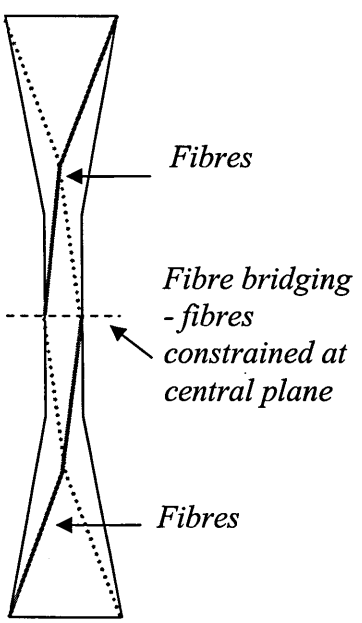

Figure 6.6. Schematic of a simulated 200mm bias extension coupon

In experiments, minor fibre slip and free tow end rotation prevent fibre bridging from causing high measured forces. The observed simulation results are therefore induced by a material model that is incapable of directly simulating these mechanisms. The clamped fibres are separated by a region of shear when simulating a 250mm length coupon, negating this effect.

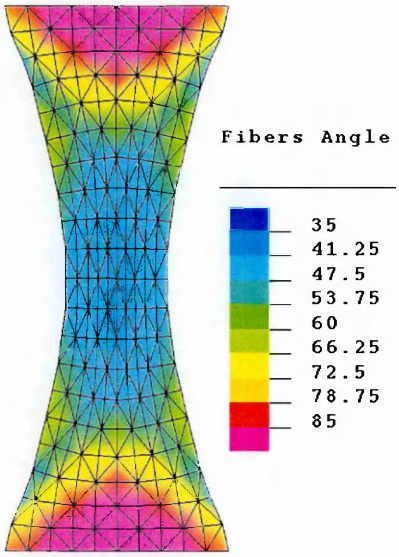

From the bias extension fibre angle example of figure 6.7, it can be deduced that using a defined shear curve of reducing shear modulus (simulation 7c) will not reduce the shear force at higher extensions. This input will promote deformation of the central high shear region and transfer loading to the lower sheared areas of the coupon edge for which a higher modulus is still in effect. This effect is also the cause of force instability for simulation 6 in figure 5.13. A lower post lock shear modulus was utilised for this simulation.

Fig. 6.7. 2/2 twill, simulation 5 bias extension fibre angle (°)

Although force data for simulation 5 is of low precision to that obtained experimentally, the inter-fibre angle distribution demonstrated in figure 6.7 shows good correlation to that observed. The three main zones of differing shear state are suitably defined. A reduction in shear angle to the coupon edges is also successfully simulated indicating, as with the experimental results, the degree of constraint on the material is of key importance to the shear induced. This model can not, however, directly simulate any fibre-slip or tow end rotation as occurs in experimental testing.

Results for the NCF representation vary to those of the twill in the deformation present in the central shear region. Buckling parallel to the coupon length is induced as demonstrated by shading in figure 5.16. This deformation type is not observed during the experimental work as fibre slippage and stitch breakage are preferential deformation mechanisms. As neither of these mechanisms are accounted for in the simulated material model, the presence of buckling is reasonable, but imprecise.

In addition, the NCF representation can not account for preferential zone II slip as observed during experimentation. The spot-weld elements permit relative displacement in any orientation. This is unlike the stitching of the actual fabric for which only longitudinal tow slip is permitted.

6.2.3 PICTURE FRAME SIMULATION DISCUSSION

Results for the picture frame simulations are more precise than those of the bias extension shear characterisation.

For the 2/2 twill fabric, figure 5.20 demonstrates comparatively good correlations between the simulated and experimental force curves could be obtained. As with the bias extension simulations, the optimal calibrated material data utilises a lower fibre modulus of 6GPa for this simulation.

The use of a low fibre modulus is justified since the fibres can still be considered inextensible. Results of the 250mm, 2/2 twill bias extension simulation (number 5a) prove this with <0.14% fibre strain at 20% axial extension. Useful fibre strain data can not be ascertained from the picture frame test directly since only pure shear is induced.

The use of a decreasing shear modulus with shear angle is necessary to prevent the force level from increasing prematurely. This indicates a limitation of the material code in fully representing the forces induced by the various deformation mechanisms of the picture frame test (described in figure 3.7).

This is to be expected since inter-tow friction, transverse tow compaction moduli and buckling criteria can not be explicitly accounted for without a refined tow model of the fabric. A simplified coupling model is therefore implemented for which further calibration may be required. Simulation times for such refined models would be excessively high and require alternative testing to ascertain the required material parameters.

Currently, such a refined model would not be a useful tool for industry since faster simulation techniques are preferred, even if precision is reduced.

The data of simulation A has been chosen for the final draping validation model since the force curve of figure 5.20 is optimal up to shear angles of ~55°. The draping trials indicate this upper limit to the model precision will not be exceeded.

NCF picture frame simulations produced force behaviour results of lower precision compared to the 2/2 twill. Once again, the force behaviour displayed in figure 5.21 indicates a lower fibre modulus of 1GPa to be optimal. However, it has been found necessary to use a high transverse fibre modulus of 0.1GPa to prevent premature initiation of buckling within the simulated NCF specimen.

The transverse tensile moduli of the unidirectional NCF fibre layers are low and depend upon stitching constraints. However, tow *compaction* is to be simulated during fibre shear, therefore the use of a relatively high transverse modulus is justified qualitatively.

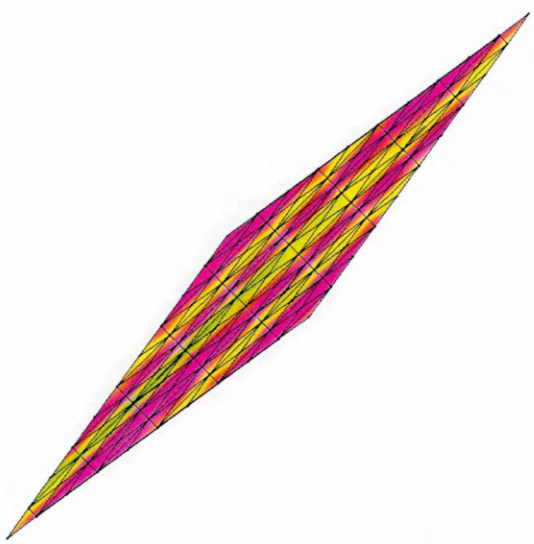

Figure 6.8 demonstrates the style of wrinkling in the NCF picture frame test of simulation E (using a high transverse fibre modulus) at 72° shear angle. With buckling transverse to the shear extension direction, the buckling style is identical to that observed during experimental testing. In part this validates the use of simulation E material data

Fig. 6.8. NCF picture frame buckling style of simulation E

Differences between the experimental test and simulation are present since fabric is not clamped at each corner of the experimental frame. This is due to the mechanical requirement of fitting and permitting movement of bearings at each corner.

The result of this is assumed negligible since the area of material effectively missing from the experimental frame is minor at 4.3%. Also, the simulation material representations produce perfect pure shear and can not simulate additional corner complexities such as superimposed micro-buckling of the fibre tows.

Picture frame simulations A and E produced optimal outputs for the twill fabric and NCF respectively. The material data used in these simulations is, therefore, subsequently utilised for the draping material models.

The use of picture frame material data in draping trials infers the draping simulation is only valid when the deformation mechanism required is pure shear. Calibration and use of the bias extension simulation data would permit the effects of tow slip and free tow end rotation to be included. However, it is then possible the calibrated material data is valid only for the calibrated mesh geometry. Ideally the calibrated material data would be similar for both tests. Difficulties in calibrating the bias extension material data have prevented this from being possible in the time available.

6.2.4 FLEXURAL RIGIDITY SIMULATION DISCUSSION

Results of the flexural rigidity simulation indicate the coupling of the bending factor in the material code is not functioning as originally intended. As previously described, the bending factor of the material 140 model has been created to permit reduction of the bending stiffness this it is calculated as a function of the high fibre moduli.

In this study the factor is used to increase the bending rigidity since a low fibre elastic modulus has been found optimal. This should still be permitted by the code. As described in 5.3.6, the results indicate the bending behaviour to be seemingly independent of the bending factor and, as such, could not be calibrated. In each simulation only minor resistance to bending is observed.

Fibres aligned at O°-90° have been dominantly used in the simulations conducted since the flexural rigidity is theoretically at a maximum, as found experimentally.

This is due to the effective longitudinal coupon modulus being equal to that of the fibres and, therefore, also at a maximum.

The implication of a low bending stiffness on the draping procedure is an increased likelihood of wrinkling. For compression of the fibres to induce wrinkling the effective bending rigidity of the fabric must be overcome. A low bending factor therefore indicates lower resistance to wrinkling.

6.2.5 DRAPING TRIAL SIMULATION DISCUSSION

Draping simulations results are provided in 5.4.7 and 5.4.8 for the twill fabric and NCF respectively.

Results for the twill fabric are very promising. For both the 0°-90° and ±45° single sheet draping simulations (pages 81-82) the fabric shape produced is comparable to that measured by experimental draping. This indicates the material model is suitably calibrated in simulating the dominating in-plane shear deformation of the material.

Minor wrinkling of the 0°-90° fabric sheet is simulated at the fabric perimeter, in areas of fibre alignment with the larger hemisphere centre. This wrinkling is not unreasonable since localised compression is induced by the surrounding regions of high shear deformation. In addition, surface constraints on the fabric are low since the rubber membrane of the forming equipment is not simulated.

The lack of additional pressure and constraint induced by this membrane is believed to be a major contributing factor to all wrinkling observed in the simulated draping trials. Low flexural rigidity is an additional factor. Time constraints of the project prevented any subsequent analyses simulating the membrane from being conducted.

In both single sheet, 2/2 twill simulations a minor degree of hemisphere bridging is simulated, which is in agreement to the observed experimental results and contributes to producing the highly satisfactory perimeter shape.

Fibre angle images generally define low shear regions around fibres aligned with the hemisphere centres. Superposition of these regions from each individual hemisphere results in distinctive distributions of shear deformation.

Simulation results obtained using two sheets of 2/2 twill are provided on pages 83-84. Simulating more than one 2/2 twill fabric sheet causes a higher state of wrinkling, dominantly occurring around the base of the larger hemisphere. This is induced by frictional interaction between the sheets and a comparatively higher degree of shear required for fabric to conform to the larger hemisphere. Since individual fabric layers have preferential shear directions at 45° to each other, a higher state of wrinkling is to be expected. Once again, lack of an additional rubber membrane constraint is believed to permit a higher degree of out-of-plane deformation. This is not present in the experimental trials.

Wrinkling between the two mould hemispheres is only produced during an experimental trial using a ±45° on 0°-90° 2/2 twill lay-up. Wrinkling is also more dominant for the simulated ±45° on 0°-90° lay-up. Differing contact frictions for each layer in the shell element sequence is believed to permit one fabric sheet to dominate buckling.

For both two layer 2/2 twill simulations the individual sheets maintain the characteristic shape noted in the single layer simulations. This results in the lower sheet protruding from the upper in areas that the characteristic draped shapes differ. This is also observed in experimental draping trials and indicates a suitable degree of fabric interaction is simulated through the contact algorithm.

Simulated wrinkling of the two layer, 2/2 twill simulations also results in a reduced state of shear when comparing the results of individual sheets to those obtained for single sheet simulations.

Appendix C includes images of simulated fibre strain. This is to ascertain if excessive fibre strain is produced as a result of using low fibre elastic moduli, calibrated from the picture frame simulation.

The images indicate fibre stain to be negligible, occurring in bands perpendicular to the simulated fibre direction as expected from the lower transverse elastic modulus.

Similar images are provided for the NCF draping simulations. The results are similar and also indicate fibre strain to be negligible.

NCF draping simulations are less satisfactory compared to those of the 2/2 twill since a high degree of wrinkling is simulated for all single and double lay-up sequences. The main contributing factor to this wrinkling is thought to be the lack of simulated rubber membrane. However, additional considerations are necessary for the NCF due to the variation in material representations.

A limitation of the NCF representation is a high number of degrees of freedom available to the spot-weld elements, connecting the separate shell element layers. This is described in 6.2.2. The effect of this is expected to be minimal for the current study as in-plane shear is the dominant deformation mechanism. Larger simulation/experimental result discrepancy may be induced by this fact when more complex shapes, of increased fibre-slip, are studied.

Simulated draping of the single NCF sheets dominantly produces wrinkling around the base of the larger hemisphere where required deformation is highest. Bridging is noted in orientations parallel to the simulated fibre directions. Despite this, the perimeter deformation still dominantly occurs in areas parallel to fibres aligned to the hemisphere centres. This is demonstrated in figures 5.39 and 5.42.

These results are satisfactory when considering different longitudinal and transverse fibre moduli are simulated for each layer. This also indicates that the stitch elements, between shell element layers, produce sufficient coupling for the NCF representation to deform as a bi-directional sheet. Improved justification of these remarks is believed possible through inclusion of the rubber membrane in the draping simulation. This addition would theoretically induce higher fabric conformity to the mould geometry and reduce the occurrence of wrinkling.

Simulations of draping two fabric sheets produced an even higher state of wrinkling than the single sheets. This is attributed to interaction between the sheets preventing preferential shear of each individual sheet. This constraint on the ability of the sheets to shear therefore induces fabric buckling as the only alternative deformation mechanism. This interpretation is justified by considering the inter-fibre angle induced in each layer as demonstrated on pages 87-88.

Appendix C includes images of fibre strain distribution. Once, again fibre stain is negligible and has not produced errors in the simulation results.

6.2.6 MATERIAL MODEL DISCUSSION

From the discussions of the simulations conducted a number of material model considerations require discussion.

Firstly, the material model 140, used for both fabrics, is understood to have no direct method of simulating inter-fibre slip. This could be a major drawback for deep-drawn mould geometries and fabrics which have an increased tendency to deform by this mechanism, such as NCF. However, the majority of any fabric deformation will occur by in-plane shear and permit application of the FE simulation code.

If in-plane shear is the only mechanism directly simulated it may appear that the FE model implemented is of little improvement to geometrical methods. The dominant simulated deformation mechanisms are currently similar for both techniques, however, the FE model permits simulation of;

- fabric interaction with tooling,
- fabric interaction with additional fabric sheets,
- fibre locking angle,
- flexural rigidity,
- buckling.

The ability of a fabric to conform to a surface is observed to be dependant on these five factors and more. The continued research into FE simulation methods is therefore justified. Geometric mapping methods still are, as yet, limited to producing inter-fibre angle data only. No hemisphere bridging or fabric wrinkling would be observed with such simulation techniques as demonstrated by figures 6.9 and 6.10.

The material representation of the NCF has limitations as previously described, but is, to the author's knowledge, the only currently investigated model concerning the additional constraint placed upon a fabric by through thickness stitching. This representation permits differential slip of the unidirectional plies as controlled by the connecting spot-weld elements. This representation can not simulate localised inter-fibre slip as observed with the bias coupon tests.

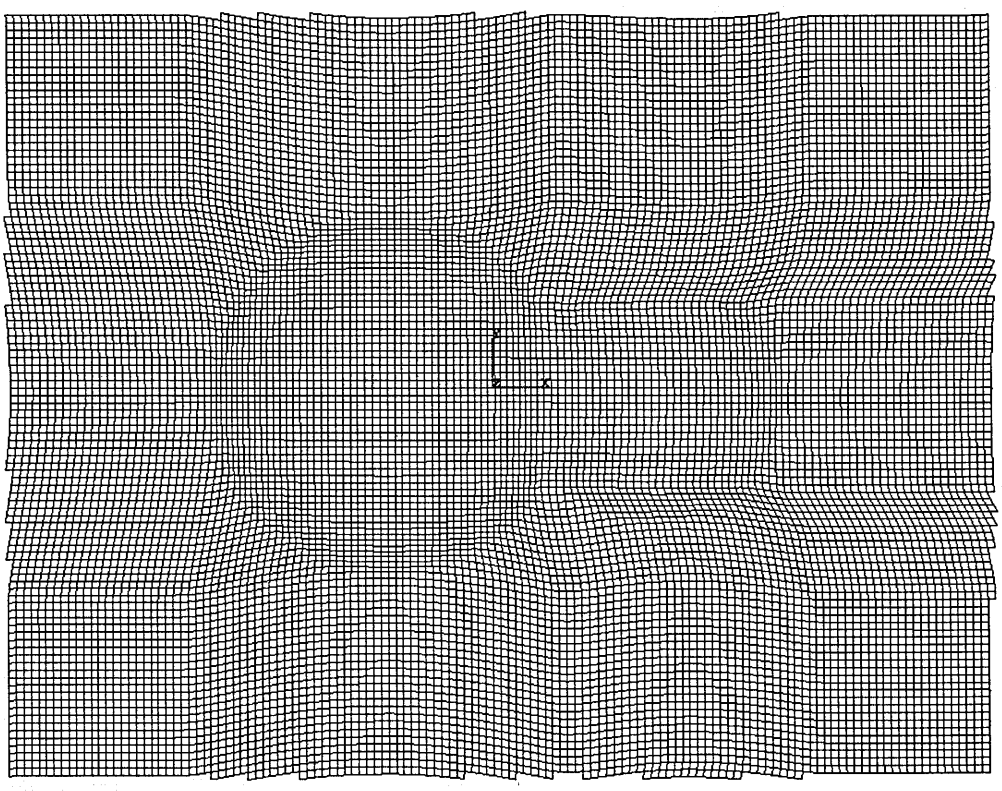

Fig. 6.9. Geometrical mapping simulation result for a 0°-90° initial fibre orientation

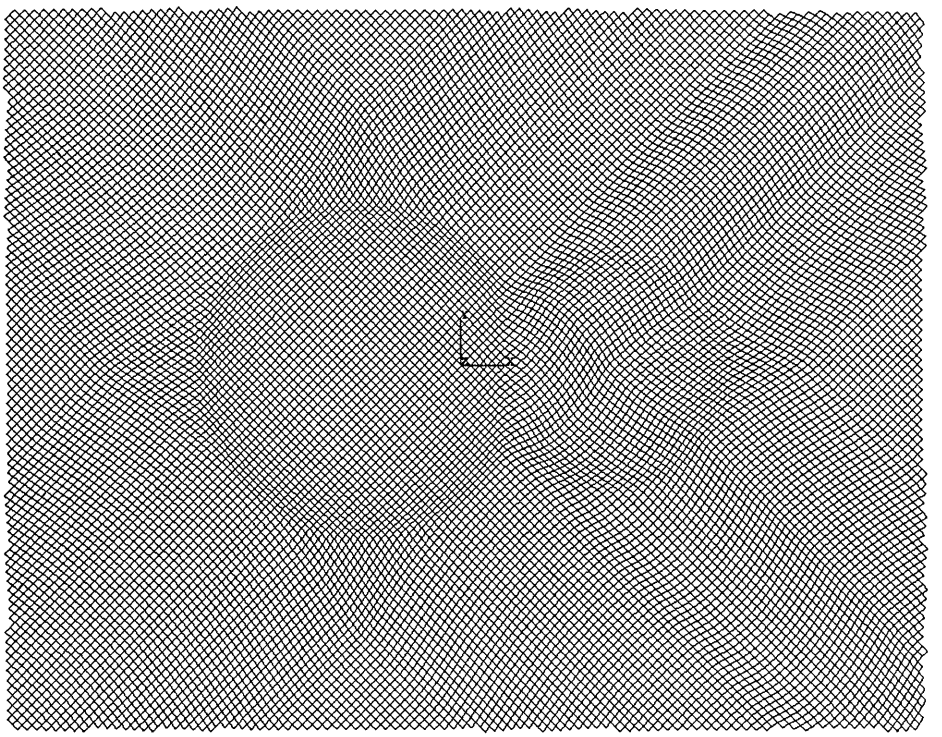

Fig. 6.10. Geometrical mapping simulation result for a ±45° initial fibre orientation

At the end of the project, simulation results were obtained from a geometrical mapping software package; QUIKFORM™ [50]. The results are provided in figures 6.9 and 6.10. These are included for comparison to the results obtained by FE simulation.

Both mapped simulations produce similar observed fibre angle results to those obtained by FE analysis for the respective original fibre orientations. This is due to in-plane shear being the dominant deformation mechanism. Differences in fibre angle distribution can, however, be simulated. For example, corners of the FE simulation with fibres aligned 0°-90° includes shear of approximately 8°, as indicated in figure 5.24. The mapped solution produces in no deformation, as indicated in figure 6.9 (a comprehensive qualitative comparison was not permitted due to time constraints).

This demonstrates that even for relatively simple mould geometries, differences between mapped and finite element simulations will be produced with FE calibration to a specific material. With suitable calibration, the FE models can therefore provide much greater scope for material and tooling specific results.

7 CONCLUSIONS

This project has successfully characterised both a 2/2 twill fabric and NCF for the main modes of deformation during pre-form manufacture. An extensive testing programme has been implemented including two shear characterisation testing procedures commonly used in research; the bias extension and picture frame tests.

Separation of the 2/2 twill indicates the bias extension test to be of limited use for fabrics of low stability. However, non-uniform shear permits preferential slip to be observed in the NCF due to stitching constraints.

Additional testing has successfully characterised bending behaviour and frictional behaviour between the fabrics and pre-form manufacturing tooling. Consideration has been given to the effects of varying fibre orientations in each experiment.

Special attention has been given to the NCF, for which the effect of through thickness stitching on inter-fibre slip has been investigated. A tow pull-out test is successfully used to measure this effect.

Using the proposed material models, simulations of the bias extension test have indicated limitations of the models and software code. Low fibre elastic moduli (3-9GPa) are found optimal to properly simulate the shear force behaviour and deformational characteristics of the materials.

Improved precision is obtained in force behaviour through simulation of the picture frame test since pure shear is induced. Low fibre elastic moduli are optimal, although, reasonable results can be obtained through the use of reasonable 300GPa moduli.

Simulations to calibrate the fabric bending stiffness indicate the simulation code is currently unable to permit sufficient user control of this variable. As such, this could not be validated. However, simulation of the NCF tow-pull out test has successfully calibrated 'spot-weld' moduli data for the NCF material representation.

Vacuum forming draping trials have been successfully conducted over a double hemisphere mould. This is for final validation of the material models, calibrated from previous tests. These tests are conducted with fabric fibres at ±45° and 0°-90° and using two fabric sheets with a ±45° layer on a 0°-90° layer and vice-versa. The mould geometry has been chosen to induce extra shear variation compared to a single hemisphere and reduce symmetry, although the required shear state of the draped material is low. In-plane shear is the dominant deformational mechanism for both fabrics. Both fabrics are also proved highly conformable with low buckling inter-fibre angles.

Simulation of these trials has indicated the twill material model to be highly satisfactory in simulating the draping process. The fabric shape is compared from measurements of edge movement and is found to be most precise when only one sheet is simulated. A higher degree of wrinkling is induced in simulations of two fabric layers, which are not observed in experimental draping trials. However, differential shear of the two layer simulations is successfully simulated.

NCF draping trials show promise for the material representation as the characteristic shape of the single fabric layer is partially observed. However, a high degree of wrinkling is simulated which does not occur in experimental trials. Differential shear of the two layer simulation is also not observed. The variation in results is believed to be an effect of incomplete tooling simulation. A higher degree of material constraint would be induced if this was included and could reduce the occurrence of wrinkling.

Comparison between finite element simulation results and those produced by mapping methods demonstrate the ability of the finite element method to produce material and tooling specific results. An ability most mapping methods are incapable of.

The study has proved the feasibility of applying FE simulation tools to the pre-form manufacturing process. This is at the expense of an extensive testing programme, although this is currently justified as sufficient data is required for calibration and validation purposes.

8 FUTURE WORK

From this study a number of issues have been raised which could improve the material model included in PAMFORM™.

Firstly, simulations of the draping trials to include the rubber membrane are necessary. This is to investigate if additional constraint reduces the occurrence of wrinkling within the simulated fabric.

Investigation into the FE material coding should be conducted to ascertain how the fibre modulus is coupled to the shear behaviour. The aim of this is to permit realistic values of shear to be produced when using high fibre moduli.

The FE coding should also be investigated to ascertain how the bending factor is implemented. The aim of this is to induce a higher degree of user control on the flexural rigidity of the simulated fabric.

Validation of the material models using a more complex geometry could be investigated to ascertain the limits of model applicability.

Additionally, further work into understanding the deformational behaviour of the fibre tows would be useful to understand how deformation is affected by mould pressure and tow compaction. The use of a unit cell model is proposed for this study as additional permeability and mechanical data could be obtained.

A unit cell model of the 2/2 twill fabric has been constructed during this project (figure 8.1), but due to time constraints could not be fully investigated. Similar models for the NCF should include representation of the through thickness stitching.

Fig. 8.1. 2/2 twill unit cell representation

9 REFERENCES

1. Rudd C D, Long A C, Kendall K N, Mangin C G E. Liquid moulding technologies. 1997, Woodhead Publishing, Cambridge, England.

2. Bickerton S, Simacek P, Guglielmi S E, Advani S. Investigation of Draping and its Effect on the Mold Filling Process During Manufacture of a Compound Curved Composite Part. *Composites Part A,* 1997, Vol. 28A, pp 801-816.

3. Long A C. An Iterative Draping Simulation Based on Fabric Mechanics. *4th International ESAFORM Conference on Material Forming.* 23-25th April 2001, Belgium, Leige, pp 99-102.

4. Mohammed U, Lekalou C, Bader M G. Expermiental Studies and Computer Simulations of the Draping of Woven Fabrics. *5th International Conference on Flow Processes in Composite Materials.* 12-14th July 1999, United Kingdom, Plymouth, pp 53-60.

5. Lamers E A D, Akkerman R, Wijskamp S. Fibre Orientation Modelling for Rubber Press Forming of Thermoplastic Laminates. *Distributed electronically.*

6. Daniel J L, Soulat D, Boisse Ph. Simulations of Fibres Fabrics. *5th International Conference on Computational Structures Technology and the 2nd International conference on Engineering Computational Technology.* 6-8th September 2000, United Kingdom, Edinburgh, pp 299-307.

7. Shiao S W, Kikuchi N. *Computational Methods of Applied Mechanical Engineering.* 1999, 177, pp 1-34.

8. Smith P, Rudd C D, Long A C. *Composites Science and Technology* 1997, Vol. 57, 3, pp 327-344.

9. Leong K H, Ramakrishna S, Huang Z M, Bibo G A. The Potential of Knitting for Engineering Composites. *Composites: Part A*, 2000, Vol. 31, pp 197-220.

10. Anard S. Warp Knitted Structures in Composites. *Proceedings of the 7th European Conference on Composite Materials (ECCM-7),* United Kingdom, London, Vol. 2, pp 407-413.

11. Backhouse R, Blakeman C, Irving P E. *Mechanisms of Toughness Enhancement in Carbon Fibre Non-Crimp Fabrics.* 27-29th March 1995. Institute of Metals. United Kingdom, University of Surrey, Guildford. pp 307-316.

12. Souter B J, Long A C, Robitaille F, Rudd C D. The influence of Fabric Mechanics on Draping. *6th International Conference on Advanced Composites (ICAC-99).* September 1999. United Kingdom, Bristol, pp 55-62.

13. Clifford M J, Long A C. Intra-ply Shear of Textile Composites. *Proceedings of the 8th International Conference on Fibre Reinforced Composites. 13-15 September 2000. United Kingdom, Newcastle upon Tyne.*

14. Potter K D. Deformation mechanisms of fibre reinforcements and their influence on the fabrication of complex structural parts. *Advances in composite materials; Proceedings of the Third International Conference on Composite Materials.* 26-29th August 1980. Paris, France. Volume 2. (A81-40501 18-24) Oxford, Pergamon Press, pp 1564-1579.

15. Pickett A K. Review of Finite Element Simulation Methods Applied to Manufacture and Failure Prediction in Composite Structures. *Applied Composite Materials.* 2002, Vol. 9, pp 43-58.

16. Potter K D. *Composites.* 1979, Vol. 10, pp 161-167.

17. Wang J, Page J R Paton R. Experimental Investigation into the Draping Properties of Reinforcement Fabrics. *Journal of Composite Science and Technology.* 1998, Vol. 58(2). pp 229-237.

18. Long A C, Rudd C D, Blagdon M, Smith P. Characterising the Processing and Performance of Aligned Reinforcements During Preform Manufacture. *Composites: Part A.* 1996, Vol. 27A, pp 247-253.

19. Mohammed U, Lekakou L, Dong L, Bader M G. Shear Deformation and Micromechanics of Woven Fabrics. *Composites: Part A.* 2000, Vol. 31, pp 299-308.

20. Hu J-L, Zhang Y-T. The KES Shear Test for Fabrics. *Textile Research Journal.* 1997, Vol. 67(9), pp 654-664.

21. Sidhu R M J S, Averill R C, Riaz M, Pourboghrat F. Finite Element Analysis of Textile Composite Preform Stamping. *Composite Structures.* 2001, Vol. 52, pp 483-497.

22. Bibo G A, Hogg P J, Kemp M. Mechanical characterisation of Glass- and Carbon-Fibre Reinforced Composites Made With Non-Crimp Fabrics. *Composite Science and Technology.* 1997, Vol. 57, pp 1221-1241.

23. Harrison P, Clifford M J, Long A C, Rudd C D. Constitutive Modelling of Impregnated Continuous Fibre Reinforcement Composites Micromechanical Approach. *Plastics, Rubbers and Composites.* 2002, Vol. 31, No.2, pp 76-97.

24. Takano N, Ohnishi Y, Zako M, Nishiyabu K. Microstructure-Based Deep-Drawing Simulation of Knitted Fabric Reinforced Thermoplastics by Homogenization Theory. *International Journal of Solids and Structures (UK).* Sept. 2001, Vol. 38, No. 36-37, pp 6333-6356.

25. Long A C, Souter B J, Robitaille F. Mechanical Modeling of In-Plane Shear and Draping for Woven and Non-Crimp Reinforcements. *Journal of Thermoplastic Composite Materials.* July 2001, Vol. 14, part 4, pp 316-326.

26. Gelin J C, Cherouat A, Boisse P, Sabhi H. Manufacture of Thin Composite Structures by the RTM Process : Numerical Simulation of the Shaping Operation. *Composites Science and Technology.* 1996, Vol. 56, pp 711-718.

27. Long A C, Rudd C D. Computer Integrated Design of Structural Preforms for Liquid Moulding Processes. *Proceedings of the 27th ISATA – New and Alternative Materials for the Transportation Industries.* 1994, Aachen, pp 381-390.

28. Pickett A K. Review of Finite Element Simulation Methods Applied to Manufacture and Failure Prediction in Composite Structures. *Applied Composite Materials.* 2002, Vol. 9, pp 43-58.

29. Potluri P, Sharma S, Ramgulam R. Comprehensive Drape Modelling for Moulding 3D Textile Preforms. *Composites: Part A.* 2001, Vol. 32, pp1415-1424.

30. Borouchaki H, Cherouat A, Billoet J L, de Luca P. Integration of a New Geometrical Model for Textile Forming Processes in Quickform Software. *4th International ESAFORM Conference on Material Forming.* 23-25th April 2001, Belgium, Leige, pp 103.

31. Mack C, Taylor H M. *Journal of the Textile Institute.* 1956, Vol. 47, T477.

32. Rudd C D, Turner M R, Long A C, Middleton V. Tow Placement Studies For Liquid Composite Moulding. *Composites: Part A*, 1999, Vol. 30, pp 1105–1121.

33. Van West B P, Pipes R B, Keefe M J. *Journal of the Textile Institute* 1990, Vol. 81(4), pp 448.

34. Long A C, Rudd C D. Simulation of Reinforcement Deformation During the Production of Preforms for Liquid Moulding Processes. *Proceedings of the Institution of Mechanical Engineers, Part B: Journal of Engineering Manufacture.* 1994, Vol. 208, B4, pp 269-278.

35. Bergsma OK. Computer Simulation of 3D Forming Processes of Fabric-Reinforced Plastics. *Proceedings of the 9th International Conference on Composite Materials (ICCM/9).* 1993, pp 560–567.

36. Bunday B D. Basic Optimisation Methods. 1984, Edward Arnold Ltd. London.

37. de Luca P, Lefebure P, Pickett A K. Numerical and Experimental Investigation of some Press Forming Parameters of Two Fibre Reinforced Thermoplastics: APC2-AS4 and PEI-CETEX. *Composites: Part A.* 1998, Vol. 29A, pp 101-110.

38. Boisse P, Borr M, Buet K, Cherouat A. Finite Element Simulations of Textile Composite Forming Including the Biaxial Fabric Behaviour. *Composites: Part B.* 1997, Vol. 28A, pp 453-464.

39. Dong , Lekakou C, Bader. Solid-Mechanics Finite Element Simulations of the Draping of Fabrics: A Sensitivity Analysis. *Composites: Part A.* 2000, Vol. 31, pp 639-652.

40. Quick-Form Users Guide. 2001, *ESI Software.*

41. PAM-SCL (Solid Core Library): Theory Notes Manual. 2000, *ESI Software.*

42. Fagan M J. Finite Element Analysis, Theory and Practice. Prentice Hall London, 1992.

43. ASTM G115-93. Standard Guide for Measuring and Reporting Friction Coefficients.

44. ASTM D4521-91. Standard Test Method for Coefficient of Static Friction of Corrugated and Solid Fibreboard.

45. ASTM D1388-96^{E1}. Standard Test for Stiffness of Fabrics.

46. Krevszig E. Advanced Engineering Mathematics, 8th Edition. 1999, John Wiley & Sons.

47. PAMFORM™, *ESI Software.*

48. Ashby M F, Jones D. Engineering Materials I: Introduction to their Properties and Applications. 1996, Butterworth & Henmann.

49. I-DEAS™, *Electronic Data Systems Corporation.*

50. QUIKFORM™, *ESI Software.*

APPENDIX: A

PICTURE FRAME DESIGNS

Picture Frame Design 1: Cross-head attachment

Dimensions in (mm)

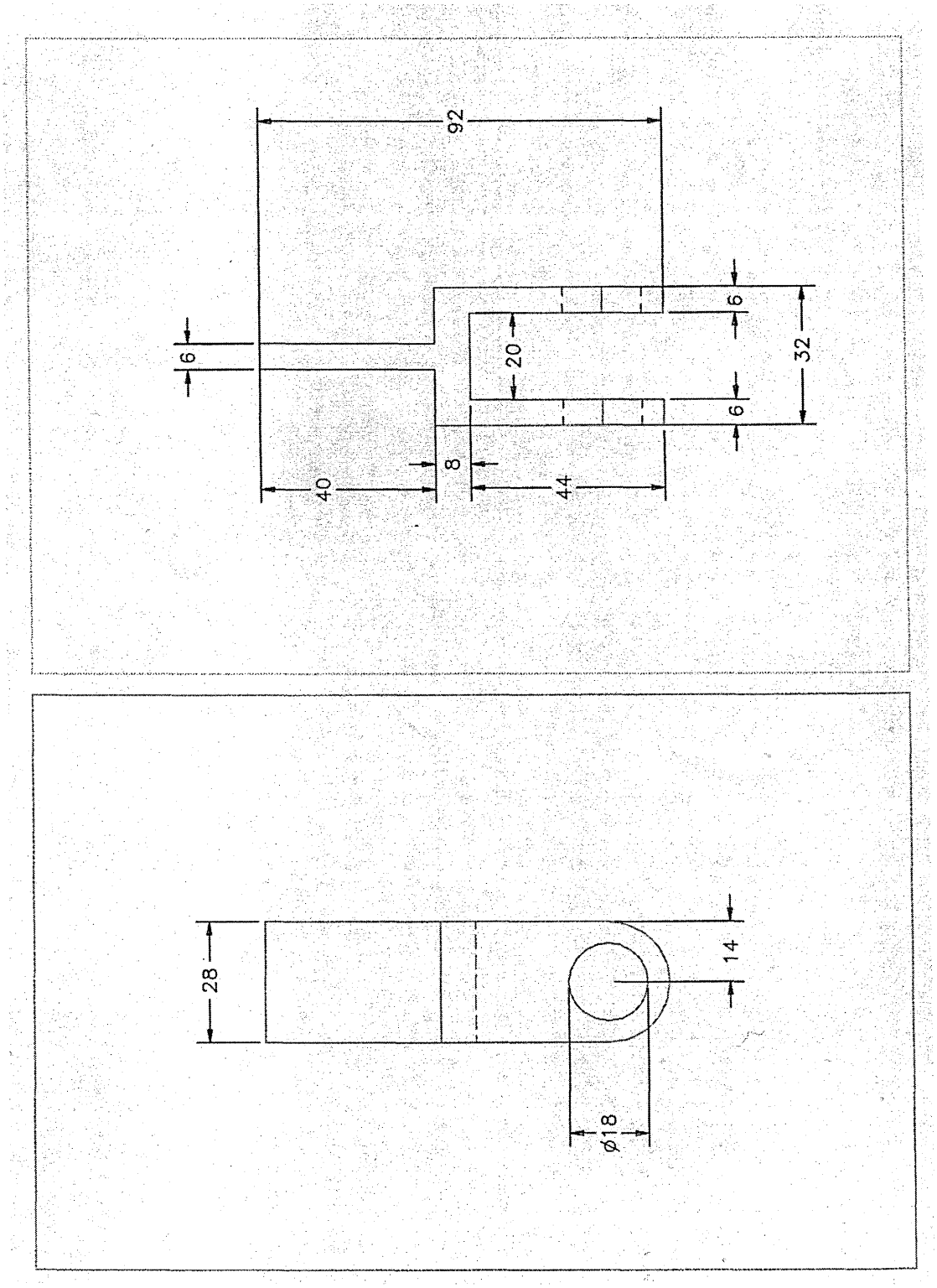

Picture Frame Design 1: I-beam clamping edge

Dimensions in (mm)

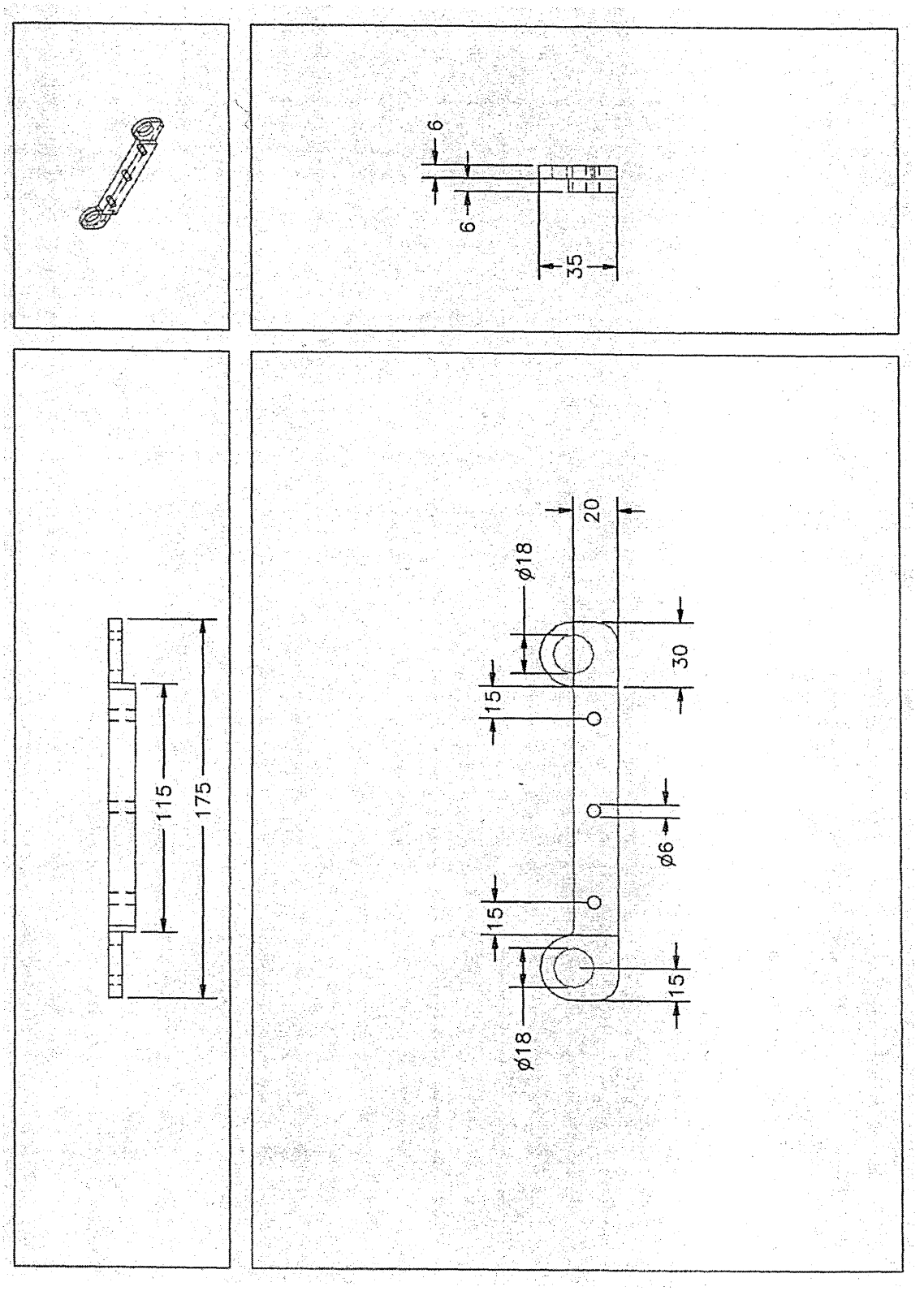

Picture Frame Design 1: U-beam clamping edge

Dimensions in (mm)

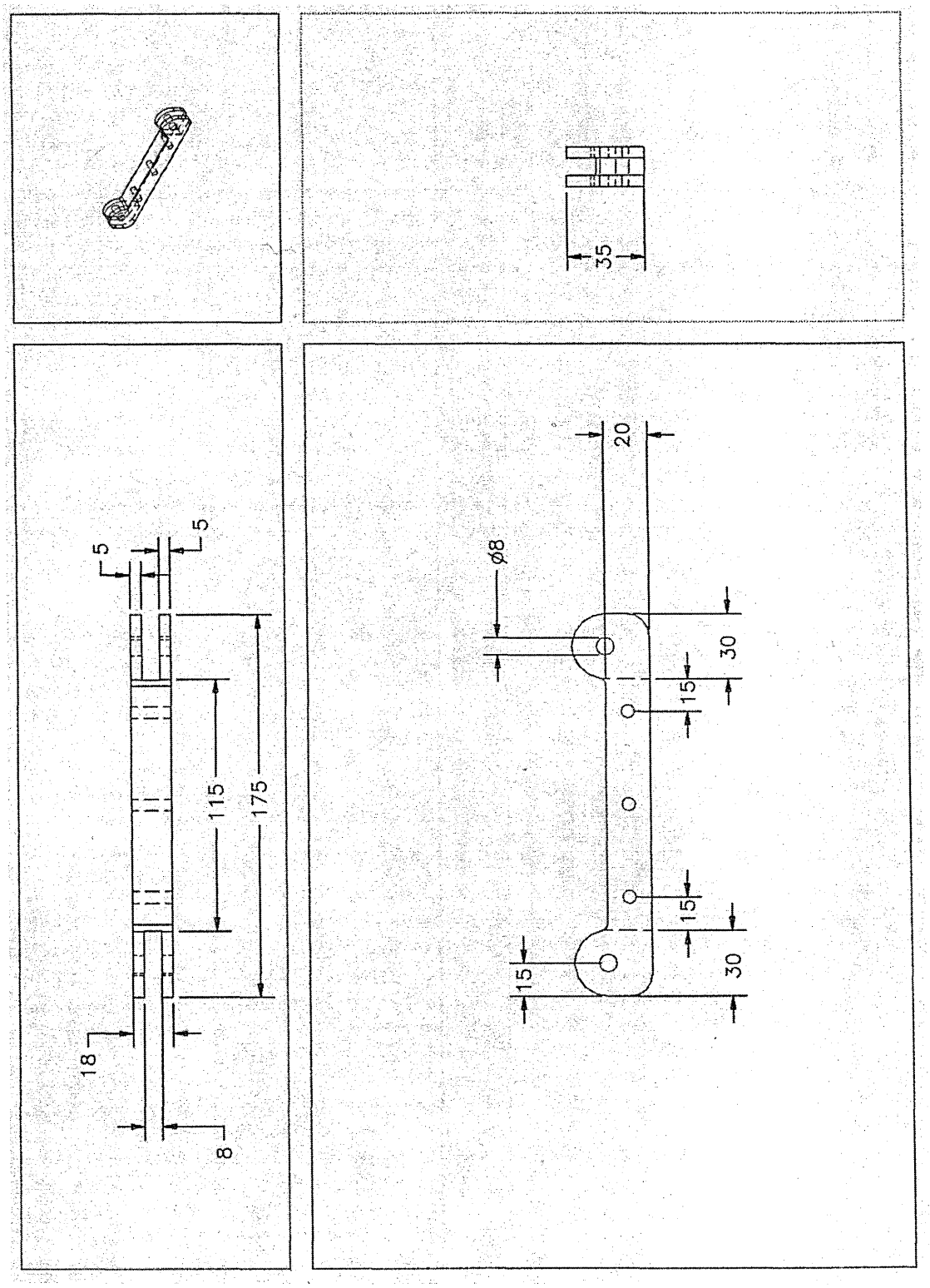

Picture Frame Design 1: Clamping plate

Dimensions in (mm)

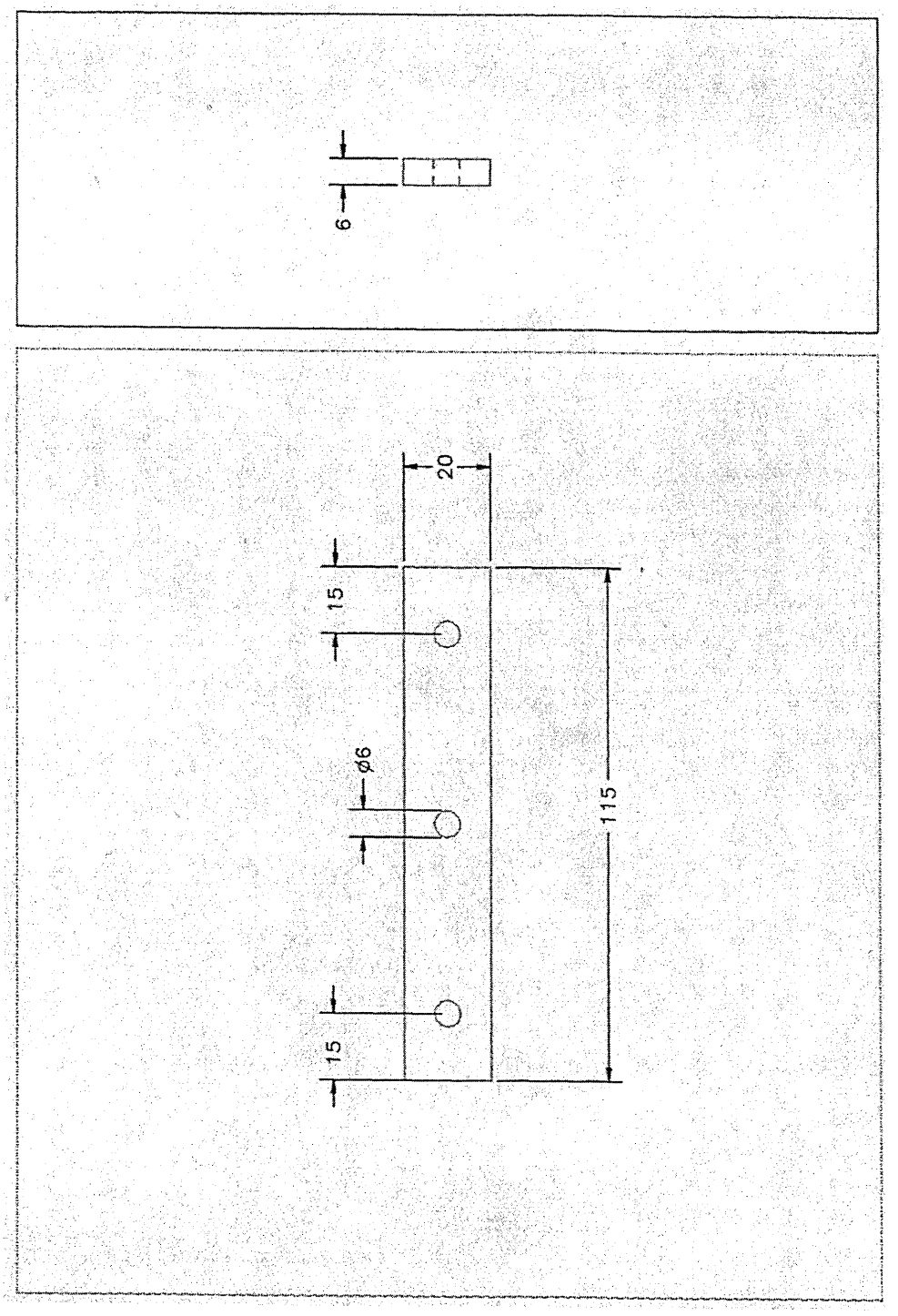

APPENDIX: B

MATERIAL CHARACTERISATION DATA

NCF Bias Extension 200mm specimen length results

Extension (mm)	Force (N) Test 1	Test 2	Test 3	Test 4	Test 5	Test 6	Test 7	Test 8	Test 9	Test 10
10	1.26	0.90	0.88	1.29	0.96	1.02	1.45	1.31	1.15	1.42
20	1.83	1.20	1.25	1.74	1.36	1.45	1.84	1.80	1.52	1.82
30	2.69	1.61	1.79	2.69	1.91	2.02	2.59	2.49	2.04	2.55
40	4.45	2.54	2.89	4.04	2.92	3.08	3.81	3.83	3.12	4.20
50	8.44	4.32	5.20	7.34	4.63	4.80	6.42	6.53	5.40	7.59
60	14.85	6.94	9.97	13.78	8.25	9.00	12.62	12.60	10.15	13.33

NCF Bias Extension 200mm specimen length squared deviations from mean

Extension (mm)	Test 1	Test 2	Test 3	Test 4	Test 5	Test 6	Test 7	Test 8	Test 9	Test 10
10	0.01	0.07	0.08	0.02	0.04	0.02	0.08	0.02	0.00	0.06
20	0.06	0.15	0.11	0.02	0.05	0.02	0.07	0.05	0.00	0.06
30	0.20	0.40	0.20	0.21	0.11	0.05	0.12	0.06	0.04	0.10
40	0.93	0.90	0.36	0.30	0.33	0.17	0.10	0.12	0.13	0.51
50	5.63	3.06	0.76	1.63	2.06	1.61	0.13	0.21	0.45	2.32
60	13.68	17.68	1.39	6.93	8.42	4.63	2.16	2.10	0.99	4.75

NCF Bias Extension 200mm specimen length data analysis

Extension (mm)	Mean Force (N)	Standard Deviation	Variance (s^2)	(s)
10	1.17	0.21	0.05	0.21
20	1.58	0.26	0.07	0.26
30	2.24	0.41	0.17	0.41
40	3.49	0.65	0.43	0.65
50	6.07	1.41	1.98	1.41
60	11.15	2.64	6.97	2.64

NCF Bias Extension 200mm specimen length t-distribution calculation [46]

Sample size

10

1) Confidence level = 95%

2) F(C) = 0.5 (1-conf) = 0.975

c(9) = 2.26

3) Variance calculated

4)

Ext. (mm)	Interval (N)
0	**0**
10	**0.1517**
20	**0.1831**
30	**0.2905**
40	**0.4674**
50	**1.0065**
60	**1.8867**

NCF Bias Extension 250mm specimen length results and analysis

Extension (mm)	Test 1	Force Test 2	(N) Test 3	Test 4	Mean Force (N)	Standard Deviation
10	0.9	1.08	1.21	1.42	1.15	0.22
20	1.27	1.53	1.67	1.95	1.60	0.28
30	1.57	2.01	2.08	2.46	2.03	0.36
40	2.08	2.78	2.77	3.26	2.72	0.48
50	2.97	4.46	4.06	4.48	3.99	0.71
60	4.21	7.55	6.50	6.95	6.30	1.46
70	6.87	12.80	10.40	10.80	10.22	2.47
80	11.83	21.32	17.67	17.80	17.16	3.93

NCF Bias Extension 250mm specimen length squared deviations from mean and variance

Extension (mm)	Test 1	Test 2	Test 3	Test 4	Variance (s^2)	(s)
10	0.06	0.01	0.00	0.07	0.02	0.13
20	0.11	0.01	0.00	0.12	0.03	0.16
30	0.21	0.00	0.00	0.18	0.04	0.21
40	0.41	0.00	0.00	0.29	0.08	0.28
50	1.05	0.22	0.00	0.24	0.17	0.41
60	4.39	1.55	0.04	0.42	0.71	0.84
70	11.21	6.67	0.03	0.34	2.03	1.42
80	28.32	17.35	0.26	0.41	5.15	2.27

NCF Bias Extension 250mm specimen length t-distribution calculation [46]

Sample size

4

1) Confidence level = 95%

2) F(C) = 0.5 (1-conf) = 0.975

c(3) = 3.18

3) Variance calculated

4)

Ext. (mm)	Interval (N)
0	**0**
10	**0.2010335**
20	**0.260367**
30	**0.3349499**
40	**0.4443606**
50	**0.6504711**
60	**1.3407035**
70	**2.2640168**
80	**3.6082386**

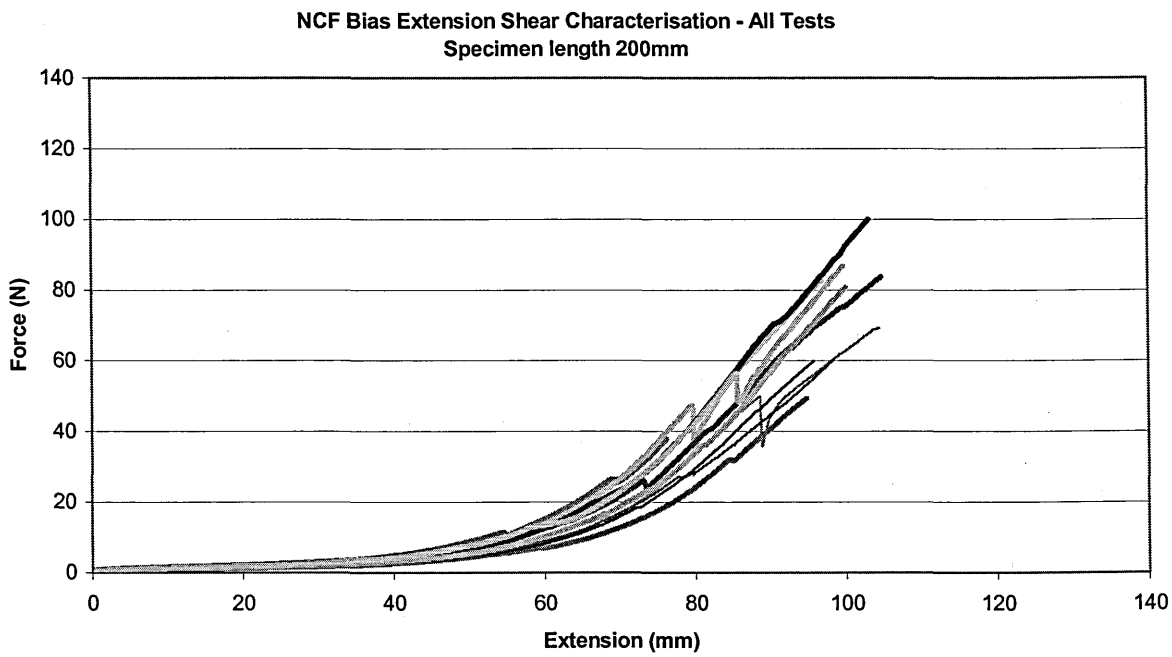
NCF Bias Extension Shear Characterisation - All Tests
Specimen length 200mm
Force (N)
Extension (mm)
0
20
40
60
80
100
120
140

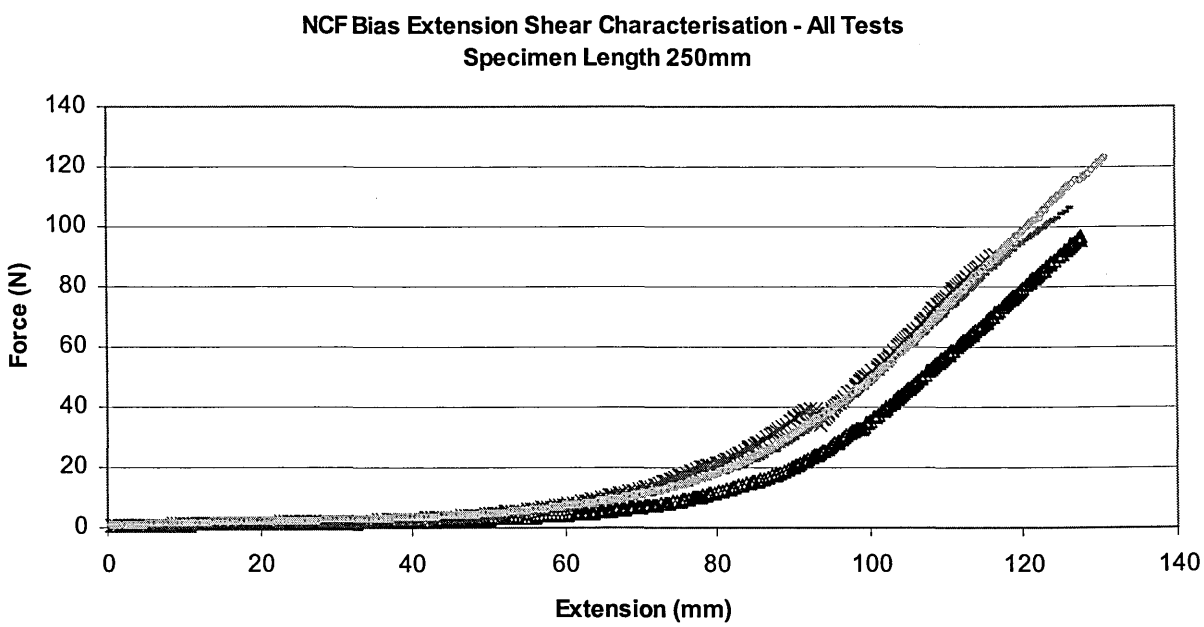
NCF Bias Extension Shear Characterisation - All Tests
Specimen Length 250mm
Force (N)
Extension (mm)
0
20
40
60
80
100
120
140

2/2 Twill Bias Extension 200mm specimen length results and analysis

Extension (mm)	Force (N) Test 1	Test 2	Test 3	Mean Force (N)	Standard Deviation
10	1.53E-01	1.43E-01	1.54E-01	1.50E-01	0.006262
20	2.17E-01	2.46E-01	2.36E-01	2.33E-01	0.014626
30	3.06E-01	3.50E-01	3.64E-01	3.40E-01	0.030087
40	4.88E-01	5.49E-01	6.28E-01	5.55E-01	0.07018
50	9.81E-01	8.56E-01	1.12E+00	9.86E-01	0.132488

2/2 Twill Bias Extension 200mm specimen length squared deviations from mean and variance

Extension (mm)	Test 1	Test 2	Test 3	Variance (s^2)	(s)
10	1.02E-05	5.21E-05	1.62E-05	3.92E-05	6.26E-03
20	2.51E-04	1.69E-04	8.01E-06	2.14E-04	1.46E-02
30	1.13E-03	8.91E-05	5.87E-04	9.05E-04	3.01E-02
40	4.49E-03	3.63E-05	5.33E-03	4.93E-03	7.02E-02
50	2.33E-05	1.69E-02	1.82E-02	1.76E-02	1.32E-01

2/2 Twill Bias Extension 200mm specimen length t-distribution calculation [46]

Sample size 3

1) Confidence level = 95%

2) F(C) = 0.5 (1+conf) = 0.975

c = 4.30

3) Variance calculated

4)

Ext. (mm)	**Interval (N)**
0	**0.00E+00**
10	**1.55E-02**
20	**3.63E-02**
30	**7.47E-02**
40	**1.74E-01**
50	**3.29E-01**

2/2 Twill Bias Extension 250mm specimen length results and analysis

Extension (mm)	Force (N) Test 1	Test 2	Test 3	Mean Force (N)	Standard Deviation
10	0.21	0.19	0.17	0.19	2.09E-02
20	0.31	0.30	0.24	0.28	3.91E-02
30	0.38	0.37	0.37	0.37	3.61E-03
40	0.55	0.52	0.47	0.51	3.86E-02
50	0.93	0.86	0.82	0.87	5.58E-02
60	1.51	1.48	1.46	1.48	2.85E-02

2/2 Twill Bias Extension 250mm specimen length squared deviations from mean and variance

Extension (mm)	Test 1	Test 2	Test 3	Variance (s^2)	(s)
10	4.38E-04	4.91E-09	4.35E-04	4.37E-04	2.09E-02
20	9.43E-04	1.79E-04	1.94E-03	1.53E-03	3.91E-02
30	1.60E-05	1.00E-06	9.01E-06	1.30E-05	3.61E-03
40	1.02E-03	1.21E-04	1.84E-03	1.49E-03	3.86E-02
50	3.64E-03	1.14E-04	2.47E-03	3.11E-03	5.58E-02
60	8.02E-04	1.00E-07	8.20E-04	8.11E-04	2.85E-02

2/2 Twill Bias Extension 250mm specimen length t-distribution calculation [46]

Sample size 3

1) Confidence level = 95%

2) F(C) = 0.5 (1+conf) = 0.975

c = 4.30

3) Variance calculated

4)

Ext. (mm)	**Interval (N)**
0	**0.00E+00**
10	**5.19E-02**
20	**9.72E-02**
30	**8.96E-03**
40	**9.58E-02**
50	**1.38E-01**
60	**7.07E-02**

2/2 Twill Bias Extension Shear Characterisation
Specimen length 250mm

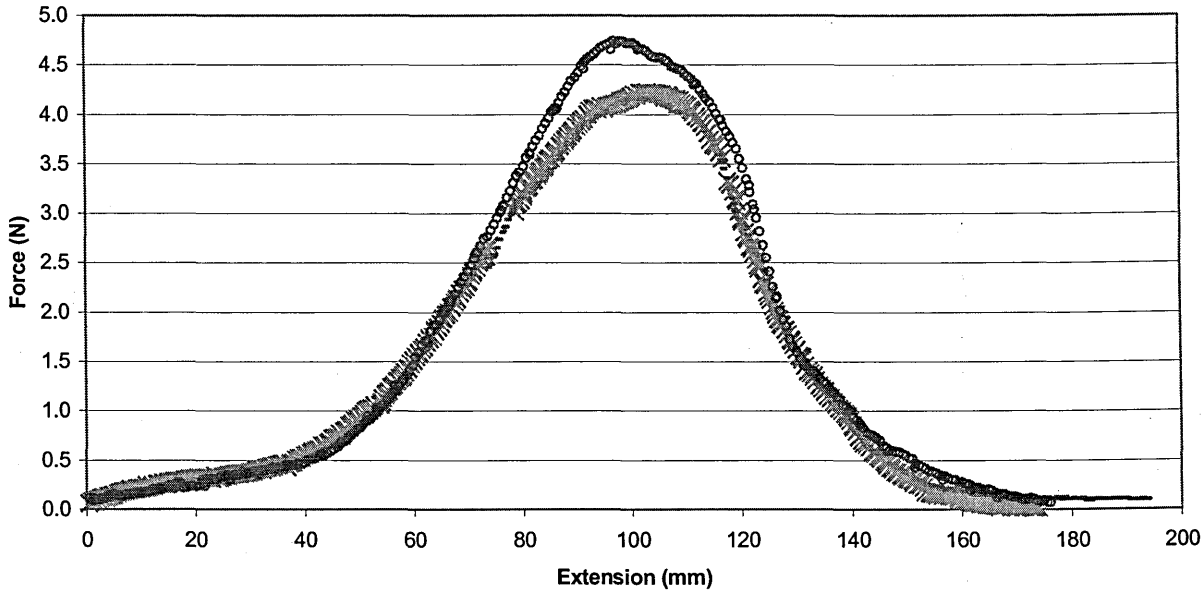

2/2 Twill Bias Extension Shear Characterisation
Specimen length 200mm

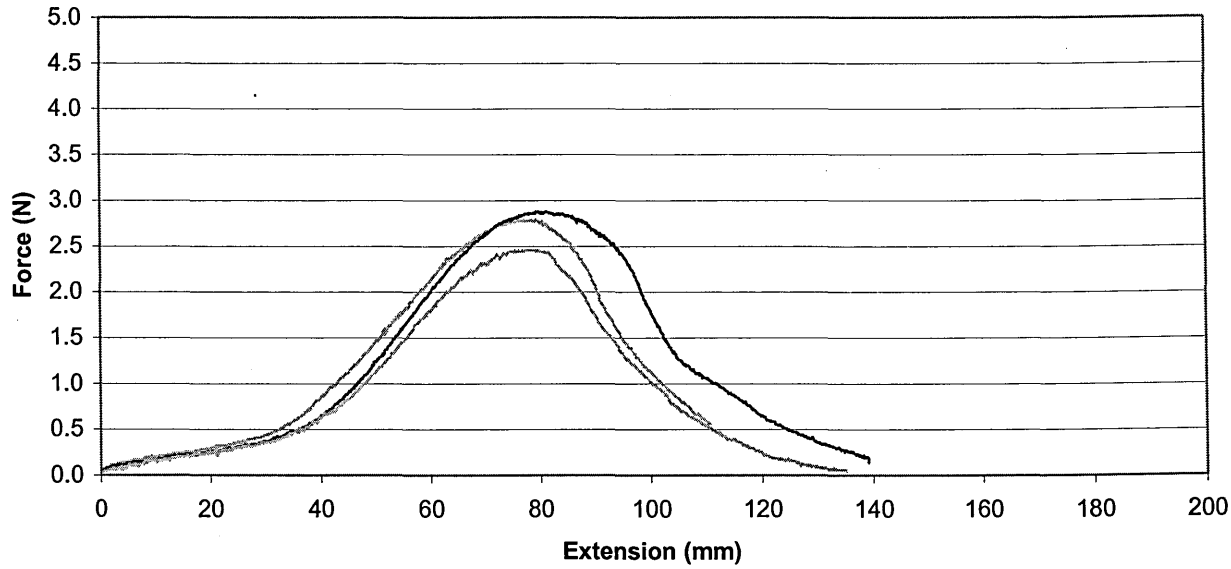

NCF picture frame results

Extension (mm)	Force (N) 1	2	3	4	5	Mean Average	Standard Deviation
10	1.74	5.25	3.03	4.43	2.91	3.47	1.38
20	4.27	9.73	6.83	6.95	4.41	6.44	2.24
30	5.62	11.00	8.81	8.12	5.61	7.83	2.29
40	6.49	11.80	11.00	9.44	6.56	9.06	2.46
50	7.23	12.00	12.00	9.67	7.30	9.64	2.37
60	7.69	12.20	12.30	9.40	7.44	9.81	2.36
70	11.10	16.40	16.50	14.50	11.10	13.92	2.69
80	43.70	62.00	55.90	57.70	40.40	51.94	9.37

NCF picture frame squared deviations from mean and variance

Extension (mm)	Squared deviation from mean 1	2	3	4	5	Variance (s^2)	(s)
10	3.00	3.16	0.20	0.92	0.32	0.84	0.92
20	4.70	10.84	0.15	0.26	4.11	2.23	1.49
30	4.89	10.04	0.96	0.08	4.94	2.32	1.52
40	6.59	7.52	3.77	0.15	6.24	2.70	1.64
50	5.81	5.57	5.57	0.00	5.48	2.49	1.58
60	4.48	5.73	6.22	0.16	5.60	2.47	1.57
70	7.95	6.15	6.66	0.34	7.95	3.23	1.80
80	67.90	101.20	15.68	33.18	133.17	39.01	6.25

NCF picture frame t-distribution calculation [46]

Sample size 4

1) Confidence level = 90%
2) F(C) = 0.5 (1-conf) = 0.95
   c(3) = 2.13
3) Variance calculated
4)

Disp. (mm)	Angle(°)	Interval (N)
0	0	0
10	5.6	0.874775
20	11.8	1.422344
30	18.2	1.451803
40	25.4	1.564273
50	33.2	1.503585
60	42	1.495777
70	53	1.711321
80	68.6	5.949885

Locking angle data; crosshead extension is measured to the nearest 0.5mm and converted to shear angle using the equation of 4.1.3;

test 1 – 68.6°
test 2 – 69.8°
test 3 – 70.9°
test 4 – 69.8°
test 5 – 70.9° Average: 70.0°

2/2 Twill picture frame results

Extension (mm)	Force (N) 1	2	3	4	5	Mean Average	Standard Deviation
10	0.71	0.28	0.63	0.86	0.57	0.61	0.21
20	3.21	0.60	1.35	2.04	2.07	1.85	0.97
30	5.44	1.76	2.94	2.37	3.84	3.27	1.44
40	7.26	4.41	5.06	4.55	7.13	5.68	1.40
50	8.13	6.83	6.47	5.25	7.59	6.85	1.11
60	8.25	8.86	7.31	7.03	11.96	8.68	1.97
70	14.62	13.40	14.38	12.13	17.70	14.45	2.06
80	79.65	73.50	111.91	49.85	95.07	81.99	23.33

2/2 Twill picture frame squared deviations from mean and variance

Extension (mm)	Squared deviation from mean 1	2	3	4	5	Variance (s^2)	(s)
10	0.01	0.11	0.00	0.06	0.00	0.02	0.14
20	1.84	1.57	0.26	0.03	0.05	0.42	0.65
30	4.72	2.29	0.11	0.82	0.33	0.92	0.96
40	2.49	1.61	0.39	1.27	2.08	0.87	0.93
50	1.63	0.00	0.15	2.57	0.54	0.54	0.74
60	0.19	0.03	1.88	2.73	10.73	1.73	1.31
70	0.03	1.10	0.00	5.35	10.56	1.89	1.38
80	5.50	72.12	894.81	1033.48	170.86	241.86	15.55

2/2 Twill picture frame t-distribution calculation [46]

Sample size 4

1) Confidence level = 90%
2) F(C) = 0.5 (1-conf) = 0.95
   c(3) = 2.13
3) Variance calculated
4)

Ext. (mm)	Angle(°)	Interval (N)
0	0	0
10	5.6	0.135717
20	11.8	0.614905
30	18.2	0.912538
40	25.4	0.889579
50	33.2	0.70212
60	42	1.25261
70	53	1.310923
80	68.6	14.81424

Locking angle data; crosshead extension is measured to the nearest 0.5mm and converted to shear angle using the equation of 4.1.3;

test 1 – 68.6°
test 2 – 69.8°
test 3 – 68.6°
test 4 – 69.8°
test 5 – 68.6° Average: 69.1°

NCF Picture Frame Shear Characterisation
Error bars to 90% confidence from 5 tests

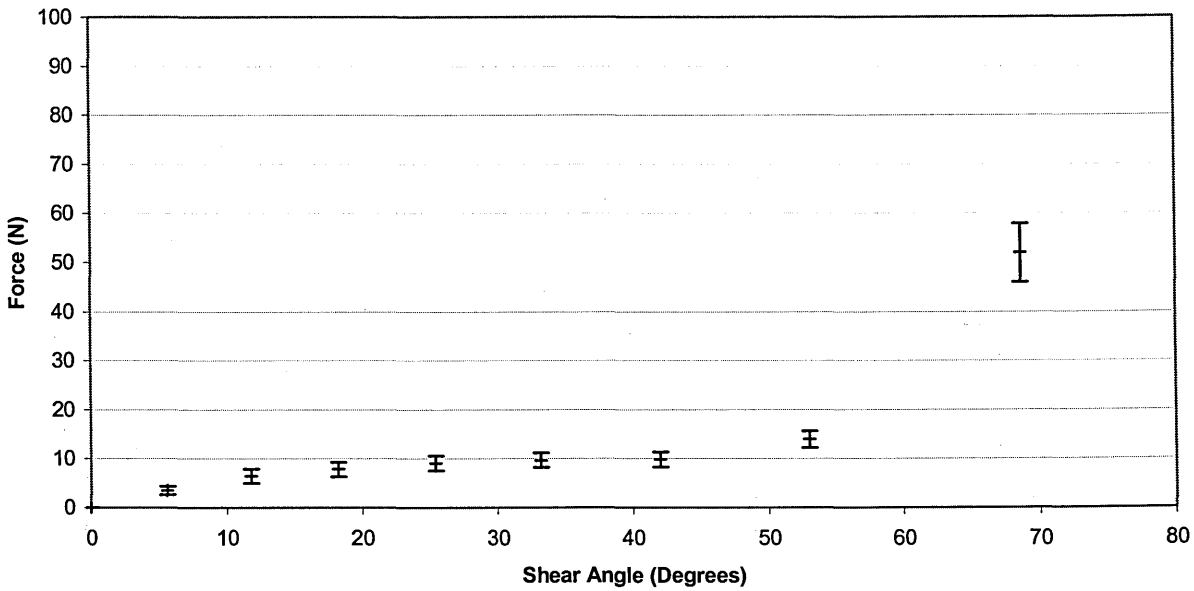

2/2 Twill Picture Frame Shear Characterisation
Error bars to 90% confidence from 5 tests

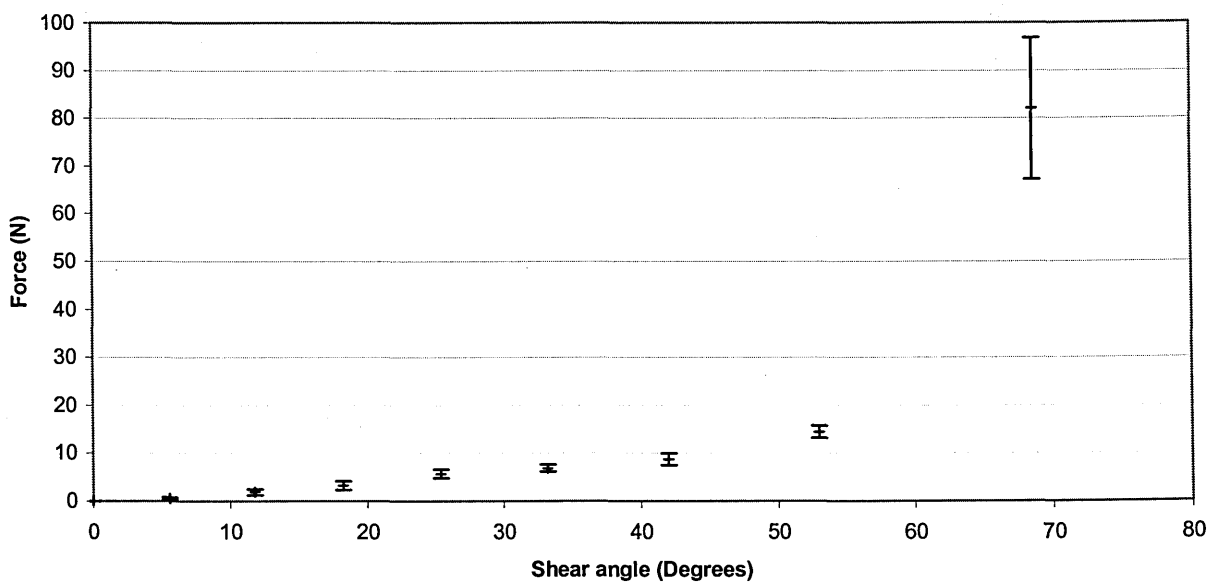

Flexural rigidity data

Fibre alignment to specimen length	Overhang length (mm) *(to nearest 1mm)*						
NCF fabric *(straight filament 'face-up')*							**AVERAGE**
±45°	84	79	80	80	80	82	**81**
0°-90° *(parallel to straight filament)*	190	185	190	186	187	189	**188**
0°-90° *(parallel to chain stitch)*	187	181	179	181	178	180	**182**
2/2 Twill fabric							
±45°	76	74	76	73	73	73	**74**
0°-90°	125	124	123	124	125	122	**124**

Friction test results

2/2 twill: total weight of test equipment (plate, fabric and 5kg mass) = 5309.8g

Interface 1	Interface 2	Force required to overcome friction (N), (Measured to nearest 0.05N)	
2/2 Twill fabric			
Twill fabric	Vacuum former base plate	0.85	0.85
		0.85	0.85
		0.85	0.85
		0.85	0.85
		0.85	0.85
Twill fabric	Mould	2.75	0.60
		2.80	0.65
		2.75	0.60
		2.80	0.60
		2.70	0.60
Twill fabric	Twill Fabric tows at ±45°	1.25	1.10
		1.25	1.10
		1.25	1.10
		1.20	1.10
		1.20	1.10
Twill fabric	Rubber forming membrane	1.90	1.35
		1.95	1.40
		2.00	1.40
		1.90	1.40
		1.95	1.45

Friction test results

NCF: total weight of test equipment (plate, fabric and 5kg mass) = 5301.8g

Interface 1	Interface 2	Force required to overcome friction (N), (Measured to nearest 0.05N)	
NCF fabric		Static	Dynamic
Weft tows (parallel to chain stitch)	Vacuum former base plate	0.95	0.55
		0.90	0.55
		0.90	0.55
		0.90	0.50
		0.90	0.50
Weft tows (perpendicular to chain stitch)	Vacuum former base plate	1.00	0.55
		1.00	0.50
		1.00	0.50
		1.00	0.50
		1.00	0.50
Weft tows (parallel to chain stitch)	Mould	1.75	1.30
		1.70	1.35
		1.70	1.35
		1.65	1.35
		1.65	1.35
Weft tows (perpendicular to chain stitch)	Mould	1.75	1.25
		1.75	1.25
		1.70	1.20
		1.70	1.20
		1.65	1.25
Weft tows (parallel to chain stitch)	Warp tows at ±45°	1.85	1.55
		1.80	1.55
		1.80	1.55
		1.80	1.55
		1.75	1.55
Weft tows (perpendicular to chain stitch)	Warp tows at ±45°	1.65	1.35
		1.65	1.40
		1.60	1.40
		1.60	1.40
		1.60	1.45
Weft tows (parallel to chain stitch)	Rubber forming membrane	1.85	1.30
		1.80	1.25
		1.75	1.20
		1.80	1.20
		1.80	1.25
Weft tows (perpendicular to chain stitch)	Rubber forming membrane	1.80	1.40
		1.80	1.40
		1.75	1.35
		1.85	1.40
		1.80	1.45

NCF tow pull-out results

Results and analysis

Extension (mm)	Force (N) Test 1	Test 2	Test 3	Mean Force (N)	Standard Deviation
1	369.3	255.0	233.9	286.1	72.8734
5	383.4	278.5	296.0	319.3	56.20874
10	399.0	330.2	330.2	353.2	39.66895
15	434.2	379.6	358.5	390.8	39.09103
20	444.1	440.7	389.0	424.6	30.87184

Squared deviations from mean and variance

Extension (mm)	Test 1	Test 2	Test 3	Variance (s^2)	(s)
1	6931.5	964.2	2725.3	5310.5	72.9
5	4110.9	1663.7	544.2	3159.4	56.2
10	2098.2	524.5	524.5	1573.6	39.7
15	1888.3	124.3	1043.6	1528.1	39.1
20	379.5	259.7	1267.0	953.1	30.9

t-distribution calculation [46]

Sample size 3

1) Confidence level = 95%

2) F(C) = 0.5 (1+conf) = 0.975

c = 4.30

3) Variance calculated

4)

Ext. (mm)	**Interval (N/m^2)**
1	**122.9**
5	**94.8**
10	**66.9**
15	**65.9**
20	**52.0**

NCF tow pull-out results

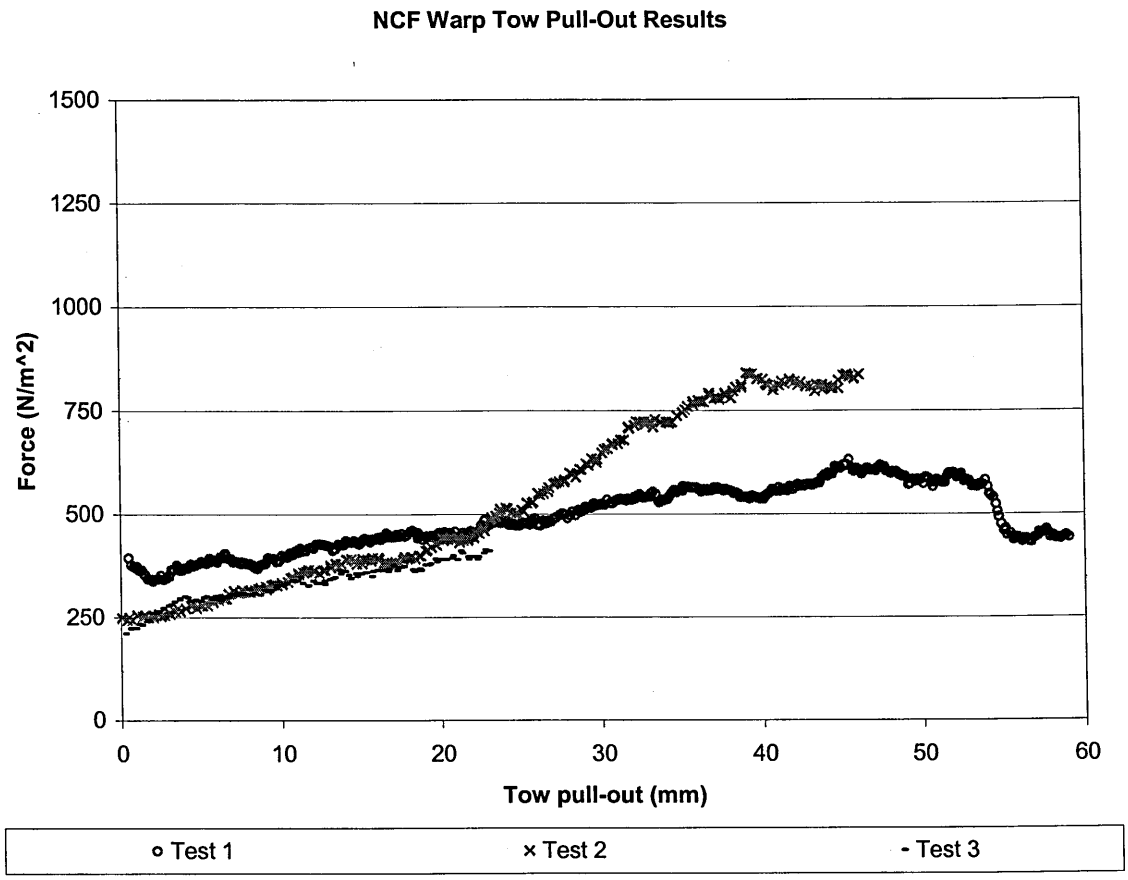

2/2 Twill tow pull-out results

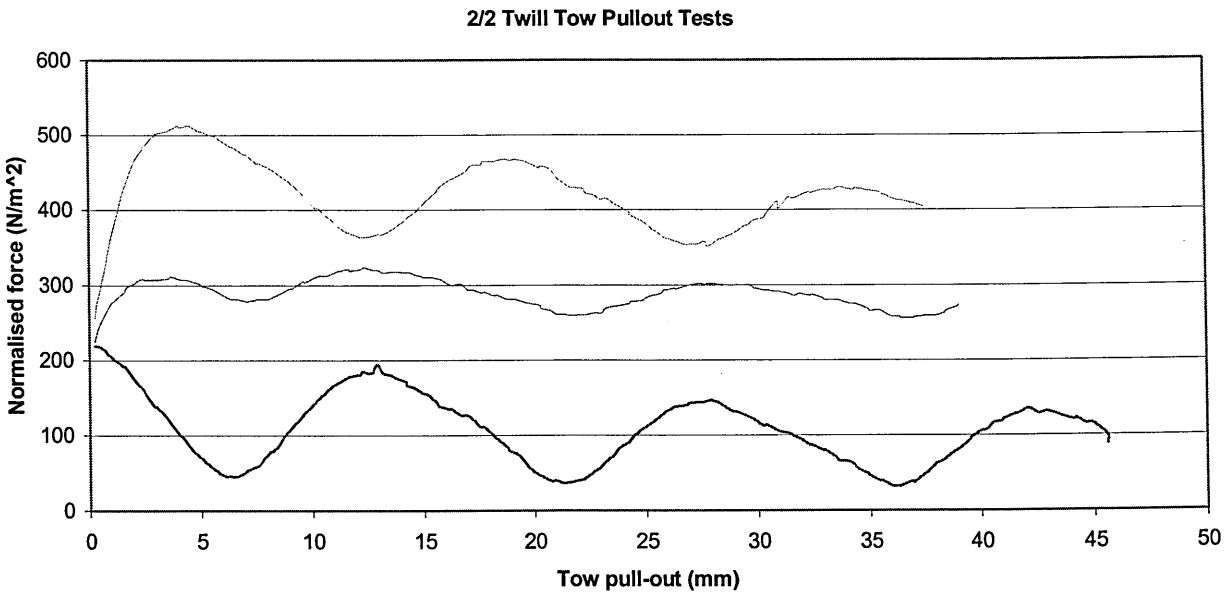

APPENDIX: C

SIMULATION DATA AND RESULTS

NCF Pull-Out Spot-weld Moduli Curve Data

ELEMENT EXTENSION (mm)	SHEAR CURVE	NORMAL CURVE
0	0	0
0.1	4.5×10^{-7}	5.6×10^{-5}
80	8.5×10^{-5}	1.6×10^{-3}

2/2 Twill bias extension material data

PARAMETER	*Simulation 1 and 1a*	*Simulation 2 and 2a*
Elastic fibre modulus 1 (GPa)	*500*	*500*
Elastic fibre modulus 2 (GPa)	*500*	*500*
Out-of-plane shear modulus (1 & 2)	*0.1*	*0.1*
Bending factor (1 & 2)	*1*	*1*
Density (kg/mm^3)	*$7.96x10^{-7}$*	*$7.96x10^{-7}$*
Thickness (mm)	*0.54*	*0.54*
Shear modulus (GPa)	*$1x10^{-6}$*	*$1x10^{-7}$*
Post-lock shear modulus	*0.1*	*0.01*
Locking angle (°)	*41*	*41*
Poisson ratio	*0.4*	*0.4*

2/2 Twill bias extension material data

PARAMETER	*Simulation 3*	*Simulation 4*	*Simulation 5 and 5a*	*Simulation 6*	*Simulation 7c (curve*)*
Elastic fibre modulus 1 (GPa)	*9*	*9*	*9*	*9*	*9*
Elastic fibre modulus 2 (GPa)	*9*	*9*	*9*	*9*	*9*
Out-of-plane shear modulus (1 & 2)	*0.1*	*0.1*	0.1	0.1	0.1
Bending factor (1 & 2)	*1*	*1*	1	1	1
Density (kg/mm^3)	*$2.2x10^{-6}$*	*$2.2x10^{-6}$*	*$2.2x10^{-6}$*	*$2.2x10^{-6}$*	*$2.2x10^{-6}$*
Thickness (mm)	*0.54*	*0.54*	*0.54*	*0.54*	*0.54*
Shear modulus (GPa)	*$5x10^{-2}$*	*$0.5x10^{-2}$*	$15x10^{-3}$	$15x10^{-3}$	N/A*
Post-lock shear modulus	*0.5*	*$0.5x10^{-2}$*	$15x10^{-3}$	$5x10^{-3}$	N/A*
Locking angle (°)	*90*	*0*	0	40	N/A*
Poisson ratio	*0.4*	*0.4*	*0.4*	*0.4*	*0.4*

A higher density of $2.2x10^{-6}$ kg/mm^3 has been used to produce faster running simulations. This value is the average density of carbon fibres and not the average density of the fabric sheet [49]

* the shear moduli are user defined by a curve with the following inputs:

Inter-fibre angle (°)	Shear modulus
90	0
89.5	0.025
80	0.01
60	$5x10^{-5}$
25	0.015
10	1
0	10

NCF bias extension. material data

PARAMETER	*Simulation 8 and 8a*		*Simulation 9 and 9a*	
Fibre orientation (°)	*45°*	*-45°*	*45°*	*-45°*
Elastic fibre modulus 1 (GPa)	*0.1*	*3*	*0.1*	*500*
Elastic fibre modulus 2 (GPa)	*3*	*0.1*	*500*	*0.1*
Out-of-plane shear modulus (1 & 2)	*10*	*10*	*10*	*10*
Bending factor (1 & 2)	*100*	*100*	*100*	*100*
Density (kg/mm^3)	$8.43x10^{-7}$	$8.43x10^{-7}$	$8.43x10^{-7}$	$8.43x10^{-7}$
Thickness (mm)	*0.255*	*0.255*	*0.255*	*0.255*
Shear modulus (GPa)	$1x10^{-7}$	$1x10^{-7}$	$1x10^{-7}$	$1x10^{-7}$
Post-lock shear modulus	*0.01*	*0.01*	*0.01*	*0.01*
Locking angle (°)	*20*	*20*	*20*	*20*
Poisson ratio	*0.4*	*0.4*	*0.4*	*0.4*

2/2 Twill picture frame material data

PARAMETER	*Simulation A*	*Simulation B*	*Simulation C*
Elastic fibre modulus 1 (GPa)	*6*	*9*	*300*
Elastic fibre modulus 2 (GPa)	*6*	*9*	*300*
Out-of-plane shear modulus (1 & 2)	*0.1*	*0.1*	0.1
Bending factor (1 & 2)	*1*	*1*	1
Density (kg/mm^3)	*$7.96x10^{-7}$*	*$7.96x10^{-7}$*	*$7.96x10^{-7}$*
Thickness (mm)	*0.54*	*0.54*	*0.54*
Shear modulus (GPa)	N/A*	N/A*	N/A*
Post-lock shear modulus	N/A*	N/A*	N/A*
Locking angle (°)	N/A*	N/A*	N/A*
Poisson ratio	*0.4*	*0.4*	*0.4*

* the shear moduli are user defined by a curve with the following inputs:

Inter-fibre angle (°)	Shear modulus
90	6
80	$6x10^{-5}$
60	$6x10^{-5}$
40	$6x10^{-8}$
20	$1x10^{-8}$
0	$6x10^{-11}$

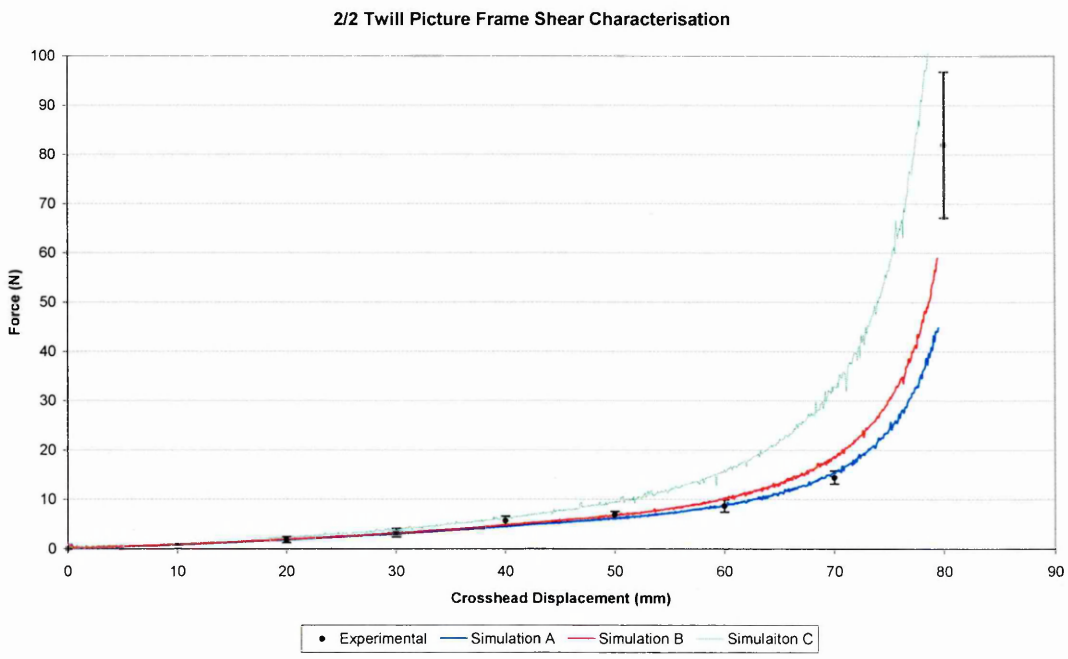

NCF picture frame material data

PARAMETER	*Simulation D*		*Simulation E*		*Simulation F*	
Fibre orientation (°)	*0°*	*90°*	*0°*	*90°*	*0°*	*90°*
Elastic fibre modulus 1 (GPa)	*1*	*0.01*	*1*	*0.1*	*300*	*0.1*
Elastic fibre modulus 2 (GPa)	*0.01*	*1*	*0.1*	*1*	*0.1*	*300*
Out-of-plane shear modulus (1 & 2)	*1*	*1*	*1*	*1*	1	1
Bending factor (1 & 2)	*1*	*1*	*1*	*1*	1	1
Density (kg/mm^3)	$2.2x10^{-6}$	$2.2x10^{-6}$	$2.2x10^{-6}$	$2.2x10^{-6}$	$2.2x10^{-6}$	$2.2x10^{-6}$
Thickness (mm)	*0.255*	*0.255*	*0.255*	*0.255*	*0.255*	*0.255*
Shear modulus (GPa)	N/A*	N/A*	N/A*	N/A*	N/A*	N/A*
Post-lock shear modulus	N/A*	N/A*	N/A*	N/A*	N/A*	N/A*
Locking angle (°)	N/A*	N/A*	N/A*	N/A*	N/A*	N/A*
Poisson ratio	*0.4*	*0.4*	*0.4*	*0.4*	*0.4*	*0.4*

A higher density of $2.2x10^{-6}$ kg/mm^3 has been used to produce faster running simulations. This value is the average density of carbon fibres and not the average density of the fabric sheet [49].

* the shear moduli are user defined by a curve with the following inputs:

Inter-fibre angle (°)	Shear modulus
90	$8x10^{-4}$
85	$8x10^{-5}$
70	$8x10^{-10}$
20	$1x10^{-15}$
10	$1x10^{-16}$
0	$1x10^{-6}$

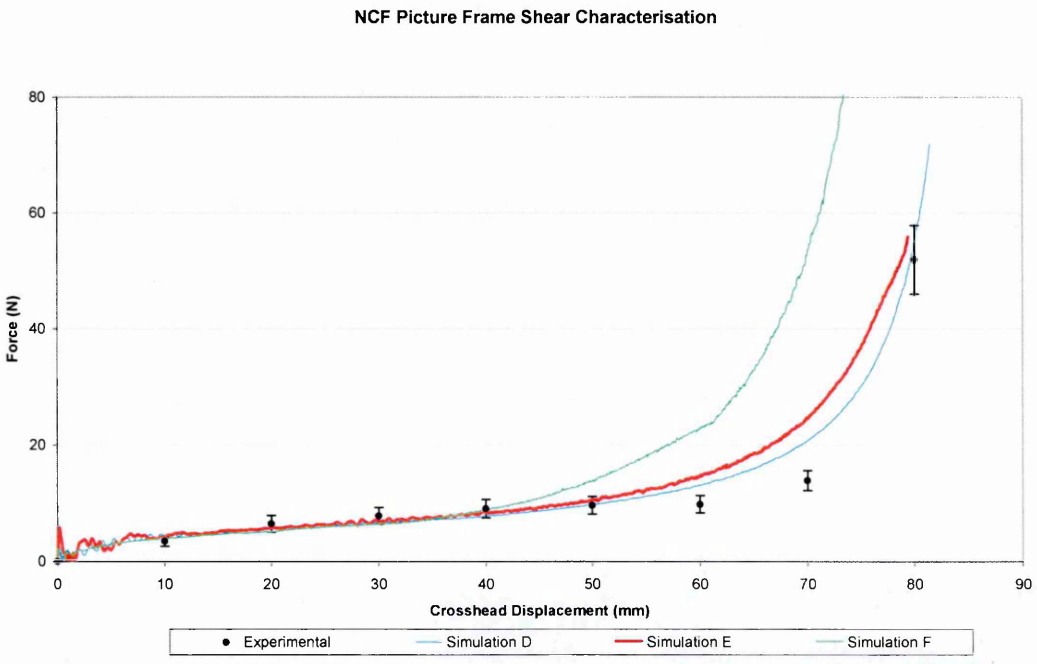

NCF Flexural rigidity simulation material data

PARAMETER	*Simulation X*		*Simulation Y*		*Simulation R*	
Fibre orientation (°) relative to coupon length	*0°*	*90°*	*+45°*	*-45°*	*0°*	*90°*
Bending length simulated (mm)	*182*		*81*		*182*	
Elastic fibre modulus 1 (GPa)	*1*	*0.1*	*1*	*0.1*	*1*	*0.1*
Elastic fibre modulus 2 (GPa)	*0.1*	*1*	*0.1*	*1*	*0.1*	*1*
Out-of-plane shear modulus (1 & 2)	*1*	*1*	*1*	*1*	*1*	*1*
Bending factor (1 & 2)	*1000*	*1000*	*1000*	*1000*	*1000*	*1000*
Density (kg/mm^3)	$2.2x10^{-6}$	$2.2x10^{-6}$	$2.2x10^{-6}$	$2.2x10^{-6}$	$8.43x10^{-7}$	$8.43x10^{-7}$
Thickness (mm)	*0.255*	*0.255*	*0.255*	*0.255*	*0.255*	*0.255*
Shear modulus (GPa)	N/A*	N/A*	N/A*	N/A*	N/A*	N/A*
Post-lock shear modulus	N/A*	N/A*	N/A*	N/A*	N/A*	N/A*
Locking angle (°)	N/A*	N/A*	N/A*	N/A*	N/A*	N/A*
Poisson ratio	*0.4*	*0.4*	*0.4*	*0.4*	*0.4*	*0.4*

PARAMETER	*Simulation S*		*Simulation T*	
Fibre orientation (°)	*0°*	*90°*	*0°*	*90°*
Bending length simulated (mm)	*182*		*182*	
Elastic fibre modulus 1 (GPa)	*1*	*0.1*	*90*	*90*
Elastic fibre modulus 2 (GPa)	*0.1*	*1*	*90*	*90*
Out-of-plane shear modulus (1 & 2)	*100*	*100*	*1*	*1*
Bending factor (1 & 2)	*1000*	*1000*	*1000*	*1000*
Density (kg/mm^3)	$2.2x10^{-6}$	$2.2x10^{-6}$	$2.2x10^{-6}$	$2.2x10^{-6}$
Thickness (mm)	*0.255*	*0.255*	*0.255*	*0.255*
Shear modulus (GPa)	N/A*	N/A*	N/A*	N/A*
Post-lock shear modulus	N/A*	N/A*	N/A*	N/A*
Locking angle (°)	N/A*	N/A*	N/A*	N/A*
Poisson ratio	*0.4*	*0.4*	*0.4*	*0.4*

* the shear moduli are user defined by a curve with the following inputs:

Inter-fibre angle (°)	Shear modulus
90	$8x10^{-4}$
85	$8x10^{-5}$
70	$8x10^{-10}$
20	$1x10^{-15}$
10	$1x10^{-16}$
0	$1x10^{-6}$

EXAMPLE DRAPING SINULATION PAMFORM FILE: NCF 0°-90° ON +/-45°

Node, spot-weld and element cards are not included

```
$
$ This file is generated by PAM-GENERIS version 2001
$        PAM-GENERIS Version 2001 - Compiled 2001/06/14
$
FREE
SOLVER STAMP
NOLIS
NOPRINT
SIGNAL YES
FILE Hemisphere_NCF_090_on_45
DATACHECK  NO
TIMESTEP  LARGE BEND
SHLPLOT ALL
SHLTHP ALL
BEAPLOT ALL
NODPLOT DFLT
PIPE  NO
DEBUG  NO
TITLE /  Hemisphere - two part mould
$
$   CONTROL CARDS
$
$       TIME      TIOD      PIOD      IRD  NLOG DTO       SLFAC     ISTR IPHG IS
$
$---5---10----5---20----5---30----5---40----5---50----5---60----5---70----5---80
CTRL  /         36     1000S       15S    0   10         0       0.6    0    0 0
$
$   SOLID VISCOSITY AND TIME STEP CARDS
$
$---5---10----5---20----5---30----5---40----5---50----5---60----5---70----5---80
               1.2      0.06         0       0.9         0         0         2
                 0         0         0         0    0         1    0    0    0
            1         0         0    0
$
$  MATERIAL DATA CARDS
$
$---5---10----5---20----5---30----5---40----5---50----5---60----5---70----5---80
MATER /        1     100           7e-06

 Mould
      0.01                 0.3         1



MATER /        2     100           7e-06

 Plate
      0.01                 0.3         1



MATER /        3     140        8.43e-07       0               0

  45 bottom ply
                                  0.255      0.01      0.01      0.01    0.8333
        1                 100        10    1         1         1         0
      0.1                 100        10    1        -1         1         0
     CURVE         8       0.4         0         0
     1e-20                                                                     0

        0         0         0         0                  0.1         0
MATER /        6     140        8.43e-07       0               0

  45 top ply
                                  0.255      0.01      0.01      0.01    0.8333
      0.1                 100        10    1         1         1         0
        1                 100        10    1        -1         1         0
     CURVE         8       0.4         0         0
     1e-20                                                                     0
```

```
        0         0         0         0                  0.1         0
MATER /        9     140        8.43e-07       0                0

 090 top ply
                                  0.255      0.01      0.01      0.01    0.8333
        1                  100       10    1         1         0         0
      0.1                  100       10    1         0         1         0
    CURVE         8       0.4        0         0
    1e-20                                                                      0

        0         0         0         0                  0.1         0
MATER /       12     140        8.43e-07       0                0

 090 bottom ply
                                  0.255      0.01      0.01      0.01    0.8333
      0.1                  100       10    1         1         0         0
        1                  100       10    1         0         1         0
    CURVE         8       0.4        0         0
    1e-20                                                                      0

        0         0         0         0                  0.1         0
MATER /       13     200           1e-05
```

```
$
$  DISPLACEMENT BOUNDARY CONDITION
$
$---5---10----5---20----5---30----5---40----5---50----5---60----5---70----5---80
#GPNAM Tooling constraint
BOUNC /        0  111111
        MAT           1        2
        END
$
$  FUNCTIONS CARDS
$
$---5---10----5---20----5---30----5---40----5---50----5---60----5---70----5---80
#GPNAM Pressure_curve
FUNCT /        1       3       1       1       0       0
                               0               0
                               1           1e-07
                            1000           1e-07
#GPNAM funct normal - for non-linear spotweld
FUNCT /        3       3       1       1       0       0
                               0               0
                            0.01           6e-05
                              80           0.002
#GPNAM funct shear - for non-linear spotweld
FUNCT /        4       3       1       1       0       0
                               0               0
                            0.01           5e-07
                              80           9e-05
#GPNAM Curve fabric shear     8
FUNCT /        8       6       1       1       0       0
                               0           1e-06
                              10           1e-16
                              20           1e-15
                              70           8e-10
                              85           8e-05
                              90          0.0008
```

```
$
$  SHELL PRESSURE CARDS
$
$---5---10----5---20----5---30----5---40----5---50----5---60----5---70----5---80
#GPNAM pressure
PRESH /        1               1                       0
        MAT       12
        END
$
$  SLIDING INTERFACE CARDS
$
```

```
$---5---10----5---20----5---30----5---40----5---50----5---60----5---70----5---80
SLINT2/      101        0       42              0.1
 interface between lower plies (spotweld
               1        0                0        0        3        4        1
$
        MAT            6
        END
$
        MAT            3
        END
SLINT2/      102        0       42              0.1
 interface between upper plies (spotweld
               1        0                0        0        3        4        1
$
        MAT           12
        END
$
        MAT            9
        END
SLINT2/        1        0       16     0.11              0.2        0                3
 Contact_mould
               0        0                0                 0                 0
               0        0
               0
$
        MAT           -3
        END
$
        MAT           -1
        END
SLINT2/        2        0       16     0.16              0.2        0                3
 Contact_plate
               0        0                0                 0                 0
               0        0
               0
$
        MAT           -3
        END
$
        MAT           -2
        END
SLINT2/        3        0       33     0.21        0   0.125       -1        0        1
 Sheet to sheet lower
               0        0        0        0        0               10        0        0
$
        MAT           -6
        END
$
        MAT            3
        END
SLINT2/        9        0       33     0.21        0   0.125       -1        0        1
 Sheet to sheet upper
               0        0        0        0        0               10        0        0
$
        MAT          -12
        END
$
        MAT            9
        END
SLINT2/        7        0       33     0.21        0   0.125       -1        0        1
 fabric to fabric
               0        0        0        0        0               10        0        0
$
        MAT           -9
        END
$
        MAT            6
        END
ENDDATA
```

EXAMPLE DRAPING SINULATION PAMFORM FILE: 2/2 TWILL 0°-90° ON +/-45°

Node, spot-weld and element cards are not included

```
$
$ This file is generated by PAM-GENERIS version 2001
$        PAM-GENERIS Version 2001 - Compiled 2001/06/14
$
FREE
SOLVER STAMP
NOLIS
NOPRINT
SIGNAL YES
FILE Hemisphere_22T_090_on_45
DATACHECK  NO
TIMESTEP  LARGE BEND
SHLPLOT ALL
SHLTHP ALL
BEAPLOT ALL
NODPLOT DFLT
PIPE  NO
DEBUG  NO
TITLE /  Hemisphere - two part mould
$
$   CONTROL CARDS
$
$       TIME      TIOD      PIOD      IRD  NLOG DTO       SLFAC     ISTR IPHG IS
$
$---5---10----5---20----5---30----5---40----5---50----5---60----5---70----5---80
CTRL  /         34     1000S       18S    0   10         0       0.1    0    0 0
$
$   SOLID VISCOSITY AND TIME STEP CARDS
$
$---5---10----5---20----5---30----5---40----5---50----5---60----5---70----5---80
               1.2      0.06         0       0.9         0         0         1
                 0         0         0         0    0         1    0    0    0
$
$  MATERIAL DATA CARDS
$
$---5---10----5---20----5---30----5---40----5---50----5---60----5---70----5---80
MATER /        1     100           7e-06

 Mould
     0.01                 0.3         1



MATER /        2     100           7e-06

 Plate
     0.01                 0.3         1



MATER /        3     140        7.96e-07       0               0

 Fabric 45
                                   0.54      0.01      0.01      0.01    0.8333
        6                 100         1    1         1         1         0
        6                 100         1    1        -1         1         0
     CURVE         8       0.4         0         0
     1e-20                                                                      0

        0         0         0         0                 0.1         0
MATER /        6     140        7.96e-07       0               0

 Upper 090 Fabric
                                   0.54      0.01      0.01      0.01    0.8333
        6                 100         1    1         1         0         0
        6                 100         1    1         0         1         0
     CURVE         8       0.4         0         0
     1e-20                                                                      0
```

```
        0         0         0         0                   0.1         0
MATER /        7     200           1e-05

 BEAM     0

        0                   0         0         0


$
$  DISPLACEMENT BOUNDARY CONDITION
$
$---5---10----5---20----5---30----5---40----5---50----5---60----5---70----5---80
#GPNAM Tools
BOUNC /        0  111111
        MAT           1        2
        END
$
$  FUNCTIONS CARDS
$
$---5---10----5---20----5---30----5---40----5---50----5---60----5---70----5---80
#GPNAM Pressure_curve
FUNCT /        1       3       1       1       0       0
                               0               0
                               1           1e-07
                            1000           1e-07
#GPNAM Curve shear     8
FUNCT /        8       6       1       1       0       0
                               0               6
                              20           6e-11
                              40           1e-08
                              60           6e-08
                              80           6e-05
                              90           6e-05
$
$  SHELL PRESSURE CARDS
$
$---5---10----5---20----5---30----5---40----5---50----5---60----5---70----5---80
#GPNAM pressure
PRESH /        1       0       1                       0
        MAT        6
        END
$
$  SLIDING INTERFACE CARDS
$
$---5---10----5---20----5---30----5---40----5---50----5---60----5---70----5---80
SLINT2/        1       0      16    0.11            0.54       0               3
 Contact
               0       0               0               0               0
               0       0
               0
$
        MAT          -3
        END
$
        MAT          -1
        END
SLINT2/        2       0      16    0.16            0.54       0               3
 Contact_plate
               0       0               0               0               0
               0       0
               0
$
        MAT          -3
        END
$
        MAT          -2
        END
SLINT2/        3       0      33    0.21     0.1    0.54      -1     0.1       1
 fabric fabric
               0       0       0       0       0              10       0       0
$
        MAT          -6
        END
$
        MAT           3
        END
ENDDATA
```

2/2 TWILL FIBRE STRAIN IMAGES

2/2 TWILL 0°-90° SHEET RESULTS

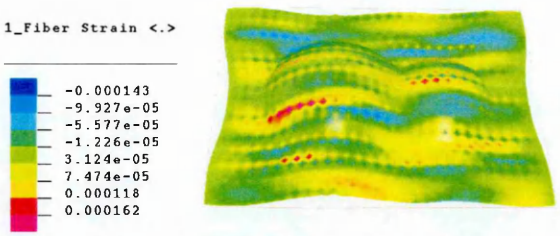

2/2 twill 0° fibre strain (%)

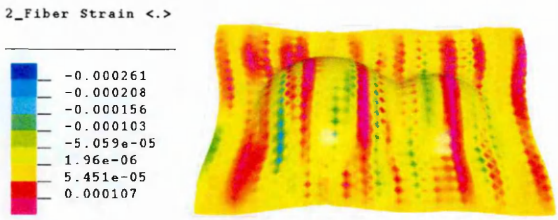

2/2 twill 90° fibre strain (%)

2/2 TWILL ±45° SHEET RESULTS

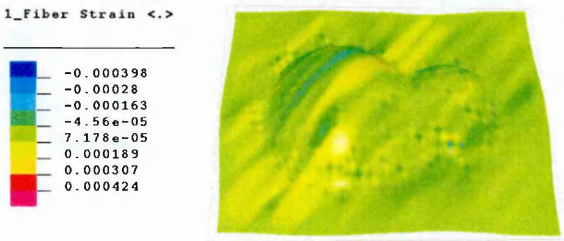

2/2 twill -45° fibre strain (%)

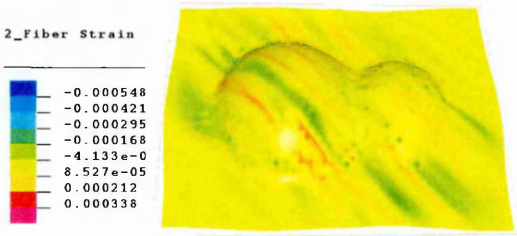

2/2 twill +45° fibre strain (%)

NCF FIBRE STRAIN IMAGES

NCF, UPPER SHELL ELEMENT LAYER, 0°-90° SHEET RESULTS

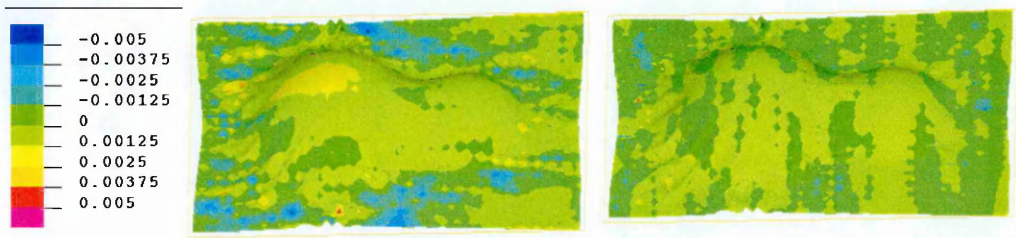

NCF 0° fibre strain (%)
(transverse to simulated fibres)

NCF 90° fibre strain (%)
(longitudinal to simulated fibres)

NCF, UPPER SHELL ELEMENT LAYER, ±45° SHEET RESULTS

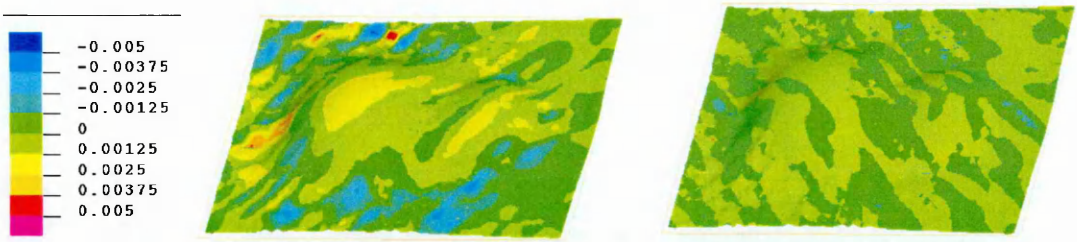

NCF -45° fibre strain (%)
(transverse to simulated fibres)

NCF +45° fibre strain (%)
(longitudinal to simulated fibres)

NCF, UPPER SHELL ELEMENT LAYER, 0°-90° SHEET ON ±45° SHEET RESULTS

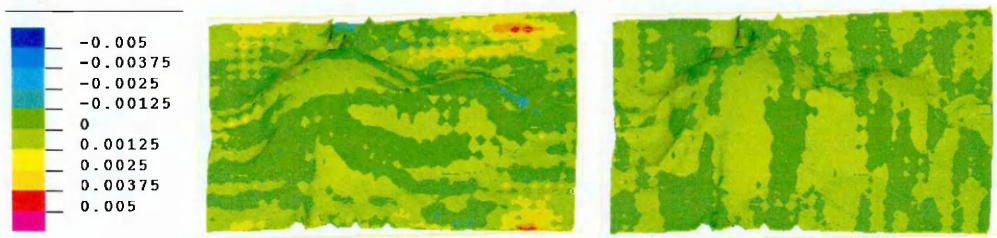

NCF 0° fibre strain (%)
(transverse to simulated fibres)

NCF 90° fibre strain (%)
(longitudinal to simulated fibres)

NCF, UPPER SHELL ELEMENT LAYER, ±45° SHEET ON 0°-90° SHEET RESULTS

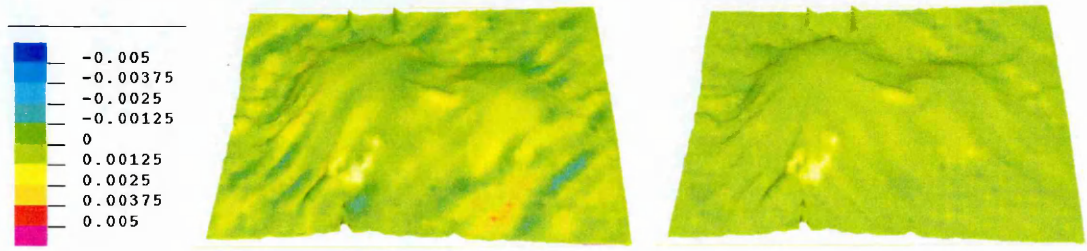

NCF -45° fibre strain (%)
(transverse to simulated fibres)

NCF +45° fibre strain (%)
(longitudinal to simulated fibres)